

Experimental characterization of a solar boiler as a sensible thermal energy storage

Sophie Vercammen

Student number: 01803706

Supervisors: Prof. dr. ir. Michel De Paepe, Dr. ir. Wim Beyne
Counsellors: Ir. Wito Plas, Maité Goderis

Master's dissertation submitted in order to obtain the academic degree of
Master of Science in de industriële wetenschappen: elektromechanica

Academic year 2022-2023

PREFACE

I selected the subject of this master thesis because I find thermodynamics and thermal energy storage an interesting and broad topic. It is a relatively new field of study where I am proud to be part of. This master thesis is mainly written as preparation for further research about sensible thermal energy storage systems.

First, I want to thank my supervisors prof. dr. ir. Michel De Paepe and dr. ir. Wim Beyne and my counsellors ir. Wito Plas and Maité Goderis. They were an enormous help and I learned a lot from them. I could always count on them and ask with my questions.

I also want to thank my girlfriend for the emotional support by telling me not to give up. Last but not least I want to thank my mother, father, plusmother and my family in general for the support during my whole school career. They always believed in me and motivated me. I have received many tips from them without which I would not be where I am today.

The author gives permission to make this master dissertation available for consultation and to copy parts of this master dissertation for personal use. In all cases of other use, the copyright terms have to be respected, in particular with regard to the obligation to state explicitly the source when quoting results from this master dissertation.

Thursday, 25 May 2023

REMARK

This master's dissertation is part of an exam. Any comments formulated by the assessment committee during the oral presentation of the master's dissertation are not included in this text.

ABSTRACT

The charging time energy fraction method is an approach to characterize the outlet state of a latent thermal energy storage heat exchanger. Common design methods for latent and sensible heat exchangers such as the logarithmic mean temperature difference method and the effectiveness number of the transfer units method are not directly applicable, as they are based on the assumption of a heat exchanger in steady state. However, a latent and sensible heat exchanger do not operate in steady state. In this paper, it is examined whether the charging time energy fraction method can be applied to a sensible thermal energy storage system. It is important to be able to predict the outlet state as a function of time of these systems, not only because it is an emerging application in domestic households, but also because sensible thermal energy storage systems in combination with a water tank are the cheapest and most used type of thermal energy storage. To investigate this, experiments were carried out on a solar boiler. To charge and discharge, the already built hot circuit is used and the cold circuit has been redesigned and closed. Six charging and six discharging tests are executed with temperatures ranging from 30°C till 50°C at flow rates ranging from 150 kg/h till 450 kg/h. Afterwards, the energy fraction in function of time is fitted between zero and one and the correlation parameters for the charging time and discharging time are found. A difference exists between the predicted integrated efflux of energy and the stored coil energy, but this thesis did not predict the outlet temperature of the experiments.

EXPERIMENTAL CHARACTERIZATION OF A SOLAR BOILER AS A SENSIBLE THERMAL ENERGY STORAGE

Sophie Vercammen, Ir. Wito Plas, Ir. Maité Goderis, Dr. ir. Wim Beyne, Prof. dr. ir. Michel De Paepe
Department of Electromechanical, Systems and Metal Engineering
Ghent University
Sint-Pietersnieuwstraat 41 – B9000 Gent – Belgium
E-mail: sophie.vercammen@ugent.be

ABSTRACT

The charging time energy fraction method is an approach to characterize the outlet state of a latent thermal energy storage heat exchanger. Common design methods for latent and sensible heat exchangers such as the logarithmic mean temperature difference (LMTD) method and the effectiveness number of the transfer units (e-NTU) method are not directly applicable, as they assume of a heat exchanger in steady state. However, a latent and sensible heat exchanger do not operate in steady state. In this paper, it is examined whether the charging time energy fraction method can be applied to a sensible thermal energy storage system. It is important to be able to predict the outlet state as a function of time of these systems, not only because it is an emerging application in domestic households, but also because sensible thermal energy storage systems in combination with a water tank are the cheapest and most used type of thermal energy storage. To investigate this, experiments were carried out on a solar boiler. To charge and discharge, the already built hot circuit is used and the cold circuit has been redesigned and closed. Six charging and six discharging tests are executed with temperatures ranging from 30°C till 50°C at flow rates ranging from 150 kg/h till 450 kg/h. Afterwards, the energy fraction in function of time is fitted between zero and one and the correlation parameters for the charging time and discharging time are found. A difference exists between the predicted integrated efflux of energy and the stored coil energy, but this thesis did not predict the outlet temperature of the experiments.

INTRODUCTION

The world's increasing population combined with the world's rising energy consumption and thus also the concerns about environmental impacts, forces countries to adjust their way of energy use and production. Solar, biomass, wind, and hydroelectric energy sources are more and more implemented all over the world. These energy sources, however, highly fluctuate and need as such effective energy storage systems [1]. To provide society with more efficient, environmentally

NOMENCLATURE

Q	[J]	Heat
U	[J]	Internal energy of the storage material
H	[kJ/kg]	Enthalpy of heat transfer fluid (HTF)
c_p	[J/°C]	Heat capacity
T	[°C]	Temperature
t	[s]	Time
\dot{m}	[kg/s]	Mass flow rate
V	[m ³]	Volume
Special characters		
α	[-]	Energy fraction ratio
Subscripts		
f		Net efflux
o		Outgoing
i		Ingoing
c		Coils
t		Tank
max		Maximum
h		Heater
cv		Control volume
m		Mean
ch		Charging
av		Average

friendly energy use in building heating and cooling, aerospace energy and utility applications, a thermal energy storage (TES) system is a great tool. Because a TES system makes use of natural resources and waste heat, it reduces the total consumption of energy, consequently the use of fossil fuels and costly oil imports [1], [2].

The definition of thermal energy storage is energy conservation on an hourly, diurnal, daily, weekly, occasionally, or seasonally basis of high- or low- temperature energy for later use and this by heating, cooling, vaporizing, solidifying or liquefying a material or through thermochemical reactions. The stored energy is transformed into heat or coolness by reversing the process.

TES can be used for water and (overnight) space heating, cooling, and air conditioning. For example, summer or waste heat can be used for winter use, winter ice can be used for space

cooling in summer, and the electrically generated heat or cold during off-peak hours can be used during subsequent peak demand hours. Cooling TES uses water, ice, or an eutectic salt solution as storage material. It is beneficial for new buildings with large cooling loads during the day and no cooling loads at night. TES systems are also used to shift peak electricity consumption to a time of day when there is a lot of solar radiation available. This reduces the peak electricity demands and results in cost effectiveness for consumers, only if time of use tariffs exist. TES systems can also be used in thermal electrical generating systems where the energy is stored before it is converted to electricity.

There are many ways to classify TES systems. One of them is seeing TES as a spectrum, where on the one side seasonal storage exists and on the other side hourly storage. Another way of classifying TES systems is splitting them into three types: sensible thermal energy storage (STES), latent thermal energy storage (LTES) and thermochemical energy storage. In STES the storage medium temperature changes when heat is added/distracted, this in contrast with a latent TES (LTES) where the storage material does undergo a phase change.

In this paper, a solar boiler with polymer coils inside is used. It is an example of a sensible solar hot water storage system. Solar energy is utilized to heat up the tank water for later use. The energy comes from solar radiation, absorbed by collectors, and is transported to the water tank directly or indirectly. This increases the water's temperature without phase change, after which the consumer can use this demanded heat to meet his basic needs. Storage of this solar energy is absolutely required since solar energy and heat demand does not always occur at the same time [1].

For characterizing heat exchangers, many methods already exist, such as the e-NTU and the LMTD method. These methods however are based on the assumption of a heat exchanger in steady state while LTES and STES heat exchangers do not operate in steady state. This is why Beyne et al. [3] recently developed a new method for quantitatively studying TES systems: the charging time energy fraction (CTEF) method. Prediction of the outlet state as a function of time is the main benefit of the CTEFM (CTEF method).

This CTEF method is not yet used on an STES system. It is important to be able to predict the outlet state as a function of time of these systems, not only because it is an upcoming application in domestic households, but also because STES systems in combination with a water tank are the cheapest and most widely used type of TES [4].

The purpose of this master thesis is to apply this CTEF model for an STES system by charging and discharging tests. Predicting the water temperature at the outlet of the coils is done by correlating the energy fraction function $\alpha(t)$. This is the integrated efflux of energy $Q_f(t)$ divided by maximum integrated efflux of energy $\max Q_f$, as can be seen in Eq. (1) [3].

$$\alpha(t) = \frac{Q_f(t)}{\max Q_f} \quad (1)$$

The net efflux of energy $\dot{Q}_f(t)$ can be correlated instead of the outlet state. To do this, the inlet state and so the mass flow rate

and the inlet water temperature must also be known and be constant to use Eq. (2).

$$\dot{Q}_f = \dot{m}(h_{out} - h_{in}) \quad (2)$$

METHODOLOGY

Experimental set-up

The old set-up consisted of a closed hot and an open cold circuit connected to the solar boiler. Figure 1 shows the current experimental set-up consisting of a closed hot circuit (in red), a closed cold circuit (in blue), a chiller circuit (in green) and a solar boiler (in purple). To do the experiments for this master thesis, the cold circuit has been redesigned and closed. With the new closed cold circuit, no water is wasted by using the same water each time for the tests, and no hot water is discharged into the sewer. There are several mechanical 3 way "T" port ball valves to control the direction of the water flow and a loop to the chiller has been added to the set-up.

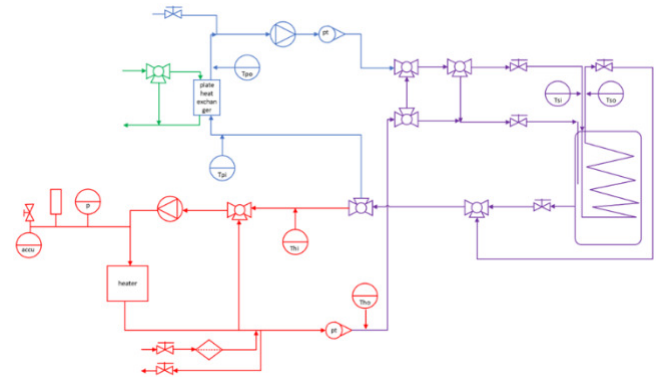


Figure 1: Set-up of the solar boiler.

Charging and discharging experiments are performed on this set-up and the CTEFM is applied. For the charging and discharging test, separate circuits are needed. Because no collectors are present in the setup, a heater is used. For the charging test, the heater in the hot circuit delivers of a constant temperature to the water flowing into the coils (heat transfer fluid HTF). The heater also ensures that a sufficiently high tank temperature is attained prior to the discharging tests. When the tank water has the right temperature, the cold and chiller circuit guarantee a constant cold inlet temperature in the coils during discharge testing.

Design of the solar boiler

The solar boiler is an open, pressure free ROTEX Sanitube INOX water storage tank. Inside the tank, there is a corrugated helical coil made of cross-linked polyethylene (PEX) with an aluminium layer inside a polymer matrix. This coil is placed in the middle of the tank and consists of two parallel helical coils of 51 and 46 m. The total length of the coils is 97 m. The outer diameter of the tube of the coil itself is 32 mm and the wall has a thickness of 2 mm [5]. The inside dimensions of the solar boiler are 138.5 x 48 x 48 cm. The boiler has a storage capacity of 300 l and has a double walled jacket made of polypropylene with PUR hard foam heat insulation [5].

A tube, where thermocouples are positioned, is connected to the lid of the tank. All thermocouples in the circuit are K-type thermocouples. There are six thermocouples in the circuit:

before and after the plate heat exchanger, before the three-way valve in the hot circuit, after the hot mass flow meter (so before and after the heater) and at the inlet and outlet of the coils. There are 11 operating thermocouples located in the tank tube. The top thermocouple is placed just below the water level. All the thermocouples are placed with a 15 mm vertical distance from each other. The tank is divided into eight control volumes with each one or two thermocouples, as can be seen in Figure 2.

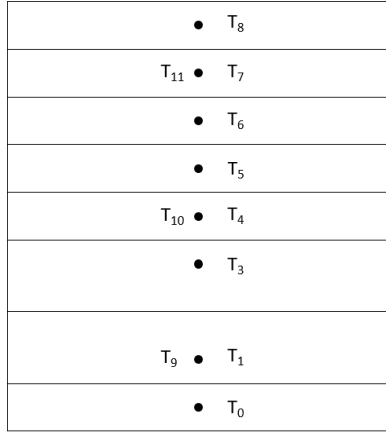


Figure 2: Control volumes of the tank.

Measurement procedure

Charging tests

To have uniform conditions in every experiment, the tank needs to be initialized prior to each experiment to meet the inlet conditions. The test is started when the tank water has a temperature of maximum 20°C, the coil inlet has a constant temperature of 30, 40 or 50°C and the mass flow rate of the HTF remains 150, 300 or 450 kg/h, as is summarized in Table 1.

	30°C	40°C	50°C
150 kg/h	X	X	X
300 kg/h	X	X	
450 kg/h	X		

Table 1: Charging test matrix.

The test is stopped when the difference between the coil inlet and outlet temperature remains the same. The scheme of a charging test is presented in Figure 3.

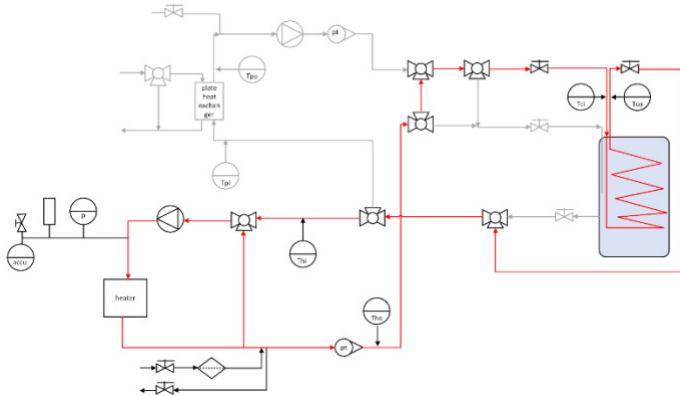


Figure 3: Scheme of solar boiler set-up during charging.

Discharging tests

To have uniform conditions in every experiment, the tank also needs to be initialized prior to each discharging experiment to meet the inlet conditions. The procedure of a discharging test is the following: the water at the inlet of the coils must have a temperature of 20°C and the water in the tank must have a temperature of 30 or 50°C. The mass flow rates are 300, 450 and 600 kg/h, as summarized in Table 2. A scheme of a discharging test is presented in Figure 4.

	30°C	50°C
300 kg/h	X	X
450 kg/h	X	X
600 kg/h	X	X

Table 2: Discharging test matrix.

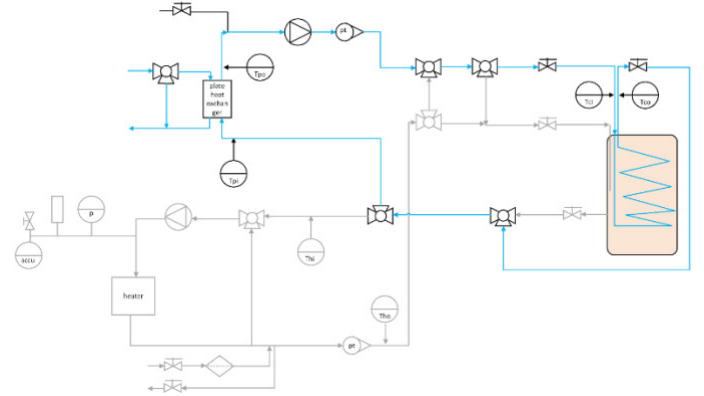


Figure 4: Scheme of solar boiler set-up during discharging.

Data reduction

For the charging tests, as well as for the discharging tests, the energy balance should be correct if the heat loss to the environment is neglected, as can be seen in Eq. (3).

$$\begin{aligned}
 Q_c(t) &= \dot{m}_c c_{p,c,av} (T_{co}(t) - T_{ci}(t)) \cdot \Delta t_{5s} \\
 &= \sum_{k=cv0}^{cv8} \rho_k V_k c_{p,t,av} (T_k(t + \Delta t_{5s}) - T_k(t)) \\
 &= Q_t(t)
 \end{aligned} \tag{3}$$

$$\begin{aligned}
 Q_{total,c} &= Q_{previous} + Q_{new} \\
 &= Q_{previous} + \dot{m}_c c_{p,c,av} (T_{co}(t) - T_{ci}(t)) \\
 &\quad \cdot \Delta t_{5s}
 \end{aligned} \tag{4}$$

$$Q_{total,c}(t) = \sum_{i=0}^t \dot{m}_c c_{p,c,av} (T_{co}(i) - T_{ci}(i)) * \Delta t_{5s} \tag{5}$$

$$Q_{total,t}(t) = \sum_{i=0}^t \sum_{k=cv0}^{cv8} \rho_k V_k c_{p,t,av} (T_k(i + \Delta t_{5s}) - T_k(i)) \tag{6}$$

The thermocouples measure the temperature every five seconds. In order to discretise the derivative in time of the internal energy, the difference of the internal energies at a time, $t + \Delta t$ and t is divided by the elapsed time between these two

measurements, Δt . Q_c is the amount of energy which is transferred from the coils to the tank water at any given moment t . Q_t is the amount of energy added to the tank water at any given moment t , added in an arbitrary time interval Δt . In order to get the total stored energy, these values therefore must be calculated for every period, and be added to the previous value, as is presented in Eq. (4). These values are thus an integrated values. Eq. (5) and (6) show the stored amount of heat in the coils and tank, respectively, at a certain time.

It is now possible to calculate the energy that is delivered to the tank by using the left-hand side of the equation, but also by using the right-hand side of the equation. If there are no or negligible heat losses present, both should be equal. This is called closing the energy balance. Both the left-hand side and the right-hand side of the equation quantify an energy, expressed in Joules.

The formula to calculate the energy fraction $\alpha(t)$ can be found in Eq. (7).

$$\alpha(t) = \frac{Q_c(t)}{\max(Q_c)} \quad (7)$$

Eq. (8) represents the charging time set $t_c(\alpha_i) \forall \alpha_i$ in α in Eq. (7).

$$t_c(\alpha_i) \text{ for which } Q_c(t) = \alpha_i \max Q_c(t) \quad (8)$$

If a charging time correlation is fitted (Eq. (9)), then the correlation parameters $p(\alpha_i)$ (Eq. (10) and (9)) for all energy fractions α_i in the base set α are known.

$$t_c = \frac{\text{Slope}}{\Delta T} + \text{Intercept} \quad (9)$$

$$\text{Slope} = A(\alpha) + \frac{B(\alpha)}{\dot{m}} \quad (10)$$

$$\text{Intercept} = C(\alpha) + \frac{D(\alpha)}{\dot{m}} \quad (11)$$

RESULTS AND DISCUSSION

Charging tests

The initial condition for each experiment is a constant inlet mass flow rate of the HTF flowing through the coils and a constant inlet temperature. The tank's initial temperature is 20°C. To meet the initial conditions, PID controllers in LabVIEW are used. The used PI parameters for the heater and valve in the hot circuit can be found in Table 3.

		30°C		40°C		50°C	
		Heater	Valve	Heater	Valve	Heater	Valve
150 kg/h	K_c [-]	0.6627	0.0182	0.6627	0.009	0.663	0.015
	T_i [min]	0.7952	0.2351	0.7952	0.488	0.795	0.235
300 kg/h	K_c [-]	0.6627	0.015	0.6627	0.015		
	T_i [min]	0.95	0.2351	0.7952	0.2351		
450 kg/h	K_c [-]	0.6627	0.007				
	T_i [min]	0.2351	0.125				

Table 3: PI parameters of heater and valve for charging experiments.

Figure 5 shows that the total energy released by the coils and heater are not completely equal. The difference is due to the heat loss to the environment. The heat absorbed by the tank

water exceeds the delivered coils' heat in the beginning of the test but is caught up towards the end. This can be the result of the tank thermocouples that are calibrated based on the thermocouple at the inlet of the coil, which is not calibrated and because the heat loss between the heater's outlet and coils' inlet is unknown and is thus not deducted from the new thermocouple values after performing linear regression. The tests with a mass flow rate of 150 kg/h show the same pattern, same as the tests with a mass flow rate of 300 kg/h. During the 300 kg/h tests, the difference between the stored tank energy and the total coil energy is larger than the 150 kg/h tests, but also bigger than the 450 kg/h test, which should not be possible because the greater the mass flow rate, the greater the turbulence, the better the exchange of heat [1].

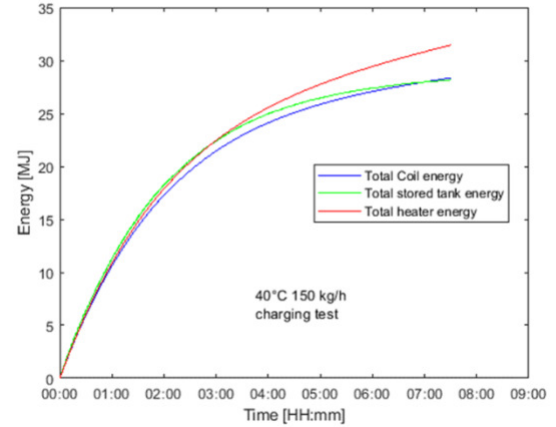


Figure 5: Energies of coils, tank and heater for the charging test with an inlet temperature of 40°C and mass flow 150 kg/h.

The charging time in function of the energy fraction of the 30°C 450 kg/h test is shown in Figure 6. It increases fast in the beginning of the test but slows down at the end.

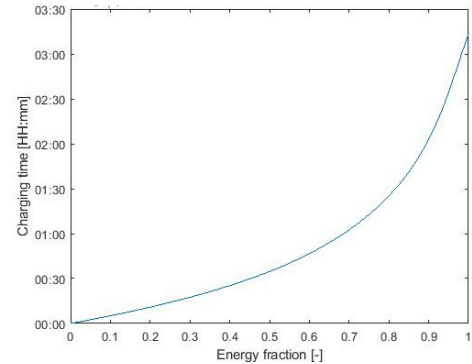


Figure 6: Energy fraction function of the 30°C 450 kg/h charging test.

Figure 7 shows the correlation parameters for all energy fractions. $B(\alpha)$ is negative, because the charging time of the 300 kg/h tests in function of $\frac{1}{\Delta T}$ is descending more than the charging time of the 150 kg/h tests in function of $\frac{1}{\Delta T}$.

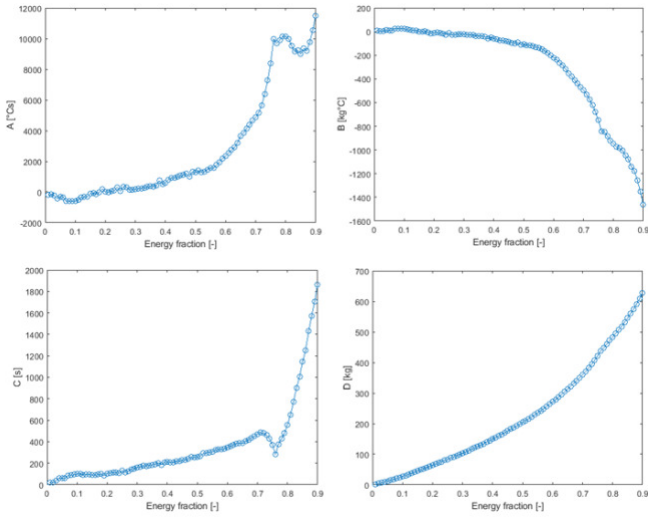


Figure 7: Correlation parameters of the charging time.

The predicted total energy $\alpha(t)\Delta U$ and stored coil energy $Q_{total,c}$ of the 50°C 150 kg/h test is displayed in Figure 8. The curves are almost equal, but not completely, because in $\alpha(t)\Delta U$ there is assumed that the average tank temperature will over time be exactly equal to the coils' inlet temperature, but this does not actually happen. So according to $\alpha(t)\Delta U$, the tank has absorbed more heat than it actually does.

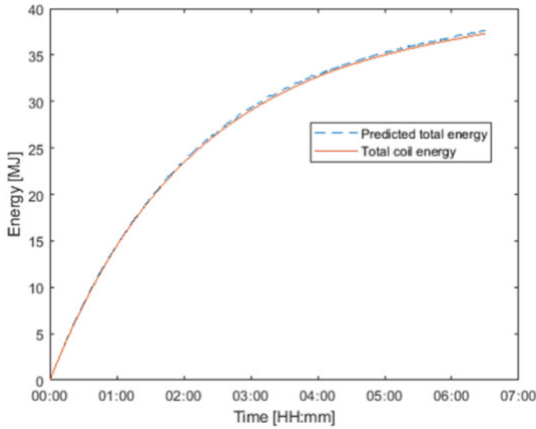


Figure 8: Predicted integrated efflux of energy and the stored coil energy of the 50°C 150 kg/h charging test.

Discharging tests

The initial conditions for each discharging experiment is a constant inlet mass flow rate of the HTF flowing through the coils (300, 450 or 600 kg/h) and a constant inlet coil temperature of 20°C. The tank is initially 30 or 50°C warm. The used PID parameters for the pump in the cold circuit and valve in the chiller circuit can be found in Table 4.

		30°C		50°C	
		Pump	Valve	Pump	Valve
300 kg/h	K_c	0.003	-0.012	0.003	-0.035
	T_i [min]	0.068	0.189	0.068	0.063
	T_d [min]	0	0.029	0	0.017
450 kg/h	K_c	0.003	-0.035	0.003	-0.035
	T_i [min]	0.068	0.063	0.068	0.076

	T_d [min]	0	0.017	0	0.017
600 kg/h	K_c	0.003	-0.035	0.003	-0.004
	T_i [min]	0.068	0.063	0.057	0.120
	T_d [min]	0	0.017	0	0

Table 4: PID parameters of the pump and chiller valve for the discharging experiments.

In Figure 9 the absorbed coil heat, heat of plate heat exchanger and transferred tank heat are displayed for a discharging test of 50°C and 300 kg/h. The difference in coil and tank energy can be the result of heat loss to the environment. However, the difference between the heat exchanger's energy and the energy of the coil and tank is great. The reason for this can be the fact that the thermocouples at the in- and outlet of the plate heat exchanger are newly bought thermocouples which are not calibrated. The read-out values of those thermocouples can have an offset in comparison with the older thermocouples in the tank and the older thermocouples at the in- and outlet of the heater. This can also be the result of the tank thermocouples that are calibrated based on the thermocouple at the inlet of the coil, which is not calibrated and because the heat loss between the coils' outlet and plate heat exchanger's inlet is unknown and is thus not deducted from the new thermocouple values after performing linear regression.

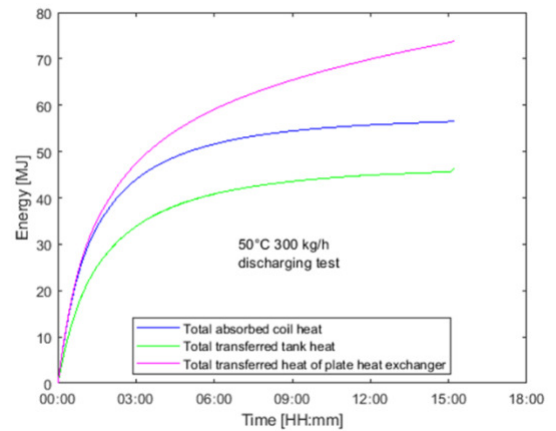


Figure 9: Coil and plate heat exchanger energies of the 50°C 300 kg/h discharging test.

The energy fraction of the 50°C 300 kg/h discharging test increases at a fast rate in the beginning of the test and increases slower at the end as can be seen in Figure 10.

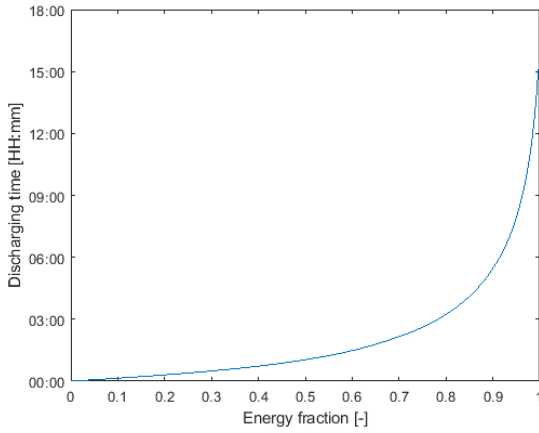


Figure 10: Discharging time of 50° 300 kg/h discharging test.

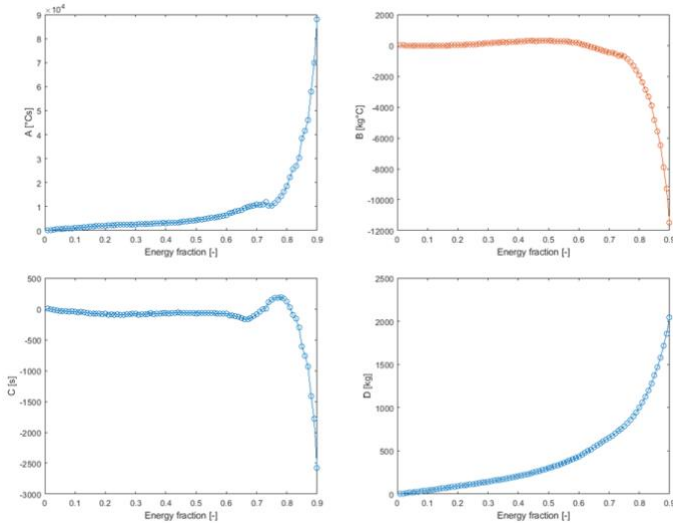


Figure 11: Correlation parameters for the discharging time.

The correlation parameters in function of the energy fraction are given in Figure 11. The predicted total energy $\alpha(t)\Delta U$ and the stored coil energy Q_c of the 50°C 300 kg/h discharging test is displayed in Figure 12. The reason why the total predicted energy is lower than the stored coil energy can be the heat loss to the environment.

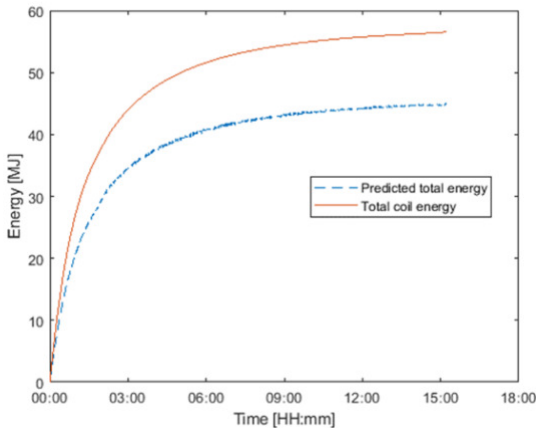


Figure 12: Predicted integrated efflux of energy and the stored coil energy of the 50°C 300 kg/h discharging test.

CONCLUSION

A previously built set-up is expanded with, among other things, a cold circuit to perform charging and discharging tests. These tests were made to verify if the CTEF method is applicable for a STES heat exchanger. Twelve tests were performed with each another heat transfer fluid inlet temperature and/or at a different flow rate. The energy fraction as a function of time is fitted between zero and one. The correlation parameters for the charging and discharging test are found. A difference exist between the predicted integrated efflux of energy and the stored coil energy, but this thesis did not predict the outlet temperature of the experiments.

REFERENCES

- [1] I. Dinçer and M. (Marc A.) Rosen, “Thermal energy storage systems and applications”, Accessed: Jan. 10, 2023. [Online]. Available: https://books.google.com/books/about/Thermal_Energy_Storage.html?hl=nl&id=4SY9EAAAQBAJ
- [2] P. Arce, M. Medrano, A. Gil, E. Oró, and L. F. Cabeza, “Overview of thermal energy storage (TES) potential energy savings and climate change mitigation in Spain and Europe,” *Appl Energy*, vol. 88, no. 8, pp. 2764–2774, Aug. 2011, doi: 10.1016/J.APENERGY.2011.01.067.
- [3] W. Beyne, K. Couvreur, I. T’ Jollyn, R. Tassenoy, S. Lecompte, and M. De Paepe, “A charging time energy fraction method for evaluating the performance of a latent thermal energy storage heat exchanger,” *Appl Therm Eng*, vol. 195, Aug. 2021, doi: 10.1016/j.applthermaleng.2021.117068.
- [4] S. Danehkar and H. Yousefi, “A comprehensive overview on water-based energy storage systems for solar applications,” *Energy Reports*, vol. 8, Elsevier Ltd, pp. 8777–8797, Nov. 01, 2022. doi: 10.1016/j.egy.2022.06.057.
- [5] S. Martinez Fernandez De Cordova, “Thermal analysis and comparison of a metal helical coil heat exchanger and its plastic alternative for a domestic water storage tank.”

EXPERIMENTELE KARAKTERISERING VAN EEN ZONNEBOILER ALS EEN VOELBARE THERMISCHE ENERGIEOPSLAG

Sophie Vercammen, Ir. Wito Plas, Maité Goderis, Dr. ir. Wim Beyne, Prof. dr. ir. Michel De Paepe
Vakgroep Elektromechanica, Systeem- en Metaalengineering
Universiteit Gent
Sint-Pietersnieuwstraat 41 – B9000 Gent – België
E-mail: sophie.vercammen@ugent.be

ABSTRACT

De *charging time energy fraction (CTEF) method* is een benadering om de uitlaattoestand van een warmtewisselaar met latente thermische energieopslag te karakteriseren. Gangbare ontwerpmethoden voor latente en voelbare warmtewisselaars, zoals de *logarithmic mean temperature difference (LMTD)* en de *effectiveness number of transfer units (e-NTU)* methode, zijn niet direct toepasbaar, aangezien ze zijn gebaseerd op de aanname van een warmtewisselaar in evenwichtstoestand. Een latente en voelbare warmtewisselaar werken echter niet in evenwichtstoestand. In dit artikel wordt onderzocht of de *charging time energy fraction method* kan worden toegepast op een voelbaar (*thermal energy storage*) TES-systeem. Het is belangrijk om de uitlaattoestand van de warmtedrager als functie van de tijd van deze systemen te kunnen voorspellen, niet alleen omdat het een opkomende toepassing is in huishoudens, maar ook omdat voelbare TES-systemen in combinatie met een watertank de goedkoopste en meest gebruikte vorm van TES zijn. Om dit te onderzoeken is er geëxperimenteerd met een zonneboiler. Voor het laden en ontladen gebruik gemaakt van het reeds gebouwde warme circuit en is het koude circuit herontworpen en gesloten. Zes laad- en zes ontladtesten worden uitgevoerd met temperaturen variërend van 30°C tot 50°C bij debieten variërend van 150 kg/h tot 450 kg/h. Daarna wordt de energiefractie in functie van de tijd tussen nul en één geplot en worden de correlatieparameters voor laadtijd en ontladtijd gevonden. Er bestaat een verschil tussen de voorspelde geïntegreerde efflux van energie en de opgeslagen wikkelingenergie, maar dit proefschrift voorspelde geen uitlaattemperatuur van de experimenten.

INTRODUCTIE

De toenemende wereldbevolking in combinatie met het wereldwijd stijgende energieverbruik en daarmee ook de zorgen over milieueffecten, dwingt landen tot aanpassing van hun manier van energieverbruik en -productie. Zonne-, biomassa-, wind- en waterkrachtbronnen worden over de hele wereld steeds vaker toegepast. Deze energiebronnen zijn echter sterk

NOMENCLATUUR

Q	[J]	Warmte
U	[J]	Interne energie van het opslagmateriaal
H	[kJ/kg]	Enthalpie van warmteoverdrachtsvloeistof
c_p	[J/°C]	warmtecapaciteit
T	[°C]	Temperatuur
t	[s]	Tijd
\dot{m}	[kg/s]	Massadebiet
V	[m ³]	Volume

Speciale karakter		
α	[-]	Energiefractieverhouding

Subscripts		
f		Netto uitstroom
o		Uitgaande
i		Ingaande
c		wikkelingen
t		Tank
max		Maximum
h		Verwarming
cv		Controle volume
m		gemiddeld
ch		laden
av		gemiddeld

fluctuerend en hebben daarom effectieve energieopslagsystemen nodig [1]. Om de samenleving te voorzien van een efficiënter, milieuvriendelijker energieverbruik bij het verwarmen en koelen van gebouwen, bij ruimtevaartenergie en bij nutsvoorzieningen, is een systeem voor thermische energieopslag (*thermal energy storage TES*) een geweldig hulpmiddel. Doordat een TES-installatie gebruik maakt van natuurlijke hulpbronnen en restwarmte, vermindert dat het totale energieverbruik, dus het verbruik van fossiele brandstoffen en kostbare olie-importen [1], [2].

De definitie van thermische energieopslag is energiebehoud op uur-, dag-, week-, occasionele of seizoensbasis van hoge- of lagetemperatuurenergie voor later gebruik en dit door verwarming, koeling, verdamping, stolling of vloeibaar maken van een materiaal of door thermochemische reacties. De

opgeslagen energie wordt omgezet in warmte of koelte door het proces om te keren.

TES kan worden gebruikt voor water- en (nacht)ruimteverwarming, koeling en airconditioning. Zo kan zomer- of afvalwarmte worden gebruikt voor gebruik in de winter, kan winterijs worden gebruikt voor ruimtekoeling in de zomer en kan de elektrisch opgewekte warmte of koude tijdens de daluren worden gebruikt tijdens de daaropvolgende piekvraaguren. Koeling-TES gebruikt water, ijs of een eutectische zoutoplossing als opslagmateriaal. Het is gunstig voor nieuwe gebouwen met grote koellasten overdag en geen koellasten 's nachts. TES-installaties worden ook gebruikt om het piekverbruik van elektriciteit te verschuiven naar een tijdstip waarop er veel zonnestraling beschikbaar is. Dit reduceert de piekvraag naar elektriciteit en resulteert in kosteneffectiviteit voor de consument, alleen als er gebruikstijdtarieven bestaan.

Er zijn veel manieren om TES-systemen te classificeren. Een daarvan ziet TES als een spectrum, waar aan de ene kant seizoensopslag is en aan de andere kant opslag per uur. Een andere manier om TES-systemen te classificeren, is ze op te splitsen in drie typen: voelbare thermische energieopslag (*sensible TES*, *STES*), latente thermische energieopslag (latente TES, *LTES*) en thermochemische energieopslag. Bij *STES* verandert de temperatuur van het opslagmedium als er warmte wordt toegevoegd/afgeleid, dit in tegenstelling tot een latente TES waarbij het opslagmateriaal wel een faseverandering ondergaat.

In deze scriptie wordt een zonneboiler met daarin polymeerwikkelingen gebruikt. Het is een voorbeeld van een voelbaar opslagsysteem voor warm water op zonne-energie. Zonne-energie wordt gebruikt om het tankwater op te warmen voor later gebruik. De energie komt van zonnestraling, wordt geabsorbeerd door collectoren en wordt direct of indirect naar de watertank getransporteerd. Hierdoor stijgt de temperatuur van het water zonder faseverandering, waarna de consument deze gevraagde warmte kan gebruiken om in zijn basisbehoefte te voorzien. Opslag van deze zonne-energie is absoluut noodzakelijk omdat zonne-energie en warmtevraag niet altijd tegelijkertijd optreden [1].

Voor het karakteriseren van warmtewisselaars bestaan al vele methoden, zoals de e-NTU en de LMTD methode. Deze methoden zijn echter gebaseerd op de aanname van een warmtewisselaar in evenwichtstoestand, terwijl *LTES*- en *STES*-warmtewisselaars niet in evenwichtstoestand werken. Dit is de reden waarom Beyne et al [3] onlangs een nieuwe methode hebben ontwikkeld om TES-systemen kwantitatief te bestuderen: de CTEF-methode. Voorspelling van de uitlaatstatus als functie van de tijd is het belangrijkste voordeel van de CTEFM (CTEF-methode).

Deze CTEF-methode wordt nog niet gebruikt op een *STES*-systeem. Het is belangrijk om de uitlaattoestand als functie van de tijd van deze systemen te kunnen voorspellen, niet alleen omdat het een opkomende toepassing is in huishoudens, maar ook omdat *STES*-systemen in combinatie met een watertank de goedkoopste en meest gebruikte soort TES zijn [4].

Het doel van deze masterproef is om dit CTEF-model toe te passen voor een *STES*-systeem door middel van laad- en ontladtesten. Het voorspellen van de watertemperatuur aan de

uitlaat van de wikkelingen wordt gedaan door de energiefractiefunctie $\alpha(t)$ te correleren. Dit is de geïntegreerde energie-uitstroom $Q_f(t)$ gedeeld door de maximale geïntegreerde energie-uitstroom $\max Q_f$, zoals te zien is in Vgl. (12) [3].

$$\alpha(t) = \frac{Q_f(t)}{\max Q_f} \quad (12)$$

De netto uitstroom van energie $\dot{Q}_f(t)$ kan worden gecorreleerd in plaats van de uitlaattoestand. Hiervoor moeten ook de inlaattoestand en dus het massadebiet en de inlaatwatertemperatuur bekend en constant te gebruiken zijn, zie Vgl. (13).

$$\dot{Q}_f = \dot{m}(h_o - h_i) \quad (13)$$

METHODOLOGIE

Experimentele opstelling

De oude opstelling bestond uit een gesloten warm en een open koud circuit aangesloten op de zonneboiler. Figure 13 toont de huidige proefopstelling bestaande uit een gesloten warm circuit (in rood), een gesloten koud circuit (in blauw), een chillercircuit (in groen) en een zonneboiler (in paars). Om de experimenten voor deze masterproef te doen, is het koude circuit herontworpen en gesloten. Met het nieuwe gesloten koude circuit wordt er geen water verspild door telkens hetzelfde water te gebruiken voor de testen en wordt er geen warm water geloosd in de riool. Er zijn verschillende mechanische driewegkogelkranen met "T"-poort om de richting van de waterstroom te regelen en er is een lus naar de koelmachine toegevoegd aan de opstelling.

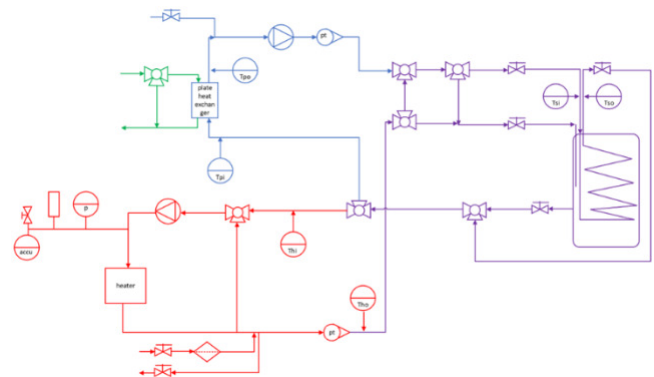


Figure 13: Opstelling van de zonneboiler.

Op deze opstelling worden laad- en ontladexperimenten uitgevoerd en wordt de CTEFM toegepast. Voor de laad- en ontladtest zijn aparte circuits nodig. Omdat er geen collectoren in de opstelling aanwezig zijn, wordt er gebruik gemaakt van een heater. Voor de laadtest levert de verwarmers in het hete circuit een constante temperatuur aan het water dat in de tank stroomt (warmtedrager). De heater zorgt er ook voor dat er voorafgaand aan de ontladtesten een voldoende hoge tanktemperatuur wordt bereikt. Wanneer het tankwater de juiste temperatuur heeft, garanderen het koude- en chillercircuit een constante koude inlaattemperatuur in de batterij tijdens de ontladtest.

Ontwerp van de zonneboiler

De zonneboiler is een open, drukloze ROTEX Sanitube INOX wateropslagtank. In de tank bevindt zich een gegolfde spiraalvormige wikkeling gemaakt van verknoopt polyethyleen (PEX) met een aluminiumlaag in een polymeermatrix. Deze wikkeling bevindt zich in het midden van de tank en bestaat uit twee parallelle spiraalvormige spoelen van 51 en 46 m. De totale lengte van de wikkelingen is 97 m. De buitendiameter van de buis van de wikkeling zelf is 32 mm en de wand heeft een dikte van 2 mm [5]. De binnenmaat van de zonneboiler is 138,5 x 48 x 48 cm. De ketel heeft een inhoud van 300 l en heeft een dubbelwandige mantel van polypropyleen met warmte-isolatie van PUR-hardschuim [5].

Een buis, waar thermokoppels in zijn geplaatst, is verbonden met het deksel van de tank. Alle thermokoppels in het circuit zijn K-type thermokoppels. Er zitten zes thermokoppels in het circuit: voor en na de platenwarmtewisselaar, voor de driewegklep in het warme circuit, na de hete massadebietmeter (dus voor en na de heater) en aan de in- en uitgang van de wikkelingen. Er zijn 11 werkende thermokoppels in de tankbuis. Het bovenste thermokoppel wordt net onder het waterniveau geplaatst. Alle thermokoppels zijn geplaatst met een verticale afstand van 15 mm van elkaar. De tank is verdeeld in acht controlevolumes met elk een of twee thermokoppels, zoals te zien is in Figure 14.

	• T_8
T_{11}	• T_7
	• T_6
	• T_5
T_{10}	• T_4
	• T_3
T_9	• T_1
	• T_0

Figure 14: Control volumes of the tank.

Meetprocedure

Oplaadtesten

Om bij elk experiment uniforme omstandigheden te hebben, moet de tank voorafgaand aan elk experiment worden geïnitieerd om aan de inlaatvoorwaarden te voldoen. De test wordt gestart wanneer het tankwater een temperatuur heeft van maximum 20°C, de inlaat van de wikkeling een constante temperatuur heeft van 30, 40 of 50°C en het massadebiet van de warmtedrager 150, 300 of 450 kg/h blijft, zoals samengevat in Table 5.

	30°C	40°C	50°C
150 kg/h	X	X	X
300 kg/h	X	X	
450 kg/h	X		

Table 5: Matrix van de oplaadtesten.

De test wordt gestopt wanneer het verschil tussen de inlaat- en uitlaattemperatuur van de wikkelingen gelijk blijft. Het schema van een laadtest wordt weergegeven in Figure 15.

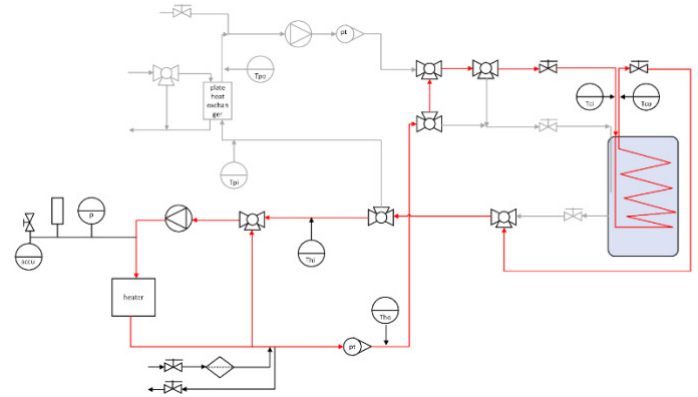


Figure 15: Schema van de zonneboileropstelling tijdens het opladen.

Ontlaadtesten

Om in elk experiment uniforme omstandigheden te hebben, moet de tank ook voorafgaand aan elk ontladexperiment worden geïnitieerd om aan de inlaatvoorwaarden te voldoen. De procedure van een ontladtest is als volgt: het water aan de inlaat van de wikkelingen moet een constante temperatuur hebben van 20°C en het water in de tank moet een temperatuur hebben van 30 of 50°C. De massadebietten zijn 300, 450 en 600 kg/h, zoals samengevat in Table 6. Een schema van een ontladtest wordt weergegeven in Figure 16.

	30°C	50°C
300 kg/h	X	X
450 kg/h	X	X
600 kg/h	X	X

Table 6: Matrix van de ontladtesten.

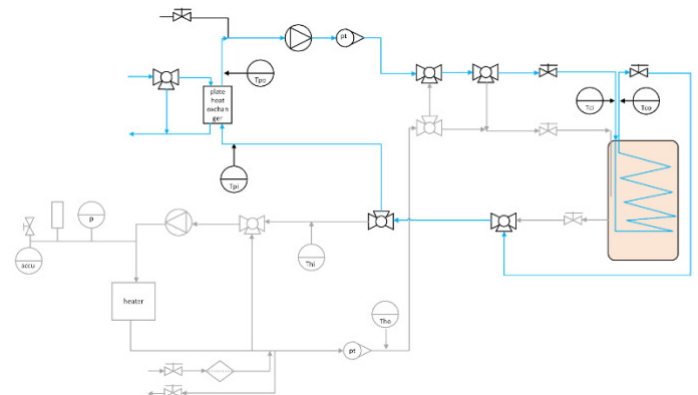


Figure 16: Schema van de zonneboileropstelling tijdens ontladen.

Datareductie

Zowel voor de laadtesten als voor de ontladtesten moet de energiebalans correct zijn als het warmteverlies naar de omgeving wordt verwaarloosd, zoals te zien is in Vgl. (14).

$$\begin{aligned}
Q_c(t) &= \dot{m}_c c_{p,c,av} (T_{co}(t) - T_{ci}(t)) \cdot \Delta t_{5s} \\
&= \sum_{k=cv0}^{cv8} \rho_k V_k c_{p,t,av} (T_k(t + \Delta t_{5s}) - T_k(t)) \\
&= Q_t(t)
\end{aligned} \tag{14}$$

$$\begin{aligned}
Q_{stored} &= Q_{previous} + Q_{new} \\
&= Q_{previous} + \dot{m}_c c_{p,c,av} (T_{co}(t) - T_{ci}(t)) \cdot \Delta t_{5s}
\end{aligned} \tag{15}$$

$$Q_{stored,coils}(t) = \sum_{i=0}^t \dot{m}_c c_{p,c,av} (T_{co}(i) - T_{ci}(i)) * \Delta t_{5s} \tag{16}$$

$$Q_{stored,tank}(t) = \sum_{i=0}^t \sum_{k=cv0}^{cv8} \rho_k V_k c_{p,t,av} (T_k(i + \Delta t_{5s}) - T_k(i)) \tag{17}$$

De thermokoppels meten elke vijf seconden de temperatuur. Om de afgeleide in de tijd van de interne energie te discretiseren, wordt het verschil van de interne energieën per keer, $t + \Delta t$ en t gedeeld door de verstreken tijd tussen deze twee metingen, Δt . Q_c is de hoeveelheid energie die op een bepaald moment t wordt overgedragen van de wikkelingen naar het tankwater. Q_t is de hoeveelheid energie die op elk moment t aan het tankwater wordt toegevoegd, toegevoegd in een willekeurig tijdsinterval Δt . Om de totale opgeslagen energie te krijgen, moeten deze waarden daarom voor elke tijdsperiode worden berekend en bij de vorige waarde worden opgeteld, zoals weergegeven in Vgl. (15).

Deze waarden zijn dus een geïntegreerde waarde. Vgl. (16) en (17) tonen de opgeslagen hoeveelheid warmte in respectievelijk de wikkelingen en de tank op een bepaald moment.

Het is nu mogelijk om de energie die aan de tank wordt geleverd te berekenen door de linkerkant van de vergelijking te gebruiken, maar ook door de rechterkant van de vergelijking te gebruiken. Als er geen of verwaarloosbare warmteverliezen aanwezig zijn, moeten beide gelijk zijn. Dit heet het sluiten van de energiebalans. Zowel de linkerkant als de rechterkant van de vergelijking kwantificeren een energie, uitgedrukt in Joules.

(18) is de formule om de energiefractie $\alpha(t)$ te berekenen.

$$\alpha(t) = \frac{Q_c(t)}{\max(Q_c)} \tag{18}$$

Vgl. (19) vertegenwoordigt de set van oplaadtijden $t_c(\alpha_i) \forall \alpha_i$ in α in Vgl. (18).

$$t_c(\alpha_i) \text{ voor dewelke } Q_c(t) = \alpha_i \max Q_c(t) \tag{19}$$

Als een oplaadtijdcorrelatie is aangebracht (vgl. (20)), dan zijn de correlatieparameters $p(\alpha_i)$ (Vgl. (21) en (22)) voor alle energiefracties α_i in de basisset α gekend.

$$t_c = \frac{Slope}{\Delta T} + Intercept \tag{20}$$

$$Slope = A(\alpha) + \frac{B(\alpha)}{\dot{m}} \tag{21}$$

$$Intercept = C(\alpha) + \frac{D(\alpha)}{\dot{m}} \tag{22}$$

RESULTATEN EN DISCUSSIE

Oplaattesten

De beginvoorwaarden voor elk experiment zijn een constant inlaatmassadebiet van de warmtedrager dat door de wikkelingen stroomt en een constante inlaattemperatuur. De begintemperatuur van de tank is 20°C. Om aan de beginvoorwaarden te voldoen, worden PID-regelaars in LabVIEW gebruikt. De gebruikte PI-parameters voor de verwarming en klep in het warme circuit zijn te vinden Table 7.

		30°C		40°C		50°C	
		Heater	Valve	Heater	Valve	Heater	Valve
150 kg/h	K _c [-]	0.6627	0.0182	0.6627	0.009	0.663	0.015
	T _i [min]	0.7952	0.2351	0.7952	0.488	0.795	0.235
300 kg/h	K _c [-]	0.6627	0.015	0.6627	0.015		
	T _i [min]	0.95	0.2351	0.7952	0.2351		
450 kg/h	K _c [-]	0.6627	0.007				
	T _i [min]	0.2351	0.125				

Table 7: PI-parameters van verwarmers en klep voor laadexperimenten.

Figure 17 laat zien dat de totale energie die vrijkomt door de wikkelingen en de verwarmers niet helemaal gelijk is. Het verschil is te wijten aan het warmteverlies aan de omgeving. De door het tankwater geabsorbeerde warmte overschrijdt de geleverde warmte door de wikkelingen aan het begin van de test, maar wordt tegen het einde ingehaald. Dit kan het gevolg zijn van de tankthermokoppels die zijn gekalibreerd op basis van het thermokoppel aan de inlaat van de wikkelingen, dat niet is gekalibreerd. Het kan ook zijn omdat het warmteverlies tussen de uitlaat van de verwarmers en de inlaat van de wikkelingen onbekend is en dus niet in mindering wordt gebracht op de nieuwe thermokoppelwaarden na lineaire regressie. De proeven met een massadebiet van 150 kg/uur laten hetzelfde patroon zien als de proeven met een massadebiet van 300 kg/uur.

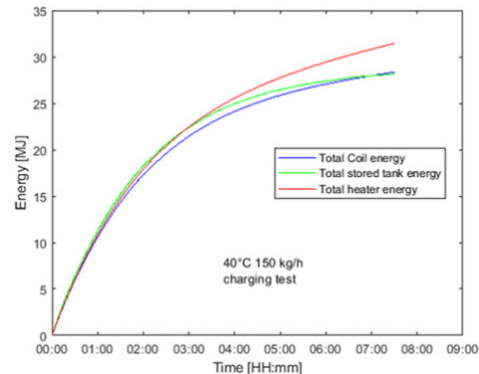


Figure 17: Energie van de wikkelingen, tank en verwarming voor de laadtest met een inlaattemperatuur van 40°C en een massastroom van 150 kg/u.

De oplaadtijd in functie van de energiefractie van de 30°C 450 kg/h test is weergegeven in Figure 18. Deze neemt snel toe in het begin van de test, maar vertraagt naar het einde toe.

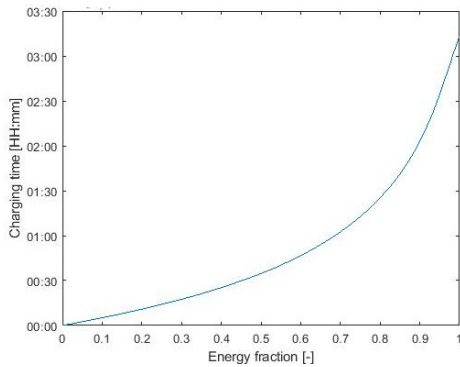


Figure 18: Energiefractiefunctie van de 30°C 450 kg/u oplaadttest.

Figure 19 toont de correlatieparameters voor alle energiefracties. $B(\alpha)$ is negatief, omdat de laadtijd van 300 kg/h in functie van $\frac{1}{\Delta T}$ sneller daalt dan de laadtijd van 150 kg/h in functie van $\frac{1}{\Delta T}$.

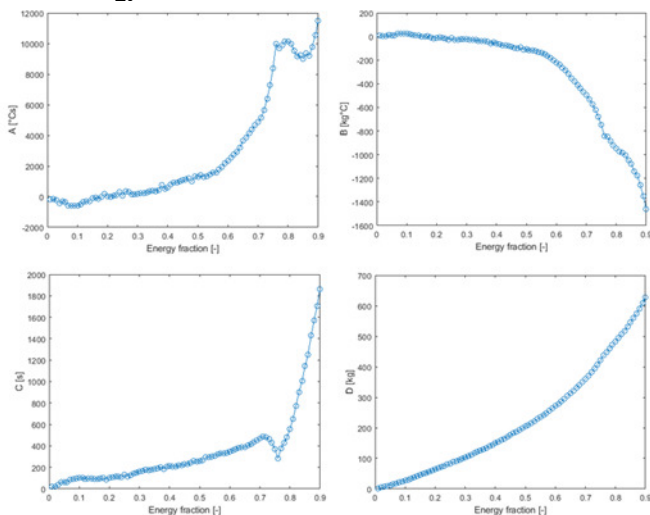


Figure 19: Correlatieparameters van de oplaadtijd.

De voorspelde totale energie $\alpha(t)\Delta U$ en de opgeslagen wikkelingenergie Q_c van de 50°C 150 kg/h test wordt weergegeven in Figure 20. De curven zijn bijna gelijk, maar niet volledig, omdat in $\alpha(t)\Delta U$ wordt aangenomen dat de gemiddelde tanktemperatuur na verloop van tijd exact gelijk zal zijn aan de inlaattemperatuur van de wikkelingen, maar dit gebeurt in werkelijkheid niet. Dus volgens $\alpha(t)\Delta U$, heeft de tank meer warmte opgenomen dan hij daadwerkelijk doet.

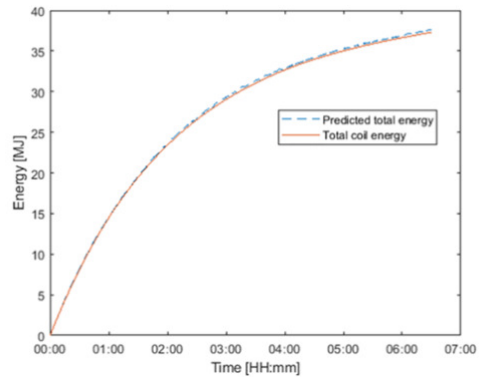


Figure 20: Voorspelde totale energie en de opgeslagen wikkelingenergie van de 50°C 150 kg/h laadttest.

Ontlaadttesten

De beginvoorwaarden voor elk ontladingsexperiment zijn een constant inlaatmassadebiet van de warmtedrager dat door de wikkelingen stroomt (300, 450 of 600 kg/u) en een constante inlaatspoeltemperatuur van 20°C. De tank is aanvankelijk 30°C of 50°C warm. De gebruikte PID-parameters voor de pomp in het koude circuit en de klep in het koelmachinecircuit zijn te vinden in Table 8.

		30°C		50°C	
		Pump	Valve	Pump	Valve
300 kg/h	K_c	0.003	-0.012	0.003	-0.035
	T_i [min]	0.068	0.189	0.068	0.063
	T_d [min]	0	0.029	0	0.017
450 kg/h	K_c	0.003	-0.035	0.003	-0.035
	T_i [min]	0.068	0.063	0.068	0.076
	T_d [min]	0	0.017	0	0.017
600 kg/h	K_c	0.003	-0.035	0.003	-0.004
	T_i [min]	0.068	0.063	0.057	0.120
	T_d [min]	0	0.017	0	0

Table 8: PID-parameters van de pomp en koelerklep voor de ontladingsexperimenten.

In Figure 21 worden de geabsorbeerde wikkelingwarmte, de warmte van de platenwarmtewisselaar en de overgedragen tankwarmte weergegeven voor een ontladingstest van 50°C en 300 kg/u. Het verschil in wikkeling- en tankenergie kan het gevolg zijn van warmteverlies naar de omgeving. Het verschil tussen de energie van de warmtewisselaar en de energie van de wikkelingen en tank is echter groot. De reden hiervoor kan zijn dat de thermokoppels aan de in- en uitlaat van de platenwarmtewisselaar nieuw gekochte thermokoppels zijn die niet gekalibreerd zijn en waarschijnlijk een offset bezitten tegenover de oudere thermokoppels in de tank en de oudere thermokoppels aan de binnenzijde. - en uitlaat van de verwarmers. Dit kan ook het gevolg zijn van de tankthermokoppels die zijn gekalibreerd op basis van het thermokoppel aan de ingang van de wikkelingen, dat niet is gekalibreerd en omdat het warmteverlies tussen de uitgang van de batterijen en de ingang van de platenwarmtewisselaar onbekend is en dus niet wordt afgetrokken van de nieuwe thermokoppelwaarden na lineaire regressie.

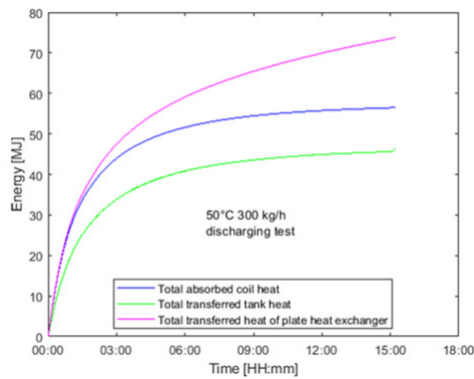


Figure 21: Energie van de spoel- en platenwarmtewisselaar van de 50°C 300 kg/h ontladingstest.

De energiefractie van de 50°C 300 kg/h ontladingstest neemt snel toe in het begin van de test en stijgt langzamer naar het einde toe, zoals te zien is in Figure 22.

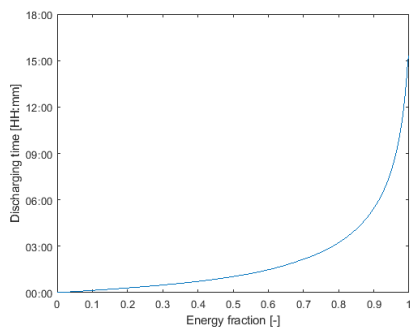


Figure 22: Ontlaadtijd van 50° 300 kg/u ontladingstest.

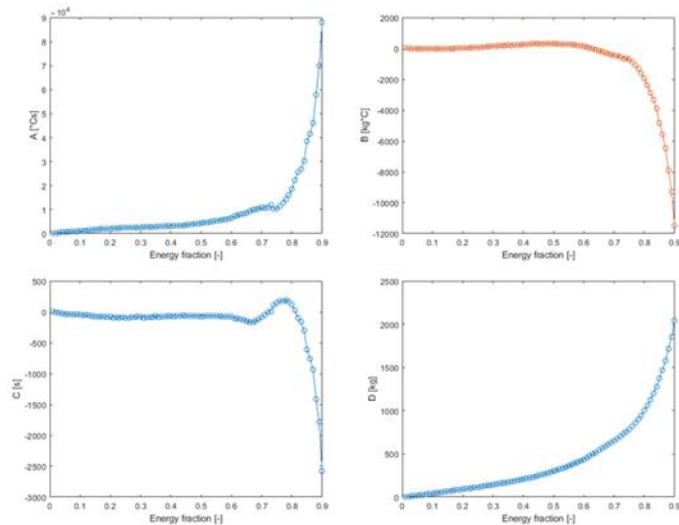


Figure 23: Correlatieparameters voor de ontladingstijd.

De correlatieparameters in functie van de energiefractie worden gegeven in Figure 23. De voorspelde totale energie $\alpha(t)\Delta U$ en de opgeslagen wikkelingenergie Q_c van de 50°C 300 kg/h ontlading test wordt weergegeven in Figure 24. De reden waarom de totale voorspelde energie lager is dan de opgeslagen wikkelingenergie kan het warmteverlies naar de omgeving zijn.

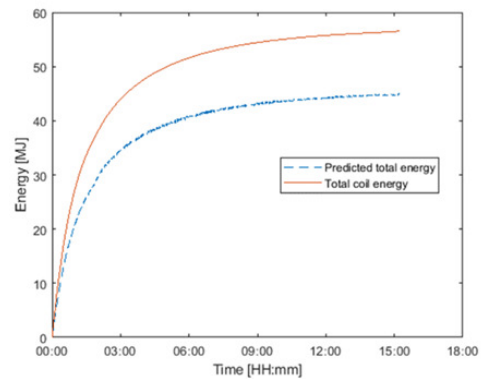


Figure 24: Voorspelde totale energie en de opgeslagen wikkelingenergie van de 50°C 300 kg/h ontladingstest.

CONCLUSIE

Een eerder gebouwde opstelling wordt uitgebreid met onder meer een koudcircuit om laad- en ontladingstesten uit te voeren. Deze testen zijn uitgevoerd om te verifiëren of de CTEF-methode toepasbaar is voor een STES warmtewisselaar. Twaalf testen zijn uitgevoerd met telkens een andere inlaattemperatuur van de warmtedrager en/of een ander debiet. De energiefractie als functie van de tijd wordt geplotted tussen nul en één. De correlatieparameters voor de laad- en ontladingstest zijn gevonden. Er bestaat een verschil tussen de voorspelde geïntegreerde efflux van energie en de opgeslagen wikkelingenergie, maar dit proefschrift voorspelde geen uitlaattemperatuur van de experimenten.

REFERETIES

- [1] I. Dinçer and M. (Marc A.) Rosen, "Thermal energy storage systems and applications", Accessed: Jan. 10, 2023. [Online]. Available: https://books.google.com/books/about/Thermal_Energy_Storage.html?hl=nl&id=4SY9EAAAQBAJ
- [2] P. Arce, M. Medrano, A. Gil, E. Oró, and L. F. Cabeza, "Overview of thermal energy storage (TES) potential energy savings and climate change mitigation in Spain and Europe," *Appl Energy*, vol. 88, no. 8, pp. 2764–2774, Aug. 2011, doi: 10.1016/J.APENERGY.2011.01.067.
- [3] W. Beyne, K. Couvreur, I. T' Jollyn, R. Tassenoy, S. Lecompte, and M. De Paepe, "A charging time energy fraction method for evaluating the performance of a latent thermal energy storage heat exchanger," *Appl Therm Eng*, vol. 195, Aug. 2021, doi: 10.1016/j.applthermaleng.2021.117068.
- [4] S. Daneshkar and H. Yousefi, "A comprehensive overview on water-based energy storage systems for solar applications," *Energy Reports*, vol. 8, Elsevier Ltd, pp. 8777–8797, Nov. 01, 2022, doi: 10.1016/j.egy.2022.06.057.
- [5] S. Martinez Fernandez De Cordova, "Thermal analysis and comparison of a metal helical coil heat exchanger and its plastic alternative for a domestic water storage tank."

CONTENTS

1	Introduction	1
2	Literature study	2
2.1	Introduction	2
2.2	Thermal energy storage	3
2.2.1	Commonly used TES applications	3
2.3	Thermal energy storage classification	6
2.4	Sensible thermal energy storage	8
2.5	Solar energy and thermal energy storage	10
2.6	The solar boiler	11
2.7	Existing characterization methods of sensible solar thermal energy systems	12
2.7.1	Modeling strategies for sensible heat thermal energy recovery	12
2.7.2	Experimental investigation of heat dispatch controllability	13
2.7.3	Experimental evaluation and improvements of a diode solar water heater	14
2.8	Problem statement	17
2.9	Charging time energy fraction method	18
3	Materials and methods	22
3.1	Experimental set-up	22
3.2	Overview of components	24
3.2.1	Solar boiler	24
3.2.2	Hot circuit	26
3.2.3	Cold circuit and chiller circuit	27
3.2.4	Thermocouples	30
3.2.5	National Instrument Data Acquisition System	32
3.3	LabVIEW program	34
3.4	Measurement procedure	41
3.4.1	Accuracies	41
3.4.2	Charging tests	41
3.4.3	Discharging tests	44
3.5	Data reduction	47
4	Results and discussion	51
4.1	Linear regression	51
4.2	Charging tests	52
4.2.1	Initial conditions	52

4.2.2	Model calibration	52
4.2.3	Model evaluation	62
4.3	Discharging tests	64
4.3.1	Initial conditions	64
4.3.2	Model calibration	66
4.3.3	Model evaluation	72
5	Conclusion	74
	Sustainability reflection	75
	References	77
	Appendices	83

LIST OF FIGURES

Figure 1: Set-up of the solar boiler.....	5
Figure 2: Control volumes of the tank.....	6
Figure 3: Scheme of solar boiler set-up during charging.....	6
Figure 4: Scheme of solar boiler set-up during discharging.....	6
Figure 5: Energies of coils, tank and heater for the charging test with an inlet temperature of 40°C and mass flow 150 kg/h.....	7
Figure 6: Energy fraction function of the 30°C 450 kg/h charging test.....	7
Figure 7: Correlation parameters of the charging time.....	8
Figure 8: Predicted integrated efflux of energy and the stored coil energy of the 50°C 150 kg/h charging test.....	8
.....	8
Figure 9: Coil and plate heat exchanger energies of the 50°C 300 kg/h discharging test.....	8
Figure 10: Discharging time of 50° 300 kg/h discharging test.....	9
Figure 11: Correlation parameters for the discharging time.....	9
Figure 12: Predicted integrated efflux of energy and the stored coil energy of the 50°C 300 kg/h discharging test.....	9
.....	9
Figure 13: Opstelling van de zonneboiler.....	11
Figure 14: Control volumes of the tank.....	12
Figure 15: Schema van de zonneboileropstelling tijdens het opladen.....	12
Figure 16: Schema van de zonneboileropstelling tijdens ontladen.....	12
Figure 17: Energie van de wikkelingen, tank en verwarming voor de laadtest met een inlaattemperatuur van 40°C en een massastroom van 150 kg/u.....	13
Figure 18: Energiefractiefunctie van de 30°C 450 kg/u oplaadtest.....	14
Figure 19: Correlatieparameters van de oplaadtijd.....	14
Figure 20: Voorspelde totale energie en de opgeslagen wikkelingenergie van de 50°C 150 kg/h laadtest.....	14
.....	14
Figure 21: Energie van de spoel- en platenwarmtewisselaar van de 50°C 300 kg/h ontladingstest.....	15
Figure 22: Ontlaadtijd van 50° 300 kg/u ontladtest.....	15
Figure 23: Correlatieparameters voor de ontladtijd.....	15
Figure 24: Voorspelde totale energie en de opgeslagen wikkelingenergie van de 50°C 300 kg/h ontladtest.....	15
.....	15
Figure 25: Storage tank in Uden to preserve summer heat [14].....	3
Figure 26: Residual load curve for Belgium for 2020 and 2030 [19].....	4
Figure 27: Demand-side management programs aiming at peak clipping (lopping), valley filling, load shifting and strategic conservation [21].....	5
Figure 28: Different types of TES systems with all possible storage materials [30].....	6
Figure 29: (a) highly stratified; (b) moderately stratified; (c) fully mixed storage tank [17].....	9
Figure 30: Dead zone in a water tank (a) large dead zones (b) small dead zones [44].....	9
Figure 31: A simple schematic of the experimental setup of the fixed beds [63].....	13
Figure 32: Experimental set-up of the vertically aligned cylindrical TES tank [64].....	14
Figure 33: Schematic diagram of solar simulation test facility [66].....	15
Figure 34: LTES heat exchanger as a control volume [3].....	18
Figure 35: Current set-up of the solar boiler.....	22
Figure 36: Scheme of solar boiler set-up with in green the newly bought components.....	24
Figure 37: Plastic coil inside solar boiler.....	25

Figure 38: Thermocouples in lid of tank.....	26
Figure 39: Comparison of the heat transfer rate for different mass flow rates at 60°C [5].	28
Figure 40: Scheme of cold circuit with components where the biggest pressure losses occur.	29
Figure 41: Scheme of chiller flow and the split-up at the mixing valve.	30
Figure 42: Thermocouples in lid of tank.	31
Figure 43: Control volumes of the tank.	32
Figure 44: Cluster of numeric temperature indicators.....	34
Figure 45: DAQ Assistant generating current or voltage.	35
Figure 46: DAQ assistant who measures current.	36
Figure 47: DAQ assistant who measures temperature with thermocouple.	37
Figure 48: DAQ assistant who generates a digital sample.	38
Figure 49: PID VI of heater in a true/false case structure.	40
Figure 50: Cooling the tank water.	42
Figure 51: Preparations of the charging test: bringing the tank water to a constant temperature.....	43
Figure 52: Scheme of solar boiler set-up during charging.	44
Figure 53: Heating up the tank.	45
Figure 54: Scheme of solar boiler set-up during discharging.	46
Figure 55: Simplified scheme of solar boiler as control volume.	47
Figure 56: Control volumes of the tank.	48
Figure 57: Linear regression on thermocouple 11.	51
Figure 58: 300 kg/h mass flow rate of the 30° charging test.....	52
Figure 59: Temperatures of 30°C 300 kg/h charging test.	53
Figure 60: Total energies of coils, tank and heater of a) the charging test with an inlet temperature of 40°C and mass flow of 150 kg/h b) the 40°C 300 kg/h charging test c) the 30°C 150 kg/h charging test d) the 30°C 300 kg/h charging test and e) the 30°C 450 kg/h charging test.	57
Figure 61: Energy fraction function of the 30°C 450 kg/h charging test.	58
Figure 62: Charging times of 300 kg/h and 150 kg/h charging tests in function of 1/ΔT for α = 0.2.	59
Figure 63: Slope of charging time for alfa = 0.2 in function of 1/(mass flow).....	60
Figure 64: Intersect of charging time for alfa = 0.2 in function of 1/(mass flow).	60
Figure 65: Correlation parameters for alle six charging tests.	61
Figure 66: Correlation parameter C for all six charging tests from alfa = 0.01 till alfa = 0.99.	62
Figure 67: Predicted total energy and the stored coil energy of the 50°C 150 kg/h charging test.	63
Figure 68: 300 kg/h mass flow rate of the 30°C discharging test.	64
Figure 69: Temperatures of set-up during 50°C 300 kg/h discharging test.	65
Figure 70: Tank temperatures of the 50°C 300 kg/h discharging test as a function of tank height after six hours.....	66
Figure 71: Total stored energies of the 50°C a) 300 kg/h discharging test b) 450 kg/h discharging test and c) 600 kg/h discharging test.	69
Figure 72: Discharging time of 50° 300 kg/h discharging test.	69
Figure 73: Discharging time functions for mass flow rates 300, 450 and 600 kg/h for an alfa = 0.20.....	70
Figure 74: Slope curve of discharging time for an alfa = 0.20.	71
Figure 75: Intersect of discharging time for alfa = 0.20.....	71
Figure 76: Correlation parameters for the discharging time.	72
Figure 77: Predicted integrated efflux of energy and the stored coil energy of the 50°C 300 kg/h discharging test.....	73
Figure 78: Sustainable development goals [82].	75

Figure 79: Coil, tank and heater energy of the 30°C 450 kg/h charging test.....	101
Figure 80: Relative difference between coil and tank energy of 30°C 450 kg/h charging test.	101

LIST OF TABLES

Table 1: Charging test matrix.	6
Table 2: Discharging test matrix.	6
Table 3: PI parameters of heater and valve for charging experiments.	7
Table 4: PID parameters of the pump and chiller valve for the discharging experiments.	8
Table 5: Matrix van de oplaadtesten.	12
Table 6: Matrix van de ontladtesten.	12
Table 7: PI-parameters van verwarmers en kleppen voor laadexperimenten.	13
Table 8: PID-parameters van de pomp en koelerskleppen voor de ontladingsexperimenten.	14
Table 9: Legend of Figure 35.	23
Table 10: NI DAQ modules with their inputs and outputs.	33
Table 11: PI parameters for control variables, calculated by the Tunerfile.	39
Table 12: measurement equipment and their accuracies.	41
Table 13: Charging test matrix.	41
Table 14: Discharging test matrix.	45
Table 15: PI parameters of heater and valve for charging experiments.	52
Table 16: PID parameters of the pump and chiller valve for the discharging experiments.	64
Table 17: Uncertainty range for the results.	102

LIST OF ABBREVIATIONS AND SYMBOLS

Abbreviation	Description
CTEF	Charging time energy fraction
CTEFM	Charging time energy fraction method
LMTD	Logarithmic mean temperature difference
e-NTU	Effectiveness number of the transfer units
TES	Thermal energy storage
STES	Sensible thermal energy storage
LTES	Latent thermal energy storage
HTF	Heat transfer fluid
PID	Proportional integral derivative
PI	Proportional integral
TESS	Thermal energy storage systems
GHG	Greenhouse gas
PCM	Phase change material
SIM	Super insulating material
ICSSWH	Integrated collector storage solar water
ICS	Integrated collector storage

Symbol	Unit	Description
Q_c	J	Transferred coil heat
U	J	Internal energy of the storage material
H	J/kg	Enthalpy of heat transfer fluid
$c_{p,c,av}$	J/°C	Average heat capacity of the HTF
T_{co}	°C	Temperature at outlet of coils
t	S	Time
M	Kg	Mass
\dot{m}_c	Kg/s	Mass flow rate through the coils
V	m ³	Volume
α	-	Energy fraction ratio
Q_f	J	Integrated efflux of energy
$c_{p,t,av}$	J/°C	Average heat capacity of tank water
T_{ci}	°C	Temperature at inlet of coils
$Q_{total,c}$	J	Total transferred coil heat
$Q_{total,t}$	J	Total transferred tank heat
t_c	s	Charging time
t_d	s	Discharging time
Q_f	J	Integrated efflux of energy
\dot{Q}_f	W	Net efflux of energy

1 INTRODUCTION

In 2021, countries of the European Union (EU) and the European Parliament approved the proposal from the Commission to enshrine in legislation the EU's political commitment to be climate neutral by 2050 [6]. Because of the increasing atmospheric concentration of greenhouse gases (GHG's), more and more heat from the earth's surface gets trapped by the atmosphere, resulting in an increase of the earth's temperature of about 1°C since 1900 [6]. Countries around the world are adapting their way of using and producing energy by using more and more natural energy sources, such as solar energy, biomass, wind and hydropower. Because these energy sources fluctuate strongly, they need effective energy storage systems [6]. A thermal energy storage (TES) system is a great tool for this. A TES system minimizes the overall energy consumption and, as a result, the usage of fossil fuels and pricey oil imports by using waste heat and natural resources [1], [7].

TES can be classified in sensible TES, latent TES and thermochemical TES. The solar boiler described in this thesis is an example of sensible TES, namely a sensible hot water storage system. It is a device that is mainly used in households to store solar heat into a water tank where it can be used on a later time. It is thus an example of a sensible heat exchanger.

Many methods already exist for characterizing heat exchangers, such as the e-NTU and the LMTD method. However, these methods are based on the assumption of steady state heat exchanger, while LTES and STES heat exchangers do not operate in steady state. Therefore, Beyne et al. [3] recently developed a new method to quantitatively study TES systems: the charging time energy fraction (CTEF) method. The prediction of the exhaust condition as a function of time is the main advantage of the CTEFM (CTEF method).

The aim of this master thesis is to apply this CTEF model for a STES system through charge and discharge tests. Predicting the water temperature at the outlet of the coils inside the solar boiler is done by correlating the energy fraction function $\alpha(t)$. This is the integrated energy outflow divided by the maximum integrated energy outflow. This is done by performing six charging and six discharging experiments with each another heat transfer fluid (HTF) inlet temperature and at different flow rates.

The next chapter of this thesis provides an overview of the literature on TES, solar energy in combination with TES and the solar boiler. Also, recent characterization methods for sensible TES systems are explained and the CTEFM is fully explained. Chapter 3 discusses the research method in which the entire set-up is reviewed. The preparation of the tests, the tests themselves and the data reduction after testing are also explained. Subsequently, chapter 4 describes the data analysis and its results. Finally, in chapter 5 the conclusion is presented.

2 LITERATURE STUDY

In this chapter a literature review is performed to highlight the importance of the current study and to provide an overview of the current state-of-the-art.

2.1 Introduction

First, a short introduction is given why thermal energy storage systems (TESS) became more and more important.

In 2021, the countries of the European Union (EU) and the European Parliament approved the Commission's proposal to legislate the EU's political commitment to be climate neutral by 2050 [6]. Because of the increasing atmospheric concentration of greenhouse gases (GHG's), more and more heat from the earth's surface gets trapped by the atmosphere. The temperature of the earth has risen about 1°C since 1900 [6]. Carbon dioxide, methane, nitrous oxide, fluorinated gases, and water vapor are the five most significant gases that cause global warming via the greenhouse effect [1], [8].

The world's increasing population combined with the world's rising energy consumption and thus also the concerns about environmental impacts, forces countries to adjust their way of energy use and production. Solar, biomass, wind, and hydroelectric energy sources are more and more implemented in the infrastructure of countries all over the world. These energy sources, however, highly fluctuate and need as such effective energy storage systems [1]. Pumped Storage Hydropower, biobased carbon nanomaterials and wind power storage plants are examples of energy storage systems for these energy sources [9]–[11].

To provide society with more efficient, environmentally friendly energy use in building heating and cooling, aerospace energy and utilities, a thermal energy storage system is a great tool. Because a TES system makes use of natural resources and waste heat, it reduces the total consumption of energy, consequently the need for fossil fuels and as a result costly oil imports [1], [7].

These systems and the body of thought behind it cannot survive if they are economically not interesting for political institutions. Because the use of waste energy and surplus heat, electrical demand charges are reduced and heating, cooling, or air-conditioning equipment purchases are avoided. Less electricity is used, so the electricity bills become lower. But, because renewable energy resources are still in development, initial investments are still high nowadays. TES is currently used in a wide variety of applications, such as active and passive solar heating, water heating, cooling, and air-conditioning and this mainly in energy intensive sectors, such as the metallurgical industry, paper plants, refineries, chemical plants, oil and gas industry, and general manufacturing [1], [12], [13].

In this literature review, first TES is explained. After that, one specific type of TES will be analyzed, namely sensible TES (STES). Also the relation between solar energy and STES is discussed. One cannot talk about the solar boiler without mentioning solar energy and its relation with TES. After that, the solar boiler will obviously be discussed. Existing characterization methods for sensible TES systems are explained and current shortcomings are pointed out. At last, the charging time energy fraction method (CTEFM) will be described, which offers a solution for the characterization of solar boilers.

2.2 Thermal energy storage

The definition of thermal energy storage is energy conservation on an hourly, diurnal, daily, weekly, occasionally, or seasonally basis of high- or low-temperature energy for later use and this by heating, cooling, vaporizing, solidifying or liquefying a material, or through thermochemical reactions. The stored energy is transformed into heat or coolness by reversing the process. By TES, a link and buffer exist between a heat source and a heat user with or without a heat transfer fluid flowing between them. A heat transfer fluid is a gas or liquid that participates in heat transfer by acting as a bridge between heating and cooling on opposite sides of a process. It also transports and stores thermal energy. The same three steps are passed every time while going through a complete storage process: charging, storing, and discharging. TES applications are designed to work on a cyclical basis [1].

2.2.1 Commonly used TES applications

TES can be used for water and (overnight) space heating, cooling, and air conditioning. For example, summer or waste heat can be used for winter use, winter ice can be used for space cooling in summer, and the electrically generated heat or cool during off-peak hours can be used during subsequent peak demand hours.

An example of using summer heat is in Uden, The Netherlands. Here, a considerable amount of heat is subterraneously stored in water in a storage tank made by Ecovat, as Figure 25 demonstrates. More than six months' worth of this heat can be stored with a 95% efficiency [14]. It has a storage capacity of 5 GWh per load cycle and a lifespan of more than 100 years [15]. This thermal tank is 16 meters deep and has a diameter of 13 meters [14].

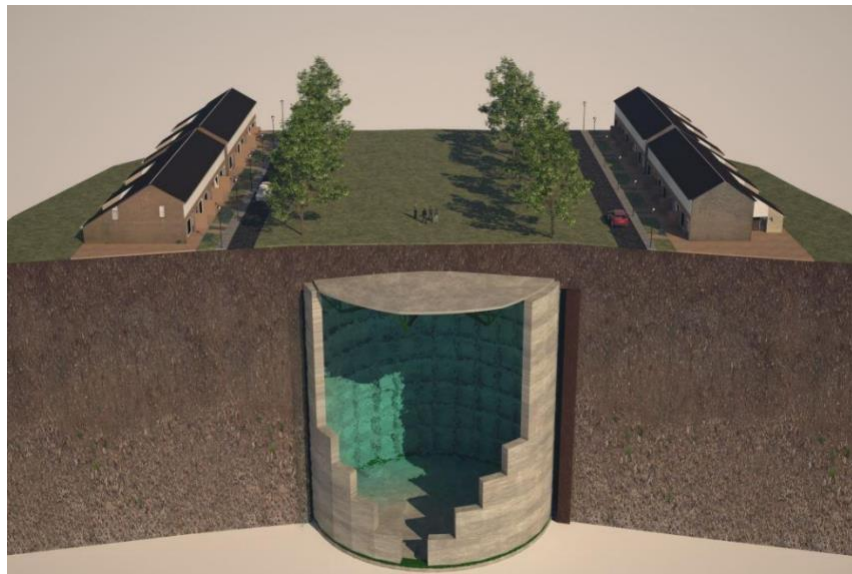


Figure 25: Storage tank in Uden to preserve summer heat [14].

Cooling TES uses water, ice, or a eutectic salt solution as storage material. It is beneficial for new buildings with large cooling loads during the day and no cooling loads at night. Baltimore Air-coil Company (Ice Chiller), Ciat Co. (Cristopia), Calmac Co. (Icebank), and Sedical Co. (Cryogel) are manufacturers that use this system on their production lines [16]. Nevertheless, cooling TES systems are only economically attractive if the old cooling system needs replacement or enlargement [17].

TES systems can be used in combination with solar installations. The storage system can shift peak electricity consumption to a time of the day when there is a lot of solar radiation available. This reduces the peak electricity demands and results in cost effectiveness for consumers, only if time of use tariffs exist [1]. The use of electricity throughout the day is high in the morning and evening, because people are spending time at home before and after their work and household tasks are being done [18]. Meanwhile, solar energy, unlike energy from fossil, nuclear, and other fuels, is not available throughout the whole day and is not available at night. In Figure 26, the duck curve for Belgium for 2020 and 2030 is presented [19]. A graph of power demand from the grid on days when solar energy output is strong and demand in the grid is low is known as the "Duck Curve." The graph's lines and curves have a noticeably duck-like appearance when plotted. The Duck Curve essentially symbolizes the possibility of instability in the electricity system as the grid tries to handle drastic variations in demand during the course of the day [20]. The mismatch of energy availability and energy demand can be prevented by using TES [1].

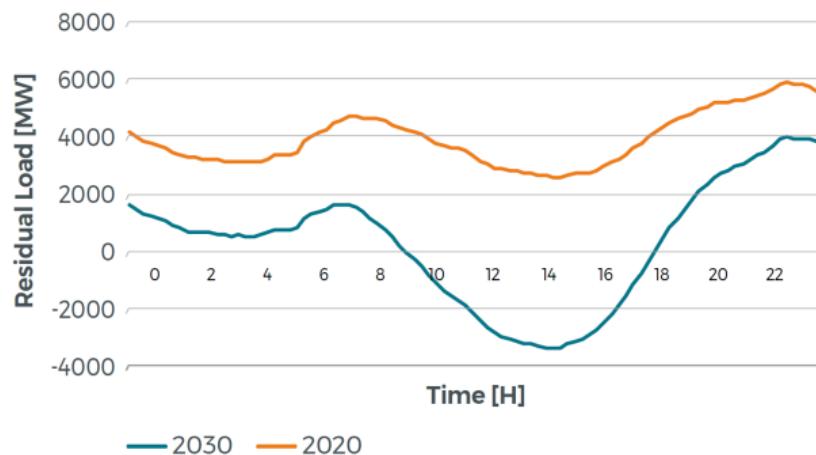


Figure 26: Residual load curve for Belgium for 2020 and 2030 [19].

There are different ways to match electricity generation and electricity demand: peak clipping (lopping), valley filling, load shifting, and strategic conservation as can be seen in Figure 27. By using TES, loads can be shifted [21]. Peak clipping is the reduction of grid load, particularly during times of high demand. Increasing the load during off-peak hours to improve system load factors is called valley filling. Load shifting involves reducing grid load during periods of peak demand while simultaneously increasing load during off-peak times. Conservation means cutting back on consumption or using more energy-efficient appliances to lighten the load throughout the day. Load building entails raising the load over the course of the day by increasing daily consumption. Flexible load shapes are agreements and fees that allow for flexible control of consumers' equipment [22]. A household device that consumes a lot of off-peak electricity is an electric storage heater [23].

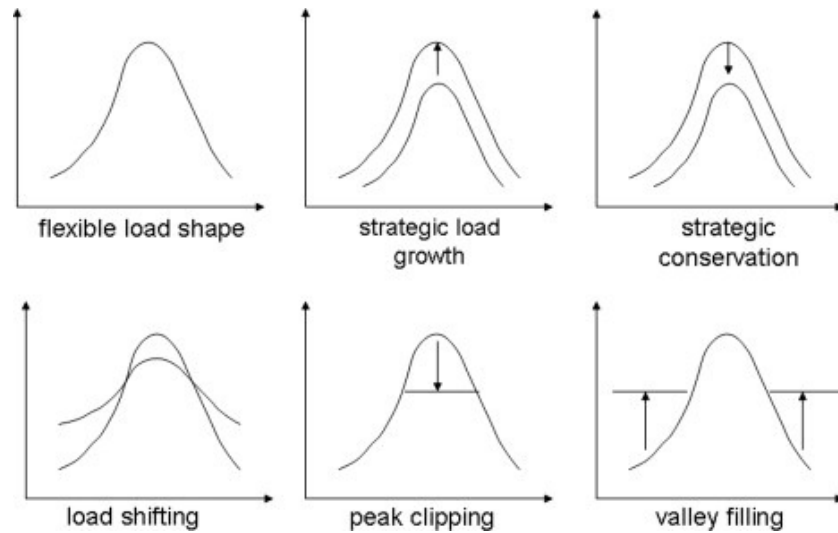


Figure 27: Demand-side management programs aiming at peak clipping (lopping), valley filling, load shifting and strategic conservation [21].

Using TES to divide electricity use throughout the day also results in an energy reduction from more expensive generating stations during peak hours. That is why TES is cost effective in commercial, industrial, utility, and residential sectors, such as offices, hospitals, schools, universities, airports and other facilities [1]. A hospital that uses TES is the Bispebjerg Hospital that houses Denmark's largest ATES (aquifer thermal energy storage) system with an energy consumption reduction of 2462 MWh/year and a total of € 209 000 savings on operating expenses [24].

TES storage can also be used in thermal electrical generating systems where the energy is stored before it is converted to electricity. This space heating system using electric TES is frequently utilized in the western world [1]. The company TEPCO Group uses thermal power generation to let generators rotate and to create electricity to improve existing facilities [25].

Other current new TES applications that are worth mentioning are enhanced waste heat/cold recovery, electrical circuit cooling, energy management in electrical and fuel cell vehicles, and photovoltaic battery cooling [1].

Before implementing TES for a certain application, there must be looked at the technical, environmental, economic, energetic, sizing, feasibility, integration, and storage aspect [1]. Ways for TES constructions to come off worst, are a wrong sizing of the system which affects the payback time, failure in the control system equipment and inexperience of operators [17].

To conclude, TES is a special form of energy storage. By using this type of energy storage for heat applications, converting energy from one form to another is not necessary, and thus conversion losses are avoided. TES systems are nowadays already used in a lot of applications, but there is still space for growth. These TES systems reduce the impact on the climate by reducing CO₂ emissions. TES is also beneficial for reducing the load on the electricity grid.

2.3 Thermal energy storage classification

There are many ways to classify TES systems. One of them is seeing TES as a spectrum, where on the one side seasonal storage exists. Seasonal fluctuations in temperature and waste heat are a handy tool for TES. Because the storage system must bridge (a) season(s), the storage must be large. To cover seasonal needs, the delay is a few weeks to multiple months [1]. An example of seasonal or annual storage is collecting the coldness of winter to charge a cool store and as such providing coolness in summer. Another example is borehole TES. Hereby, waste heat is used to warm up a volume of earth via heat exchangers in boreholes. This heat can later be used for space and water heating [26]. The disadvantage of this type is that the energy supply grid must be placed in the ground beneath the structure so that is only suitable for new constructions [17].

On the other side of the spectrum lies hourly storage. Here, the storage volume is of less importance. With this short-term storage, the size of the storage is reduced, and the stored energy can be used during off-peak electricity demand hours where the price is lower. Hereby, the power loads are managed for a few hours to a day [27]. An example of hourly storage is an electric hot water tank with sizing of hundred liters, generally installed in individual households in high electrified countries [28].

Another way of classifying TES systems is splitting them into three types: sensible thermal energy storage (STES), latent thermal energy storage (LTES) and thermochemical energy storage. STES is storage by causing a storage material to increase or decrease in temperature by adding/distracting heat, but without undergoing phase change. In LTES, the phase change material (PCM) undergoes a phase change when adding heat to/distracting heat from the storage. The combination of the sensible and latent TES is also possible. Examples of LTES are ice, paraffin wax and a steam generator [1], [29]. In thermochemical storage, the storage absorbs energy by reversing an endothermic chemical reaction. In these reactions, chemical bonds break and are being formed again. These reactions can be catalytic reactions and thermal dissociation reactions involving metal oxides and metal hydrides. Examples of a catalytic reaction in TES are a steam reforming reaction with methane and the decomposition of sulfur trioxide. These reactions are used in high-temperature (>300°C) nuclear cycles, solar-energy systems and as topping cycles for industrial boilers [1]. Figure 28 shows a classification of all sorts of heat storage material type-based TES systems and their thermal storage media.

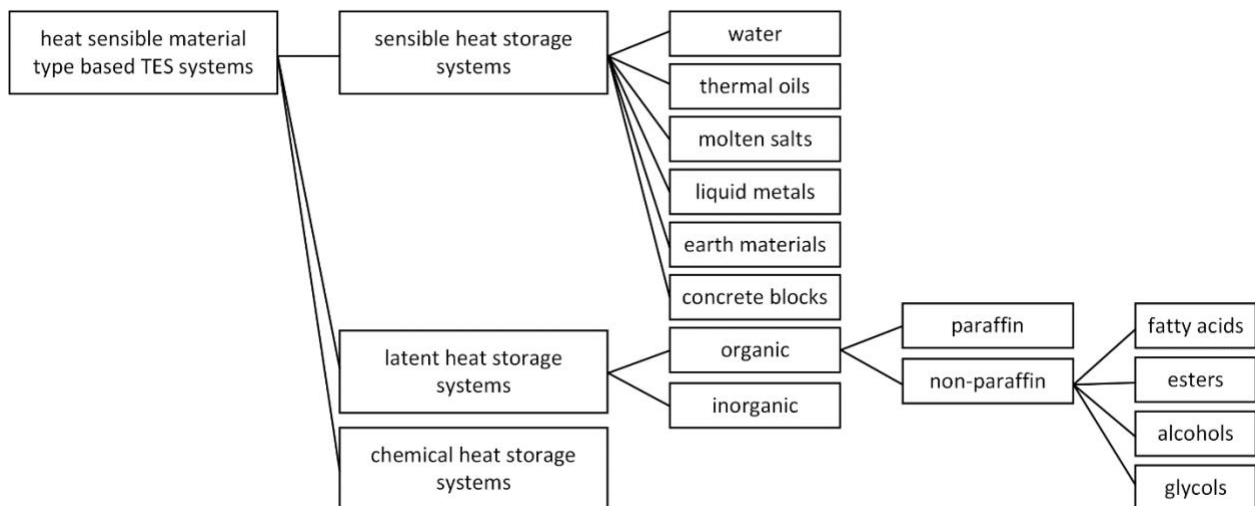


Figure 28: Different types of TES systems with all possible storage materials [30].

One material that is used a lot for storage is water. It is a user-friendly and easy material to apply as a storage medium where the three phases can be used. It can be used both as a heat transfer fluid and as a TES material. It is not toxic, not flammable, chemical stable, easily available, cheap, and has a high specific heat (4,184 kJ/kgK) [4], [30], [31]. That is what makes water perfect for home space heating, cold storage of food products and hot water supply type of applications [4]. Disadvantages of water are high vapor pressure, corrosiveness and temperature limitation for several industrial activities. Where the liquid phase is used for low temperature heat energy storage below 100°C, steam phase is used for high temperature heat energy storage. Chilled water or ice is used on its turn for cold storage [30]. The storage tank is usually made of concrete, plastic or steel [17].

2.4 Sensible thermal energy storage

For this master thesis, a specific STES system is used, namely the solar boiler. This chapter takes a closer look at STES systems.

As previously mentioned, in STES the storage medium temperature changes when heat is added/distracted. The storage material does not undergo a phase change. STES always contains the storage medium, a container, and input/output devices. The container needs to be well insulated to minimize heat losses [1].

The energy input in an STES system is proportional to the difference between the final and initial temperature, the mass and the heat capacity of the storage medium. The higher the specific heat of the storage material and, if volume is important, the denser the storage material, the more effective the system is. The amount of heat that is stored in a material, can be described as Eq. (23).

$$E = mc_p(T_2 - T_1) = \rho Vc_p(T_2 - T_1) \quad (23)$$

where m is the mass, c_p the specific heat coefficient, $T_2 - T_1$ the temperature change of the storage material, ρ the mass density and V the volume. The factor ρc_p is strongly related to the ability to store sensible heat for a certain material [1].

To make a sensible water tank TES system as effective as possible, four aspects are required:

1. Thermal stratification

Thermal stratification is the existence of a thermal gradient across the storage, even during (dis)charging periods. The higher the thermal stratification of a storage tank, the more efficient a system is. This is more difficult in a fluid storage medium than a solid one, because mixing is easier in a liquid than in a solid. Mixing leads to a thicker thermocline and thus less thermal stratification. By this, smaller tanks can be used for the same purpose. Thermal stratification is important, because if the cold and hot layer stir together, there are more thermal losses than when the thermocline layer is thinner. Figure 29 shows a tank with levels of thermal stratification and their thermocline [32].

To improve the thermal stratification and so the performance efficiency of storage tanks, a high height to diameter ratio must be taken into account, because axial wall conductivity falls when the L/d ratio rises [33]. As a result, it takes less time for hot water to be stored. Mixing is avoided by installing the water inlet and outlet precisely so that a uniform flow is made [1], [32]. Stratification can also be increased by adding phase change materials to the sensible storage as these materials have a low thermal conductivity [34]–[36]. The design of the storage normally defines the heating/cooling power. For a thermally stratified water tank, however, the flow rate from the tank to the load determines the heating/cooling power. This cannot be too high, because otherwise, the stratification will decrease [17]. The flow rate can be slowed down by installing different barriers such as flat plates or disks inside the tank [37], [38] and novel inlet designs and configurations [39], [40]. A rectangular tank placed in an oblique position also improves the degree of stratification in the tank [41]. Thermally stratified water tanks are an appealing type of TES because of their full development, availability on the market, efficiency of more than 90% [42] and the low price in the temperature range for building applications [17].

The phenomena known as dead water is high vertical density stratification brought on by, in this case, temperature [43]. The degree of thermal stratification and dead water volume in the tank relate to each other. In a naturally thermally stratified storage tank, which has no inside partitions, warm water flows to the top of the tank because of its lower density. The cooler water sinks to the bottom because of the

same principle. In this case, the amount of dead water volume is little whereby the tank volume can be decreased [1]. The more uniform the water flow is, the less the thermal stratification will be destroyed.

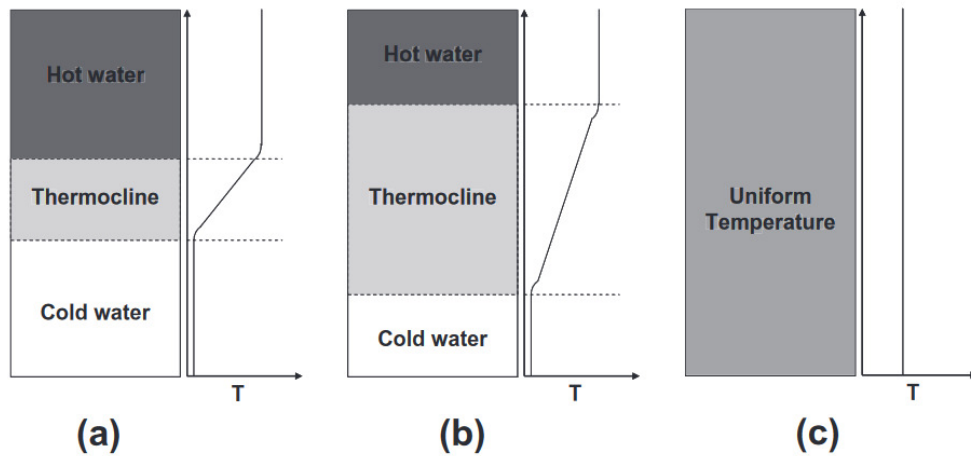


Figure 29: (a) highly stratified; (b) moderately stratified; (c) fully mixed storage tank [17].

2. Limited amount of dead water volume in the tank

By placing the inlet and outlet connections near the top and bottom of the storage volume, respectively, dead water volume is minimized, as can be seen in Figure 30. There should also be little surface area in contact with the storage water to limit the dead water volume [1]. The more dead water volume there is in the tank, the less space there is for the water on different temperatures to take part of the uniform flow of water to avoid mixing, hence decreasing the efficiency [1].

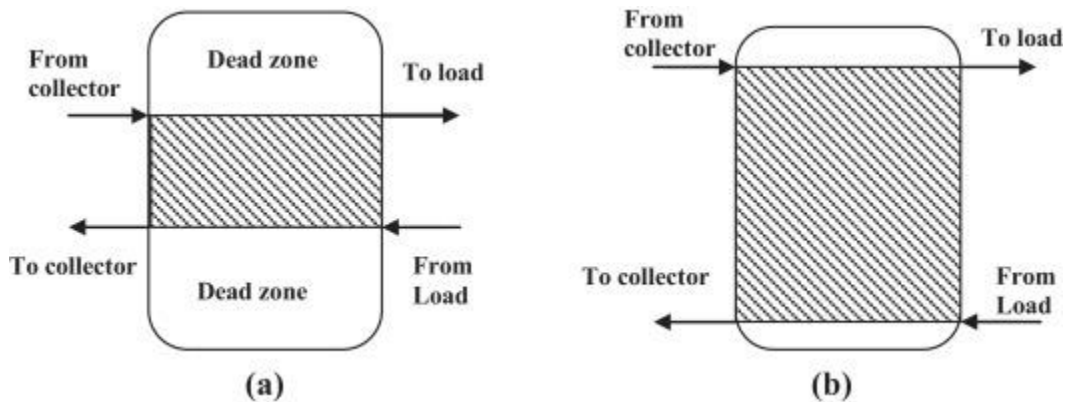


Figure 30: Dead zone in a water tank (a) large dead zones (b) small dead zones [44].

3. Well-insulated tank

With a well-insulated tank, excess heat losses are reduced which results in an increase in efficiency. The insulation of the tank must be as cheap as possible, but environmentally safe, safe to interact with other materials, must have low thermal conductivity, and a high resistance against the storage medium and surrounding environment influences. It must also not leak. Water-based seasonal storage tanks normally use mineral fiber, extruded polystyrene foam, expanded polystyrene foam, polyethylene foam, and polyurethane/polyisocyanurate foam. In Table 1, conventional insulation materials and Super Insulating Materials (SIMs) are shown. It is noticeable that the SIMs are much more expensive than the traditional insulation materials. Not all these traditional insulation materials occupy the same thermal

behavior [45]. Plus, they possess a higher thermal conductivity and therefore, a higher insulation thickness is needed. If these materials are compared with SIMs, SIMs have 5 to 10 times lower conductivity and therefore a much lower thickness is needed [46]. Nowadays, Aspen Aerogel [46], [47], polyisocyanurate foam [48], and vacuum insulation [46], [49] are the most desirable insulating materials for solar boiler systems [4].

Table 1: Tank insulating materials and their minimum cost and worldwide usage [4].

Material	Minimum Cost (\$)/per sq. ft.	Worldwide usage
Aspen Aerogel	4.89	Rare
Mineral fiber	0.20	Common
extruded polystyrene foam (XPS)	0.50	Common
expanded polystyrene foam (EPS)	8.50	Less common
polyurethane/polyisocyanurate (PUR/PIR) foam	1.50	Common
glass granules	2.40	Common
perlite	0.37	Common
foam glass gravel	5.00	Less common
fiber glass	1.29	Common
vacuum insulation	10.00	Rare

4. Tank size

Tank size also has an influence on the performance of the water storage system. The higher the height/diameter is of the tank, the higher is the performance efficiency, because axial wall conductivity falls when the L/d ratio rises [33]. As a result, it takes less time for the hot water to fill the tank [50].

Current STES applications involve oils and molten salts. Thermally stratified TES tanks, concrete, rock beds, water/rock beds, air, pit, bricks, sand, cavern, aquifer and solar pond TES systems also exist [1], [4], [17].

2.5 Solar energy and thermal energy storage

In this chapter, the relationship between solar energy and TES will be clarified and there will be explained why these two concepts go hand in hand.

Solar energy is a cyclic, time-dependent energy resource and because of the unpredictable nature of this resource, storage is needed to match the availability of this energy with the demand. The storage must be large enough to bridge periods of insufficient sunshine, but the storage system must also be designed in such way that it can handle periods of large amounts of bright sunshine and that it does not have burn-out problems. As previously mentioned, here, also diurnal, weekly and seasonal storage cycles exist [1]. Seasonal systems have larger tanks compared to short-term storage. Many of these tanks are installed underground or partially buried (water pits) [45]. However, not all solar thermal applications require storage, such as solar grain driers, solar distillers, and solar kilns [1].

Solar TES can be split up in active and passive systems. Active systems require pumps and other devices to transform the sun's energy into hot water or electricity [1], [51]. Passive systems directly use the heat or light from the sun without the presence of a heat pump. The heat transfer fluid flows from the collector to the storage tank by natural circulation [4]. Active systems are 35%-80% more efficient than passive systems, due to the excessive reliance on climatic factors, storage material properties, and building architecture [52], [53]. The drawback of these efficient systems is the fact that they are depended on electricity, the cost of

this electricity and the complexity of the system [53]. Active systems can be divided into active solar space heating, solar water heaters, photovoltaic cells and concentrated solar power. Passive systems are mostly used for small-scale domestic applications. Five main types of these passive solar TES systems are direct heat gain, heat collection and storage, sunspace, roof-top heat storage and thermosyphon [1], [51]. South-facing windows are essential to direct-gain passive solar systems because they allow solar energy to enter a building directly. The materials in the house (the floor, walls, furniture, etc.) absorb the sunlight, which warms them up. They store a part of the heat and radiate a part of the heat back into the room, warming the room [54]. Heat collection and storage is using thermal mass, heat flow, and insulation effectively to capture, transmit, and retain the heat [55]. A sunspace is a glass space that is on the southside of a building. Because of the space's natural heating and cooling, daytime temperatures can rise higher and nighttime temperatures can drop deeper than the adjacent living spaces' "comfort zone" temperatures [56]. The roof solar heating storage system works by using solar heat radiation to heat the thermal storage attic plate through the roof glass skylight and thermal convection and radiation to change the temperature between the walls, which raises the room's overall temperature [57]. At last, a thermosiphon is a passively operated heat management device that works with the natural convection and conduction forces as its drivers. These forces are used by the device to produce a fluid flow that cycles back and forth between hot and cool regions [58].

A good solar TES system consists of five parts: the heat reservoir, the heat reservoir container, the heat receptor–transmitter system, the thermal insulator and structural support. To somewhat decrease the environment impact, the TES unit materials must be abundant and be of common usage in industry. They must be obtained either from recycling or industrial wastes. The materials for the heat reservoir must possess a high energy density per unit of volume and mass. They must contain high temperature resistance and good solar radiation absorptance in the energy receptor zone. The heat reservoir container and thermal insulator require materials with low thermal conductivity and high temperature resistance [59].

Solar energy is, along with biomass and geothermal energy, one of the only three clean energies that can produce sufficient thermal energy to generate power [60], where solar energy is the most promising. The biggest disadvantages of this resource energy are its infrequency and the control difficulty of related technologies that prohibits the domination of the electricity supply market [61].

According to Danehkar et al. [4], solar pumped hydro storage is the best storage option. Number two is solar sensible thermal storage, followed by underground natural storage systems, underground man-induced storage systems and lastly water-based latent heat storages. This is based on environmental risks and reliability but neglecting the application factor [4]. When solar energy is used in combination with STES, the storage definitely needs to be large, because the energy from solar collectors is at low temperatures [1]. Speaking of solar energy in combination with STES, the solar boiler is an example of that and furthermore the subject of this master thesis.

2.6 The solar boiler

One cannot talk about the combination of solar energy and STES without mentioning the solar boiler, also being the subject of this master thesis. The solar boiler is an example of a solar hot water storage system. The energy comes from solar radiation, absorbed by collectors, and is transported to the water tank directly or indirectly. This increases the water's temperature without phase change, after which the consumer can use this demanded heat to meet his basic needs. Storage of this solar energy is absolutely required since solar energy and heat demand does not always occur at the same time [1].

Water tank storages and TES go hand in hand, because water is one of the most commonly used storage medium for thermal applications, such as water heating, building air conditioning, commercial and industrial

usage. These systems are cost-effective in storing thermal energy and the thermal stratification of water and proper insulation of the vessel ensure a high efficiency [62]. To evaluate these systems, different approaches can be used. One is to define the TES efficiency, which is the ratio of thermal energy recovered from the storage at discharge temperature to the total thermal energy input at charging temperature, as shown in Eq. (24) [32]:

$$\eta_{TES} = \frac{Q_{recovered}}{Q_{input}} \quad (24)$$

Other commonly used definitions are discharge efficiency and charging efficiency. Discharge efficiency is the total recovered energy divided by the maximum thermal energy that can be stored in a stratified tank. Charging efficiency is the thermal energy input at the end of charging to the maximum thermal energy that can be stored [32].

2.7 Existing characterization methods of sensible solar thermal energy systems

For characterizing heat exchangers, many methods already exist, such as the e-NTU method, but because these methods assume a heat exchanger in steady state, Beyne et al. [3] developed a new method for quantitatively studying thermal energy storage systems: the charging time energy fraction (CTEF) method. This methodology makes it possible to characterize the dynamic behavior of LTES heat exchangers where other models are not capable of deriving a predictive model from a set of experiments which can be implemented in process simulations for different applications.

This CTEF method is not yet used on an STES. Also, the methods to characterize an STES system are limited. It is important to be able to predict the outlet state as a function of time of these systems, not only because it is an upcoming application in domestic households, but also because STES in combination with a water tank is the cheapest and most widely used type of TES [4]. In this chapter some already existing characterization methods for STES systems are given.

2.7.1 Modeling strategies for sensible heat thermal energy recovery

In this paper, a sensible heat thermal energy recovery system was investigated experimentally and by mathematical modeling. For the experimental study, a fixed bed was built, as presented in Figure 31. Several tests were performed to investigate the impact of various operational factors on the performance of the system, such as the temperature and velocity of the incoming air as well as the material and diameter of the packings [63].

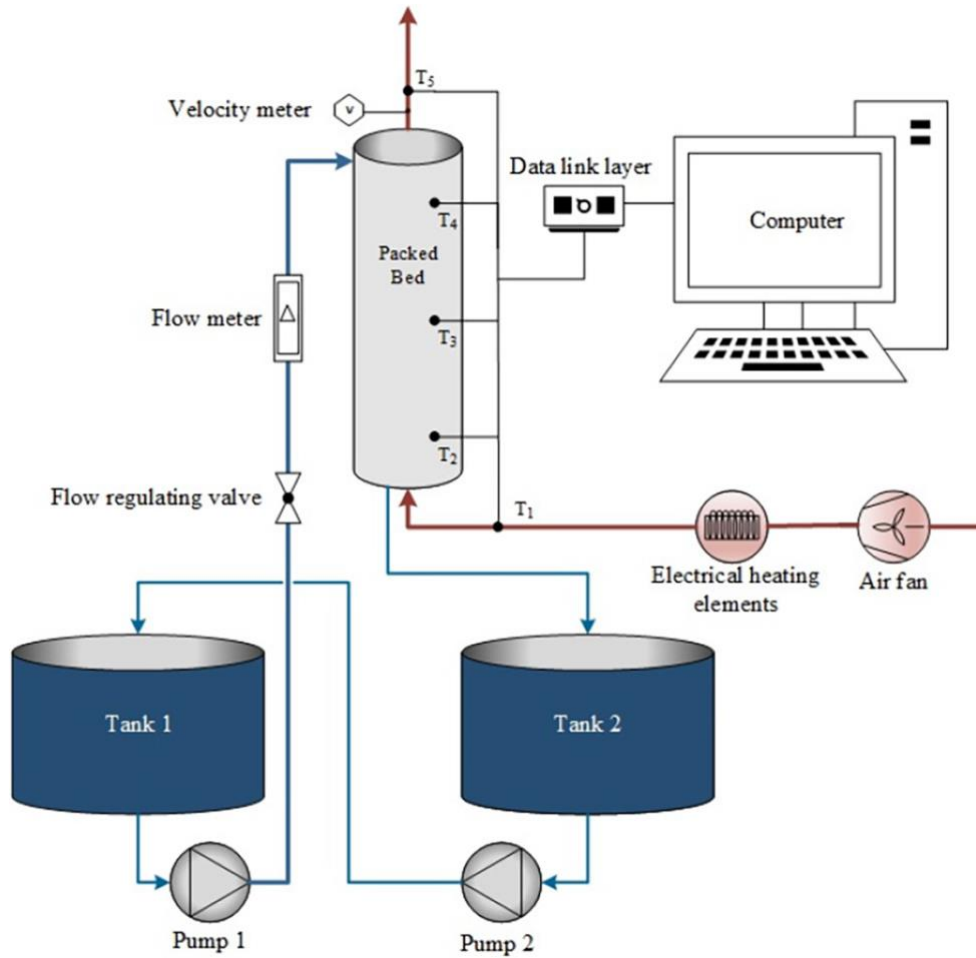
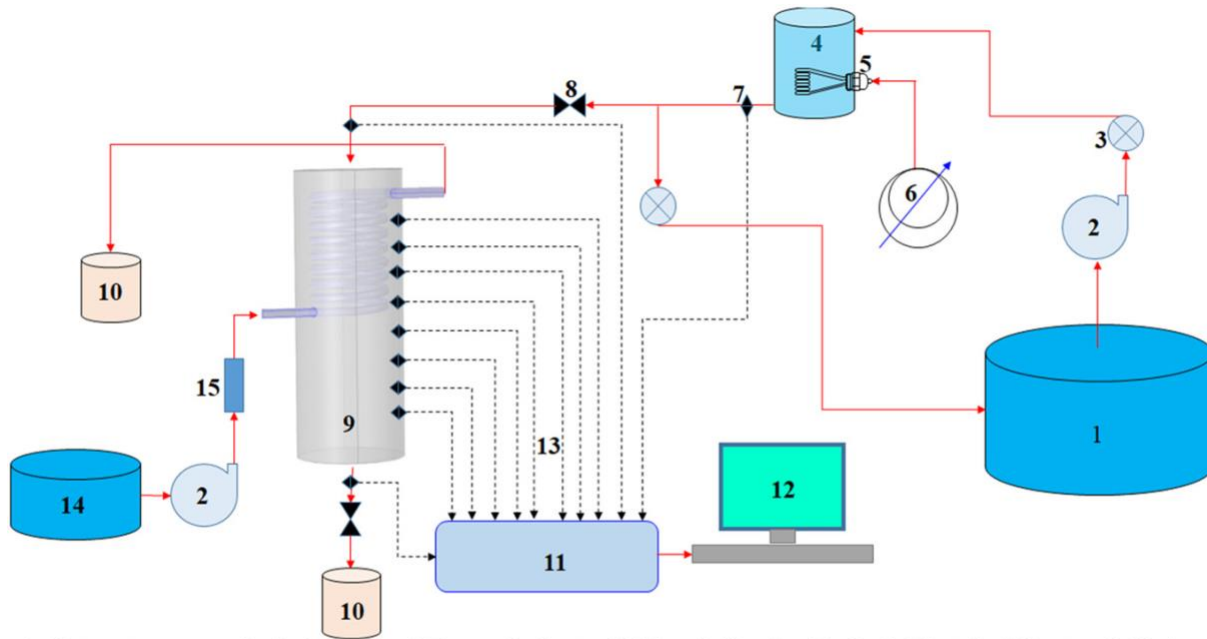


Figure 31: A simple schematic of the experimental setup of the fixed beds [63].

System modeling was done at three different levels in the mathematical modeling utilizing the energy conservation rule. Experimental data were utilized to assess the correctness of the derived models. Then, the ideal model was chosen to anticipate the system behavior. A dimensionless energy recovery efficiency parameter was established, and the experimental results were compared with those used to assess the performance of the system [63].

2.7.2 Experimental investigation of heat dispatch controllability

In this study, the seldom investigated simultaneous charging and discharging (SCAD) mode is studied as well as the discharging-alone operation following a substantial stand-alone period using a vertical cylindrical thermal energy storage tank. The experimental set-up is presented in Figure 32. These storage tank's dynamic operational modes are examined to increase the flexibility of energy content dispatch in response to load-side demand [64].



1. Hot water reservoir, 2. Centrifugal Pump, 3. Control Valve, 4. Heating Tank, 5. Electrical Heater, 6. Variac, 7. Thermocouple, 8. Needle Valve, 9. TES Tank, 10. Sump, 11. Data Logger, 12. Computer, 13. Thermocouple Wires, 14. Cold water reservoir, 15. Rotameter.

Figure 32: Experimental set-up of the vertically aligned cylindrical TES tank [64].

Based on the temporal and spatial temperature profiles of the working fluids, coil outlet temperature, temperature gradients along the storage tank height, energy analysis, and primary thermocline thickness for different discharging coil flow rates, the performance of the storage tank is examined. The main goal of this study is to evaluate the storage tank's performance under two distinct operating modes and to determine if the operational parameters are appropriate given the energy demand and supply [64].

The study uses meanly heat formulas to determine the key performance indicators (energy analysis, thermocline thickness...). It is known that the geometry of a storage tank's interior and the performance enhancement of the immersed heat exchanger coil used in discharging the tank, are still the two ways to improve the performance of solar water heating systems [65]. It was found that during the SCAD mode, the primary thermocline thickened along one side of the tank while splitting into two layers below it, named the secondary thermocline. The sustenance of this secondary thermocline, thermal gradients across the tank's height, and the discharge efficiency decrease as the flow rate increases. Prior to the discharging-alone operation, there is evidence of heat content retention within the storage tank which allows the formation of thermic stratification in the tank. The writer found out that thermal stratification takes longer in higher initial charging temperatures. Additionally, discharge time decreases with increasing coil-side flow rate, which provides more operational flexibility and controllability over tank heat content. As a result of these features, the TES system is highly versatile and able to meet various demands [64].

2.7.3 Experimental evaluation and improvements of a diode solar water heater

Here, a novel thermal diode operation is used to characterize a pre-heat integrated collector storage solar water heater (ICSSWH) to reduce ambient heat loss during non-collection periods. This is done by using a solar simulator facility, named Mark IV, that is located in Ulster University. It is intended to use this Mark IV as a sustainable pre-heat alternative to other types of solar boilers in domestic hot water installations. A

solar 433 simulation test laboratory was used to develop, produce, test, and evaluate a variety of prototypes [66].

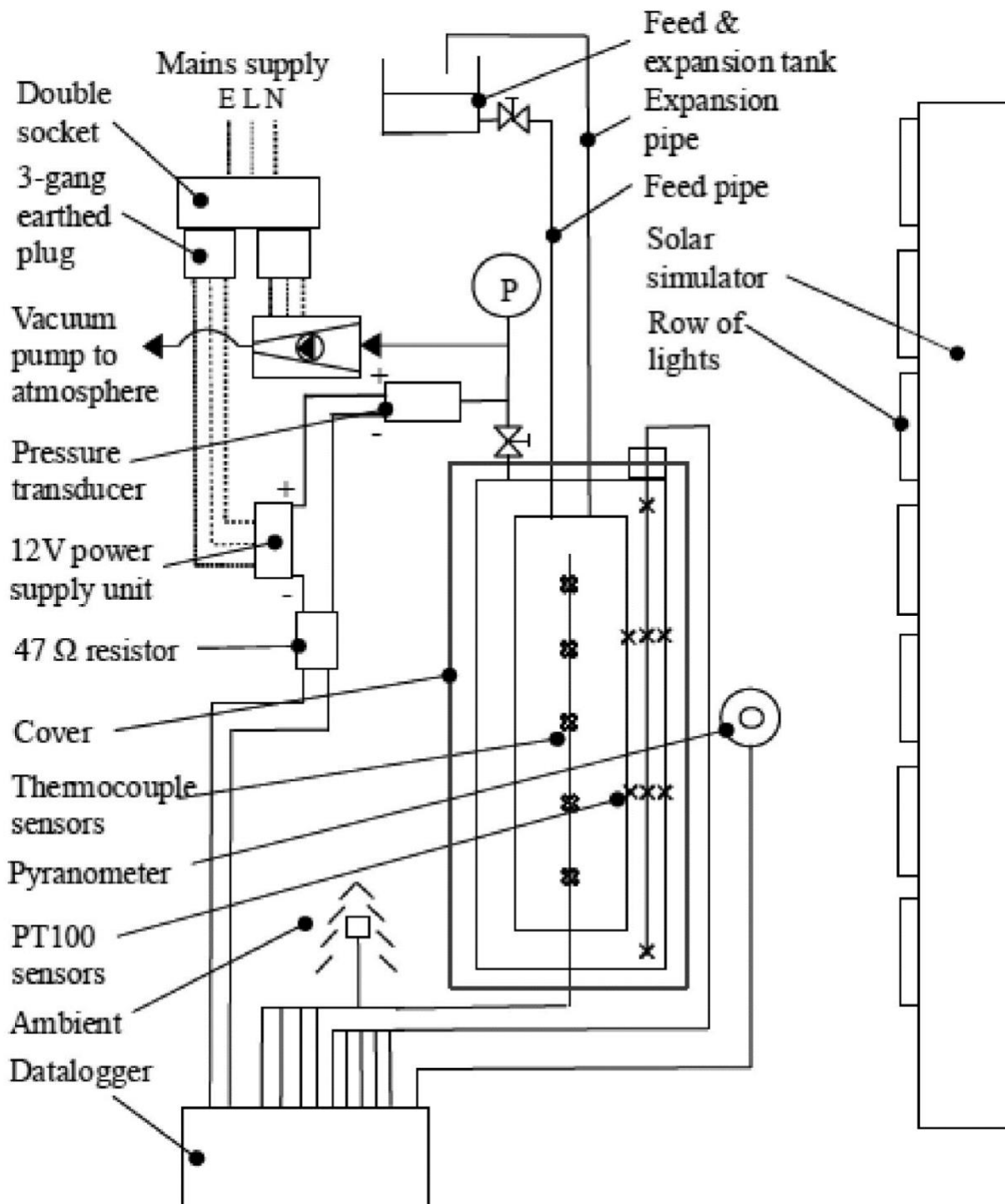


Figure 33: Schematic diagram of solar simulation test facility [66].

The testing of the thermal diode concept highlighted the importance of cover and insulation in order to ensure a steady evaporation and condensation cycle. When compared to other conventional integrated

collector storage (ICS) systems, it is clear that the current prototype units have an improved performance in terms of thermal retention during non-collection periods. The ICS units were found to have fewer thermal losses when compared with other similar systems. The study found that, when implemented in conjunction with heat retaining thermal diode features, elongated pockets and capillary matting, transparent coverings, and aperture cavity back insulation/transparent apertures, the system performance significantly improved [66].

2.8 Problem statement

Methods to characterize STES systems are limited. But [3] Beyne et al. has recently invented a technique to experimentally examine TES devices. This methodology makes it feasible to characterize thermal energy storage systems' dynamic behavior, which was previously not achievable using conventional heat exchanger techniques.

The purpose of this research is to examine whether the CTEF method can be applied on a STES heat exchanger. It is examined whether the energy fraction model of the charging time can also serve as a design model if the coefficients of the model can be found based on the geometry of the tank.

The CTEF method will be explained in the following subsection.

2.9 Charging time energy fraction method

The CTEF method is a tool to design LTES processes. With this method it is possible to predict the heat transfer fluid outlet temperature as a function time, based on the initial and input conditions. It characterizes and evaluates a latent thermal energy storage heat exchanger. Standard methods, which are based on the steady-state operation, to design these processes, are not capable, because latent thermal energy storage heat exchangers do not operate in steady state [3].

To reach this method, first the first law of thermodynamic is applied to a control volume comprising an LTES heat exchanger, which can be seen in Figure 34 [3].

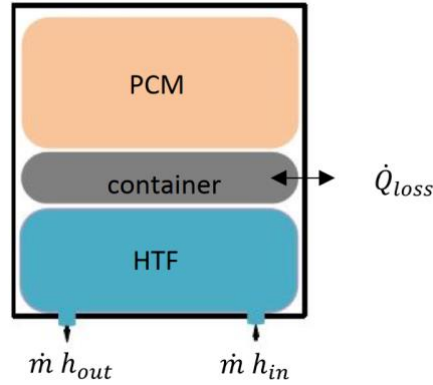


Figure 34: LTES heat exchanger as a control volume [3].

In order to determine the internal energy of an LTES heat exchanger, it is necessary to know the internal energies of the PCM U_{PCM} , U_C (container) and HTF U_{HTF} (heat transfer fluid) [3], as displayed in Eq. (25):

$$U = U_{PCM} + U_C + U_{HTF} = \int_{PCM} u_{PCM}(state)dm + \int_C u_C(state)dm + \int_{HTF} u_{HTF}(state)dm \quad (25)$$

Because the compressibility of the HTF is negligible, the thermal expansion of the HTF is also negligible. This ensures that the in- and outgoing HTF mass flow rate is equal and given by \dot{m} . The kinetic and potential energy change of the LTES heat exchanger and that between the in- and outlet of the HTF are also neglected. The resulting first law of thermodynamics is expressed with \dot{Q}_{loss} being heat losses over the boundary of LTES heat exchanger and h_{out} and h_{in} being the specific enthalpy at respective out- and inflow ports of the HTF, as Eq. (26) shows [3]:

$$\frac{dU}{dt} = \dot{Q}_{loss} + \dot{m}(h_{out} - h_{in}) \quad (26)$$

The net efflux of energy is the movement of HTF that results in a loss of energy, as can be seen in Eq. (27) [3]:

$$\dot{Q}_f = \dot{m}(h_{out} - h_{in}) \quad (27)$$

The two main components of heat loss from the battery are the heat transfer between the LTES exchanger and ambient air, as well as heating or cooling the insulation itself. By applying sufficient thermal insulation, both parts of this lost energy can be minimized. This is done by calculating how much less internal energy will need to be expended in order to maintain an equilibrium temperature within the battery using the Eq. (26). Knowing the internal energy of a battery during charging and discharging can be understood by considering a cycle between two known states. How much energy is stored at the end of the cycle is pointed out by Eq. (28):

$$\int_{t_{start}}^{t_{end}} U(state(t))dt = U(state_{end}) - U(state_{start}) = \Delta U \quad (28)$$

There is a continuous energy increase from 0 to 1 that can be written as Eq. (29) where $\alpha(t)$ is the energy fraction as a function of time. However, until there are methods to measure local states, we cannot actually determine the value of this fraction exactly [3].

$$J(t) = \int_{t_{start}}^t dU = \alpha(t)\Delta U \quad (29)$$

Integration in time is shown in Eq. (30):

$$Q_f = \int_{t_{start}}^t \dot{m}(h_{out} - h_{in})dt \quad (30)$$

Eq. (26) integrated in time in Eq. (31):

$$\alpha(t)\Delta U = Q_f(t) \quad (31)$$

Transformation of Eq. (30) and Eq. (31) results in Eq. (32).

$$\frac{d\alpha}{dt}\Delta U = \dot{m}(h_{out} - h_{in}) \quad (32)$$

The outlet state of the LTES heat exchanger can be determined, by correlating the energy fraction function $\alpha(t)$. To correlate this, two issues need to be addressed. The first is determining a parametrizable function for $\alpha(t)$ as a function of the inlet conditions and initial state. The second is making an objective function where the parameters to the measured energy fraction are fit in. It is difficult to find a parametrized function for $\alpha(t)$, as different transfer processes will be dominant throughout the charging cycle. Since thermal batteries can be located at different distances from where the HTF flows, it becomes difficult to clearly define when one phase transitions into another. The objective function is to find the outlet state that minimizes the absolute difference between correlated and measured values. The parameters can be chosen in order to achieve this goal, but it may take some time for accuracy to improve. The fitting problem can be solved by finding a correlation between the charging time for different energy fractions. This is done by choosing an α_i value close to 1, and then measuring the charging time at each α_i value [67], [68]. The problem of fitting the energy fraction function $\alpha(t)$, is thus divided into solving for a correlation between $t_c(\alpha_i)$ values as can be seen in Eq. (33).

$$t_c(\alpha_i) \text{ for which } Q_f(t) = \alpha_i \max Q_f(t) \quad (33)$$

It is not possible to predict the outlet state of a particle until its charging time has been determined. The prediction comes down to finding a function for the charging time and determining the parameters p of that function for several energy fractions α_i . By comparing Eq. (33) with Eq. (34), one can determine which fraction α_i corresponds to the measured charging time as Eq. (34) shows.

$$t_c(\alpha_i) = f(\dot{m}; h_{in}; p(\alpha_i)) \quad (34)$$

Mean efflux of energy between two energy fractions is shown in Eq. (35).

$$\bar{Q}_f^{\alpha_1, \alpha_2} = \frac{\alpha_1 - \alpha_2}{f(\dot{m}; h_{in}; p(\alpha_2)) - f(\dot{m}; h_{in}; p(\alpha_1))} \Delta U \quad (35)$$

Mean outlet state between energy fractions is shown in Eq. (36).

$$\bar{h}_{out}^{\alpha_1, \alpha_2} = h_{in}(t_m) - \frac{\bar{Q}_f^{\alpha_1, \alpha_2}}{\dot{m}(t_m^{\alpha_1, \alpha_2})} \text{ with } t_m^{\alpha_1, \alpha_2} = \frac{f(\dot{m}; h_{in}; p(\alpha_2)) + f(\dot{m}; h_{in}; p(\alpha_1))}{2} \quad (36)$$

Eq. (28), (34), (35) and (36) are necessary in the CTEF model to define the outlet state of LTES heat exchangers. Beyne et al. [69] extended an analytical solution by Bauer et al. [70] to propose a general correlation for the total charging time [3]:

$$t_c = \frac{Slope}{\Delta T} + Intercept \quad (37)$$

Since no general correlation is available between charging time and heat exchanger performance, the specific LTES energy fraction model must be fitted for each individual heat exchanger. To calibrate a model, first measurements and calculations are determined for a set of experiments with an inlet mass flow rate level \dot{m}_{level} and enthalpy level h_{level} . For each experiment, the efflux of energy $\dot{Q}_f(t)$, integrated efflux of energy $Q_f(t)$ and energy fraction $\alpha(t)$ are defined as a function of time. The charging time $t_c(\alpha_i)$ is then searched based on a set of energy fractions α . This correlation is used to find the charging times for all experiments. A model that consists of three components, can be used to predict the outlet state for given inlet and initial conditions. The inlet conditions are combined with the charging time correlation and correlation parameters to determine the charging time for all energy fractions in the base set. The total stored energy is then determined from mass and properties of the constituent materials, as well as initial and final conditions. The stored energy in an LTES heat exchanger is combined with the charging time to estimate the total stored energy. This value is then differentiated to determine how much power will be released over a specific period of time. Finally, the outlet state is determined from the $\bar{h}_{out}^{\alpha_1, \alpha_2}$ formula. The charging time energy fraction method thus requires input conditions which stay relatively stable around fixed values. It is not possible to vary these levels greatly unless a model is calibrated and validated for a real LTES heat exchanger first [3].

There has been made use of the CTEFM in a further study of Couvreur et al. [71]. Here, the charging time energy fraction method has been improved by adding a heat loss model to the charging time energy fraction model.

As can be written above, the prediction of the heat transfer fluid outlet temperature as a function of time is the main benefit of the CTEF method. It is examined whether the CTEF method can be applied on a STES system by executing charging and discharging tests. These experiments are performed on a solar boiler. To charge and discharge, both a hot and cold water circuit are build next to this solar boiler. The charging and discharging tests are executed with temperatures ranging from 30°C till 50°C at different flow rates.

3 MATERIALS AND METHODS

In order to apply the CTEFM to the solar boiler set-up, the set-up must be adapted to carry out charge and discharge tests. All set-up components are explained, as well as the LabVIEW program used. The experiments are only valid if they meet the initial conditions. That is, a constant inlet mass flow rate and a constant inlet temperature of the HTF, being the water flowing through the coils and transferring heat to the tank water. Preparations are necessary before tests are ready to be performed. The course of these preparations will be clarified. The measurement procedure and data reduction are also examined.

3.1 Experimental set-up

The original set-up consisted of a closed hot and an open cold circuit connected to the solar boiler. The current experimental set-up consists of a closed hot circuit (in red), a closed cold circuit (in blue), a chiller circuit (in green) and a solar boiler (in purple) as can be seen in Figure 35. In Table 9, the legend of Figure 35 is given.

The hot circuit is located on a skit and is not changed. To do the experiments for this master thesis, the open cold circuit is broken down and build up again on the other side of the skit with mainly new components. The chiller circuit is built from the ground up. Also, there are several non-adjustable 3 way "T" port ball valves added to control the direction of the water flow. Appendix A shows a photo of the hot circuit. Appendix B shows photos of the solar boiler and Appendix C shows a photo of the cold and chiller circuit.

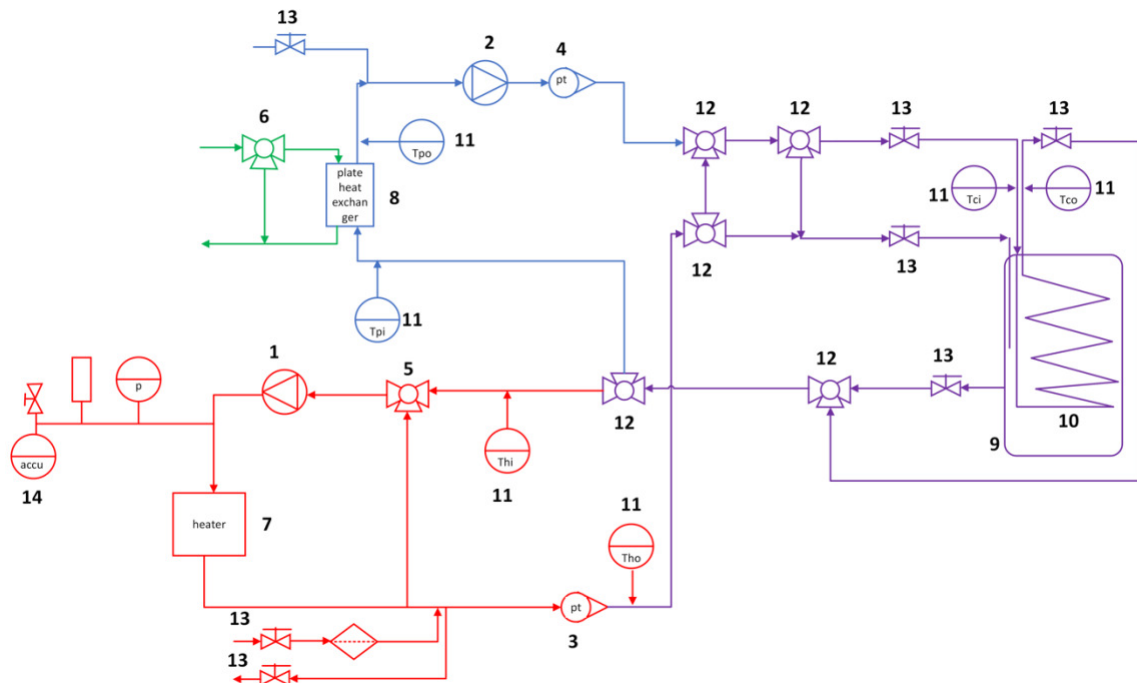


Figure 35: Current set-up of the solar boiler.

No.	Component	Brand and model
1	Circulator pump	Grundfos MAGNA 32-100 180

2	Circulator pump	Grundfos MAGNA3 25-120 180
3	Mass flow meter	Endress+Hauser PROMASS 80F
4	Mass flow meter	KROHNE OPTIFLUX 4300 C
5	Three-way mixing valve	Danfoss 065Z0217 VRB3 with actuator AME 25 082G3025
6	Three-way mixing valve	Danfoss 065Z0217 VRB3 with actuator AME 35 082G3022
7	Heater	DIRAC Industries
8	Plate heat exchanger	SWEP X-marked BX8Tx10/1P
9	Solar boiler	ROTEX Sanitube INOX
10	Polymer coils	
11	K-type thermocouple	
12	Three-way "T" port ball valves	
13	Two-way ball valve	
14	Expansion tank	

Table 9: Legend of Figure 35.

Beyne et al. [3] developed the charging time energy fraction (CTEF) model to predict the outlet state of latent thermal energy storage (LTES) systems as a function of time. The purpose of this master thesis is to validate this CTEF model for an STES system by charging and discharging tests. Predicting the water temperature at the outlet of the coils is done by correlating the energy fraction function $\alpha(t)$. This is the integrated efflux of coil energy $Q_c(t)$ divided by the difference in internal energy ΔU of the total solar boiler at the start and end of the experiment, as can be seen in Eq. (38) [3].

$$\alpha(t) = \frac{Q_c(t)}{\Delta U} \quad (38)$$

The net efflux of coil energy $Q_c(t)$ can be correlated instead of the outlet state. To do this, the inlet state must be known and so the mass flow rate of the coil water \dot{m} and the inlet water temperature T_{ci} must be known and be constant to use Eq. (39). T_{co} is the temperature at the outlet of the coils, c_p is the heat capacity of the coil water.

$$\dot{Q}_c = \dot{m}(h_{out} - h_{in}) = \dot{m}c_p(T_{co} - T_{ci}) \quad (39)$$

For the load and unload tests, separate circuits are needed. For the charging test, the heater in the hot circuit delivers a constant temperature to the water flowing into the coils. The heater also ensures a sufficiently high tank temperature needed as preparation for the discharging tests. When the tank water has the right temperature, the discharging test can start when the cold and chiller circuit guarantee a constant cold inlet temperature in the coils.



Figure 37: Plastic coil inside solar boiler.

The inside dimensions of the solar boiler are 138.5 x 48 x 48 cm. The boiler has a storage capacity of 300 l and has a double walled jacket made of polypropylene with PUR hard foam heat insulation [5]. A tube, where thermocouples are positioned, is connected to the lid of the tank as can be seen in Figure 38.



Figure 38: Thermocouples in lid of tank.

3.2.2 Hot circuit

The hot circuit was already built for other research before the start of this thesis, so all components were already there, and it was not necessary to change them in the context of this thesis.

3.2.2.1 Circulator pump

A Grundfos MAGNA 32-100 180 is used in the hot circuit. This is a circulator pump and has a delivery head of 10 m. This type of pump does not require a lot of maintenance and does not produce a great amount of noise. They are used for heating and cooling applications and for hot water recirculation. The circuit needs a pump to transport the water through the tubes, coils, heater and tank. The pump only works when there is overpressure available. In the LabVIEW code, only a start/stop button is provided to start/stop the pump. On the pump, push buttons are located to regulate the water flow in 11 operating points: zero to ten and a 'minimum flow' operating point. The datasheet of this pump is available in Appendix D.

3.2.2.2 Heater

The heater is manufactured by DIRAC Industries and delivers a maximum heat of 9 kW. The heater consists of three resistances, each with their own power controller. Resistance one and two are parallel connected. To model the heat absorbed by solar collectors, a heater is used. The temperature of the water through the pipes and coils is controlled by the heater. The voltage over the heater and so the power is regulated by the National Instruments Data-Acquisition (NI DAQ) system. A constant inlet temperature is required to implement the CTEFM on the set-up.

3.2.2.3 Three-way mixing valve

The mass flow rate in the hot circuit is controlled by the three-way mixing valve Danfoss 065Z0217 VRB3. This valve has a kvs value of 10 m³/h and actuator AME 25 082G3025. This actuator has a speed of 90.9 μm/s [72]. The valve controls the mass flow rate going into the coils by increasing or decreasing the flow through the heater. When a voltage of 10 V is applied over the valve, the valve is completely open and there is no return from the heater directly to the valve. The datasheet of this valve is displayed as Appendix E and the datasheet of the actuator is displayed as Appendix F.

3.2.2.4 Coriolis mass flow measuring system

The mass flow meter in the hot circuit is the coriolis mass flow measuring system Endress+Hauser PROMASS 80F. It has a measurement error of ±0.15% [73]. A constant mass flow is needed to implement the CTEFM on the set-up. The datasheet of this device is displayed as Appendix G.

3.2.3 Cold circuit and chiller circuit

The cold circuit is expanded and the chiller circuit is added on to the original set-up. All components in these two circuits are designed and selected, except for the mass flow meter. This meter was firstly located on the original open cold circuit.

3.2.3.1 Plate heat exchanger

The X-marked BX8Tx10/1P of manufacturer SWEP was chosen for the plate heat exchanger. The plate heat exchanger exchanges heat from the cold circuit to the chiller circuit. This plate heat exchanger is needed to extract the heat from the solar boiler during the discharge tests. The chiller circuit is connected to the chiller on the roof of the building. The hottest temperature the hot circuit has during testing is 50°C, but for safety reasons 60°C is assumed. Presume that the chiller temperature is set on maximum 10°C and presume a heat loss of 1°C between the exchanger and the inlet of the coils. The expected temperature that the cold water must have at the outlet of the heat exchanger is approximately 19°C to enter the coils with a temperature of 20°C.

The mass flow rates used in the charging experiments are 2.5, 5 and 7.5 l/min and during discharging 5, 7.5 and 10 l/min. During charging, the heat absorbed by the tank water is the same as the heat delivered from the coil water. In ideal circumstances, the tank water receives the same heat transfer rate as the heater can deliver. The heater has a maximum power of 9 kW, so the maximum power the tank water can absorb is 9 kW.

In the paper from Martinez Fernandez De Cordova S. [5] who has done tests on the same set-up and with different coil materials, it is shown that during discharging with different constant inlet mass flow rates, the heat transfer rate through polymer coils at 5.5 l/min is 11 kW and approximately 12 kW at 7.5 l/min. Figure 39 shows the heat transfer rate as a function of volumetric flow rate for metal and polymer coils. So, the coils receive 12 kW from the tank water at a flow rate of 7.5 l/min during discharging. This means that the plate heat exchanger must be able to transfer a heat load of 12 kW. With the calculation tool of SWEP, the BX8Tx10/1P is selected with a pressure drop of 2.56 kPa on the boiler side. The BX8T can handle a heat load of 12 kW and a max flow rate of 4 m³/h, see Appendix I and Appendix J. It is designed for counter current flow [74], [75].

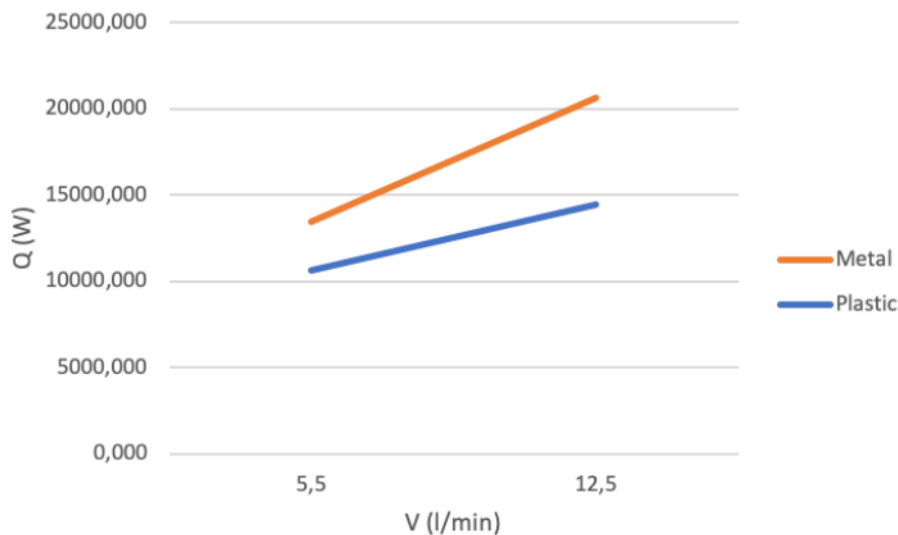


Figure 39: Comparison of the heat transfer rate for different mass flow rates at 60°C [5].

3.2.3.2 Circulator pump

The function of the three-way valve in the chiller circuit is to control the temperature in the cold circuit. By changing the flow rate through the chiller side of the plate heat exchanger, the amount of heat that is transferred through the heat exchanger is controlled. The plate heat exchanger will cool down the boiler during discharge testing. The pump in the cold circuit needs to control the mass flow rate which must be constant. A pump with 11 operating points, such as the pump in the hot circuit, is not sufficient: the pump must control the mass flow rate on a continuous basis.

There are two ways to connect the cold circuit or hot circuit to the solar boiler: that is via the coils or via the tank's in- and outlet. When the plate heat exchanger is connected to the coils inside the tank, the pressure that the pump has to overcome Δp_{pump} is that of the coils Δp_{coils} and the plate heat exchanger Δp_{phex} , see Figure 40. The pressure losses over the mass flow meter and the valves are negligible [76]. The pressure drop in the coils is 60 kPa when water is flowing through at 12 l/min and 15 kPa with a flow rate of 5.5 l/min [77]. The BX8Tx10/1P is selected with a pressure drop of 2.56 kPa on the boiler side. This means that the pump must deliver a minimum pressure of 62.56 kPa.

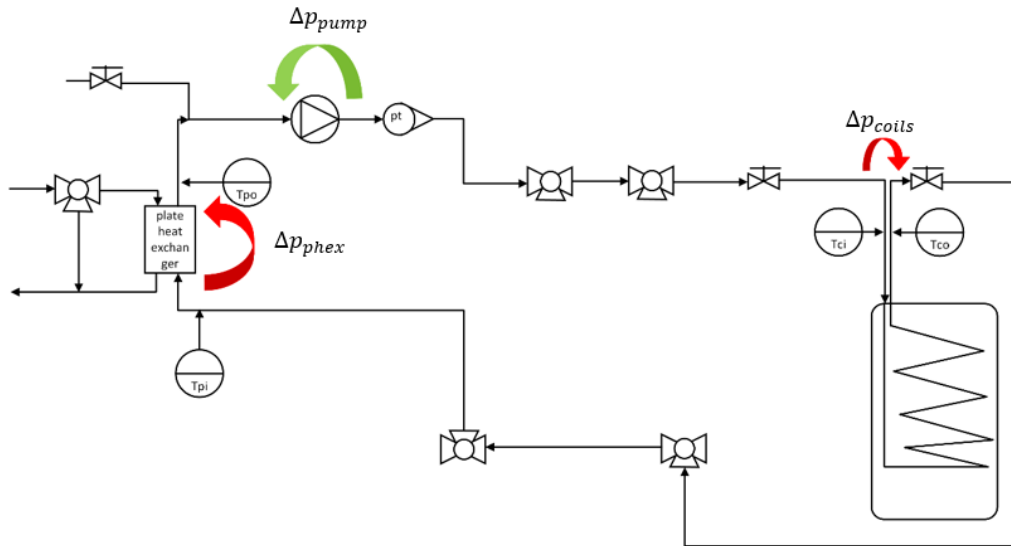


Figure 40: Scheme of cold circuit with components where the biggest pressure losses occur.

The pump in the cold circuit is the Grundfos MAGNA3 25-120 180. A circulator pump is again chosen for the same reasons as the pump in the hot circuit. In the group of circulation pumps, it was checked which pump best suits the set-up. With this kind of pump, it is possible to adjust the flowrate of the pump allowing for a variable flowrate through the set-up, without the need of an additional 3-way valve. All the other circulator pumps of Grundfos only have one, three, or more operating points, but do not work on a continuous basis. The pump has an efficiency of 73% when 12 l/min is delivered with a pressure drop of 65 kPa [78].

The pump contains eight control modes: $AUTO_{ADAPT}$, $FLOW_{ADAPT}$, proportional pressure, constant pressure, constant temperature, differential temperature, constant curve and the "assist" menu "multi-pump setup". The $AUTO_{ADAPT}$ control mode constantly adjusts pump performance based on the current system characteristics. When $FLOW_{ADAPT}$ is chosen, the pump will execute $AUTO_{ADAPT}$ to guarantee that the flow does not exceed the $FLOW_{LIMIT}$ value entered. The $FLOW_{LIMIT}$ is the maximum flow limit. The pump constantly checks and adjusts the flow to ensure that the $FLOW_{LIMIT}$ is not exceeded [79].

To execute the discharging tests, the pump's control mode 'constant curve' is chosen. This control mode is useful when an external controller is used. In 3.3, the LabVIEW program is explained and it is explained which external controller this is. The pump can switch from one constant curve to another, depending on the value of this external signal. The datasheet of the pump is given in Appendix K.

3.2.3.3 Electromagnetic flowmeter

The mass flow rate meter in the cold circuit is a magnetic inductive flowmeter KROHNE OPTIFLUX 4300 C with accuracy less than 0.5% of the measured value for a flow rate bigger than 2.5 l/min [76]. The mass flow meter in the cold circuit has the same purpose of the flow meter in the hot circuit. The datasheet of this flowmeter is attached in Appendix H.

3.2.3.4 Three-way mixing valve

The three-way mixing valve in the chiller circuit is the same as the one in the hot circuit, but it has a different actuator, namely AME 35 082G3022. This actuator has a speed of 0.33 mm/s [72]. The datasheet of this actuator is attached in Appendix L. The valve controls the mass flow rate going from the chiller \dot{m}_{chill} into the plate heat exchanger \dot{m}_{phex} . The flow coming from the chiller is split into a flow going to the plate heat exchanger and a flow that bypasses the plate heat exchanger \dot{m}_{bypass} , just as can be seen in Figure 41 and Eq. (40). Hereby, it controls the amount of heat extracted from the cool circuit and thus the water temperature at the inlet of the coils, given that a constant mass flow rate through the coils is maintained.

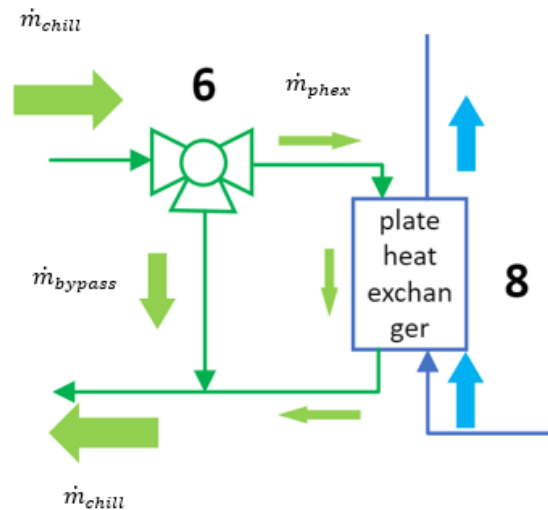


Figure 41: Scheme of chiller flow and the split-up at the mixing valve.

$$\dot{m}_{chill} = \dot{m}_{bypass} + \dot{m}_{phex}$$

(40)

3.2.4 Thermocouples

All thermocouples in the circuit are K-type thermocouples. There are six thermocouples in the circuit: before and after the plate heat exchanger, before the three-way valve in the hot circuit, after the hot mass flow meter (so before and after the heater) and before and after the coils. There are 11 operating thermocouples located in the tank tube, which can be seen in Figure 42. The top thermocouple is placed just below the water level. All the thermocouples are placed with a 15 mm vertical distance from each other.



Figure 42: Thermocouples in lid of tank.

Measuring the temperature after the heater is relevant to quantify the temperature increase of the water flowing through the heater. Measuring the temperature of the water at the inlet of the heater indicates the amount of lost energy to ambient air throughout the circuit. The thermocouple at the inlet of the coil is important because, during the test, this temperature needs to be constant at a predetermined value. The thermocouple at the outlet of the coils indicates how much energy is released/transferred to the water in the coils. The thermocouples before and after the plate heat exchanger measure the delivered heat to the chiller circuit. Finally, the thermocouples in the tank measure the temperature at different levels inside the tank. Because of stratification, the tank has different temperatures in height.

The tank is divided in 8 control volumes with each one or two thermocouples, as can be seen in Figure 43.

• T ₈
T ₁₁ • T ₇
• T ₆
• T ₅
T ₁₀ • T ₄
• T ₃
T ₉ • T ₁
• T ₀

Figure 43: Control volumes of the tank.

Thermocouple T₂ is defect so thermocouple T₁ and T₃ are located in a control volume that is 1/3rd larger than the other control volumes. The thermocouples measure the temperature every 5 seconds.

3.2.5 National Instrument Data Acquisition System

The thermocouples, pumps, electrical three-way valves, mass flow meters and the heater are connected to an NI DAQ-system. The NI DAQ-System consists of six NI-modules. All thermocouples are connected to module one and five. The second module contains the pump of the hot circuit. All mass flow meters are connected to the third module. Module four contains the pump of the cold circuit, the three heaters and the three-way mixing valve of the hot circuit. The last module encloses the three-way mixing valve of the chiller circuit, presented in Table 10.

Module	NI number	Input/output	Component
Mod1	NI 9213	7	Thermocouple outlet coils
		8	Thermocouple inlet coils
		9	Thermocouple inlet heater
		11	Thermocouple inlet plate heat exchanger
		12	Thermocouple outlet heater
Mod2	NI 9482	0	Pump hot circuit
Mod3	NI 9203	0	Mass flow meter hot circuit
		3	Mass flow meter cold circuit
Mod4	NI 9263	0	Pump cold circuit
		1	Heater one and two
		2	Heater three
		3	Three-way valve hot circuit

Mod5	NI 9213	0	Thermocouples tank
		...	
		11	
		14	Thermocouple outlet plate heat exchanger
Mod6	NI 9263	0	Three-way valve chiller circuit

Table 10: NI DAQ modules with their inputs and outputs.

3.3 LabVIEW program

To read out the values of the thermocouples and mass flow meters and to control the pumps, electrical three-way valves and the heater, a LabVIEW program is used. The front panel of the program is divided into three spaces: the charging tab (Appendix M), the discharging tab (Appendix N) and the left side that displays necessary information for both test. In Appendix O, the program code in the block diagram is shown. To program some of the code, there has been looked to an already existing LabVIEW program about the solar boiler.

The values of all thermocouples of the set-up, the position of the electrical valves, the voltage send to the cold circuit pump and to the heater are displayed using numeric indicators. The cluster of numeric indicators which indicates all temperatures in the set-up is displayed in Figure 44. The values of the thermocouples located in the tank, the temperatures at the in- and outlet of the coil, at the in- and outlet of the heater and at the in- and outlet of the plate heat exchanger are displayed using a waveform chart. This type of chart is also used to display all mass flows rates.

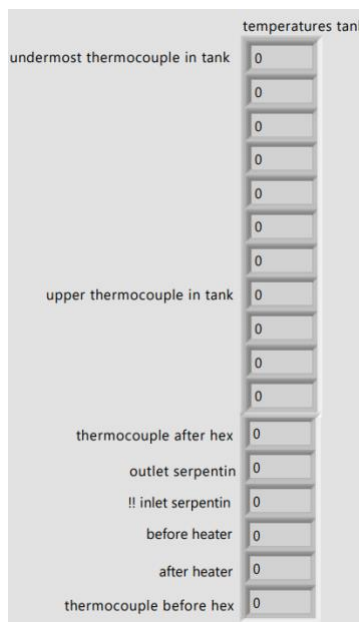


Figure 44: Cluster of numeric temperature indicators

In the LabVIEW code, DAQ assistants are used to communicate with the NI DAQ modules in the set-up. There are four types of DAQ assistants used: an assistant who ensures that an NI DAQ module generates a current or voltage to (a) specific component(s) (Figure 45), an assistant who is connected to an NI DAQ module who measures a current from (a) specific component(s) (Figure 46), an assistant who measures temperature with a thermocouple (Figure 47) and an assistant who generates a digital sample (Figure 48). Only the mass flow meters and thermocouples transmit a current to the NI DAQ system. The components who need a voltage to be driven are the valves, the pumps and the three resistances of the heater. The pump in the hot circuit is driven by a start/stop button in the front panel and uses the DAQ assistant who generates a digital sample. The pump in the hot circuit itself contains push buttons to set the desired mass flow. In Figure 46, the DAQ assistant measures currents from the mass flow meters and writes the Amperes' values to a measurement file.

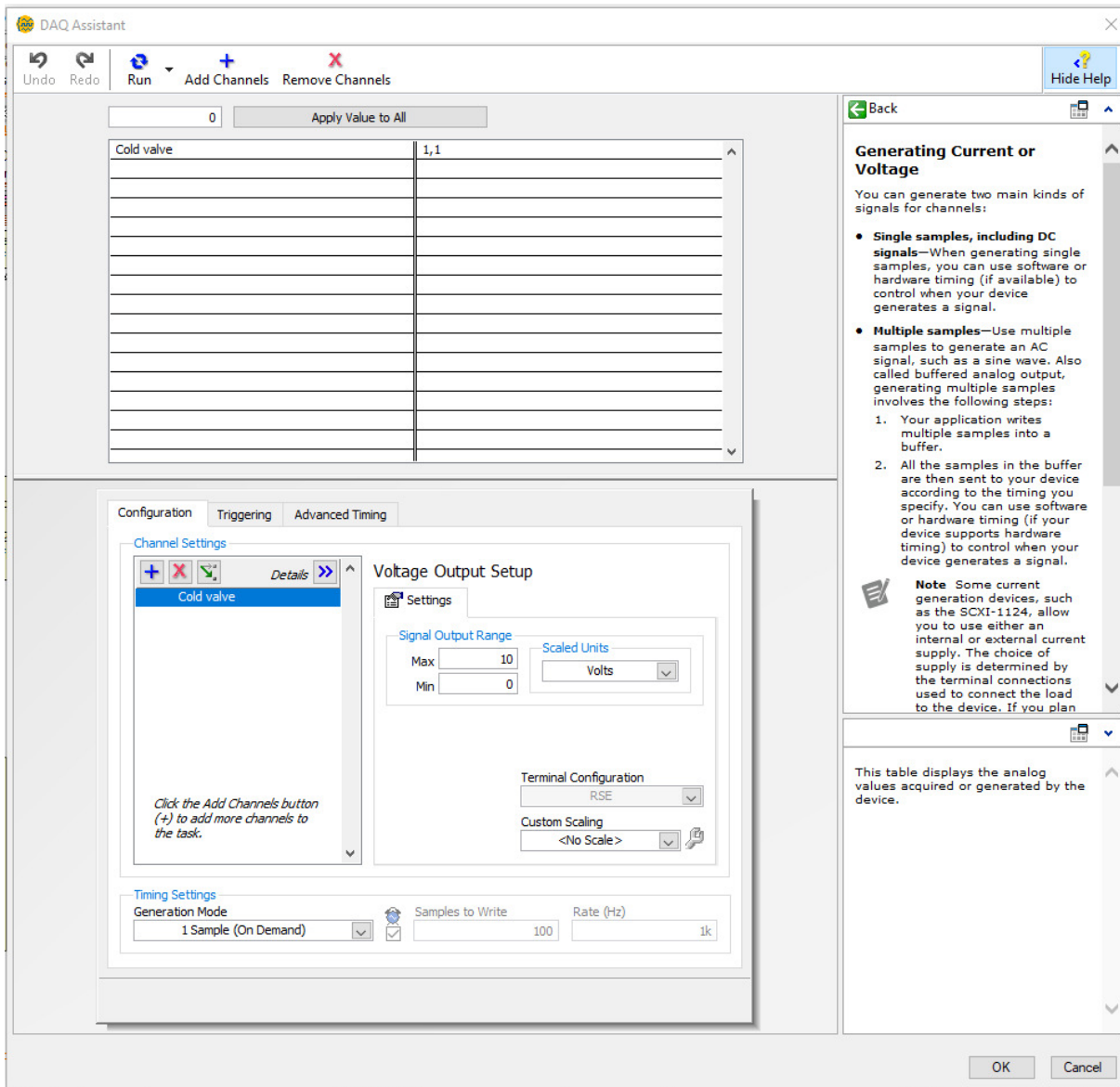


Figure 45: DAQ Assistant generating current or voltage.

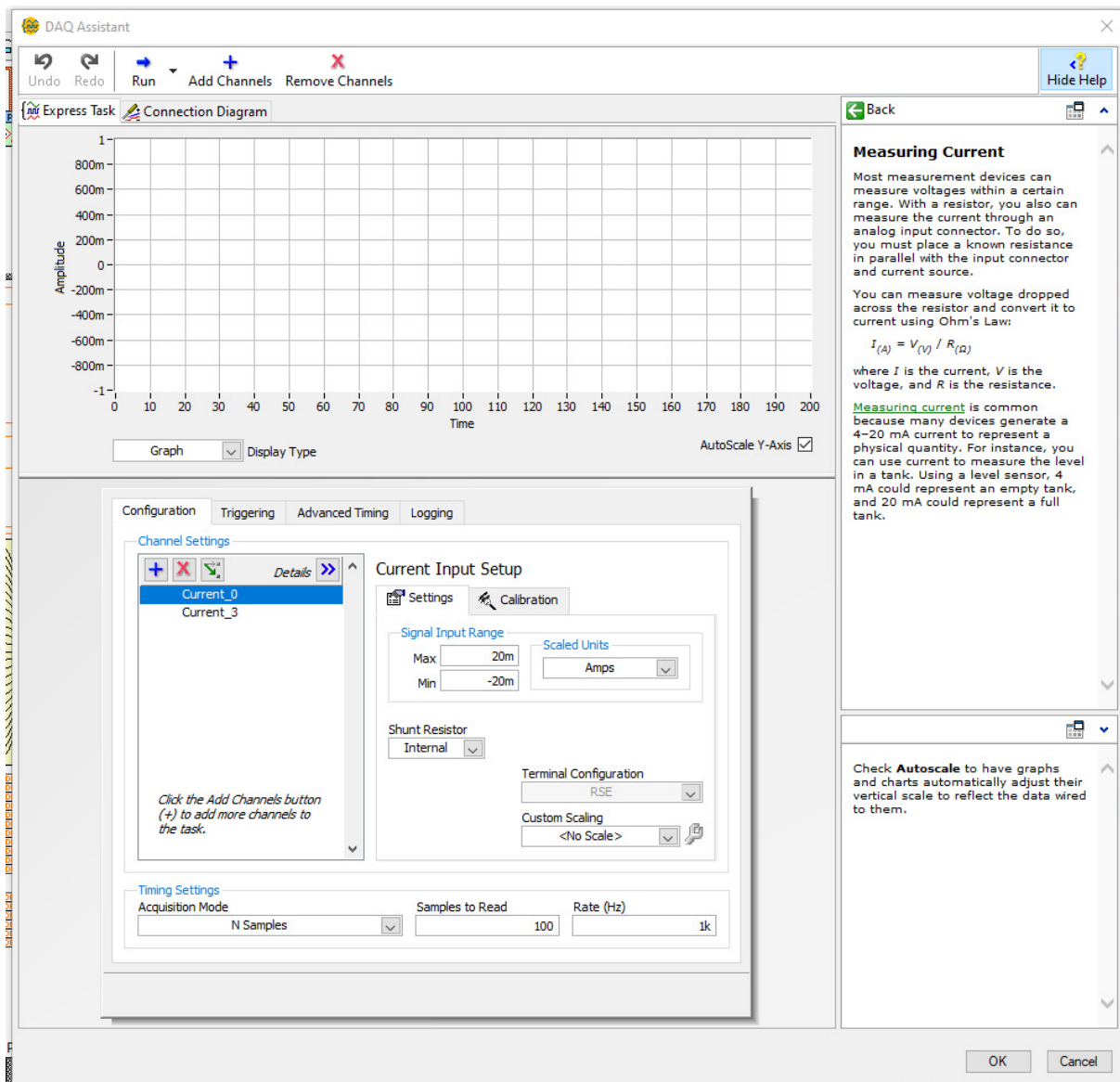


Figure 46: DAQ assistant who measures current.

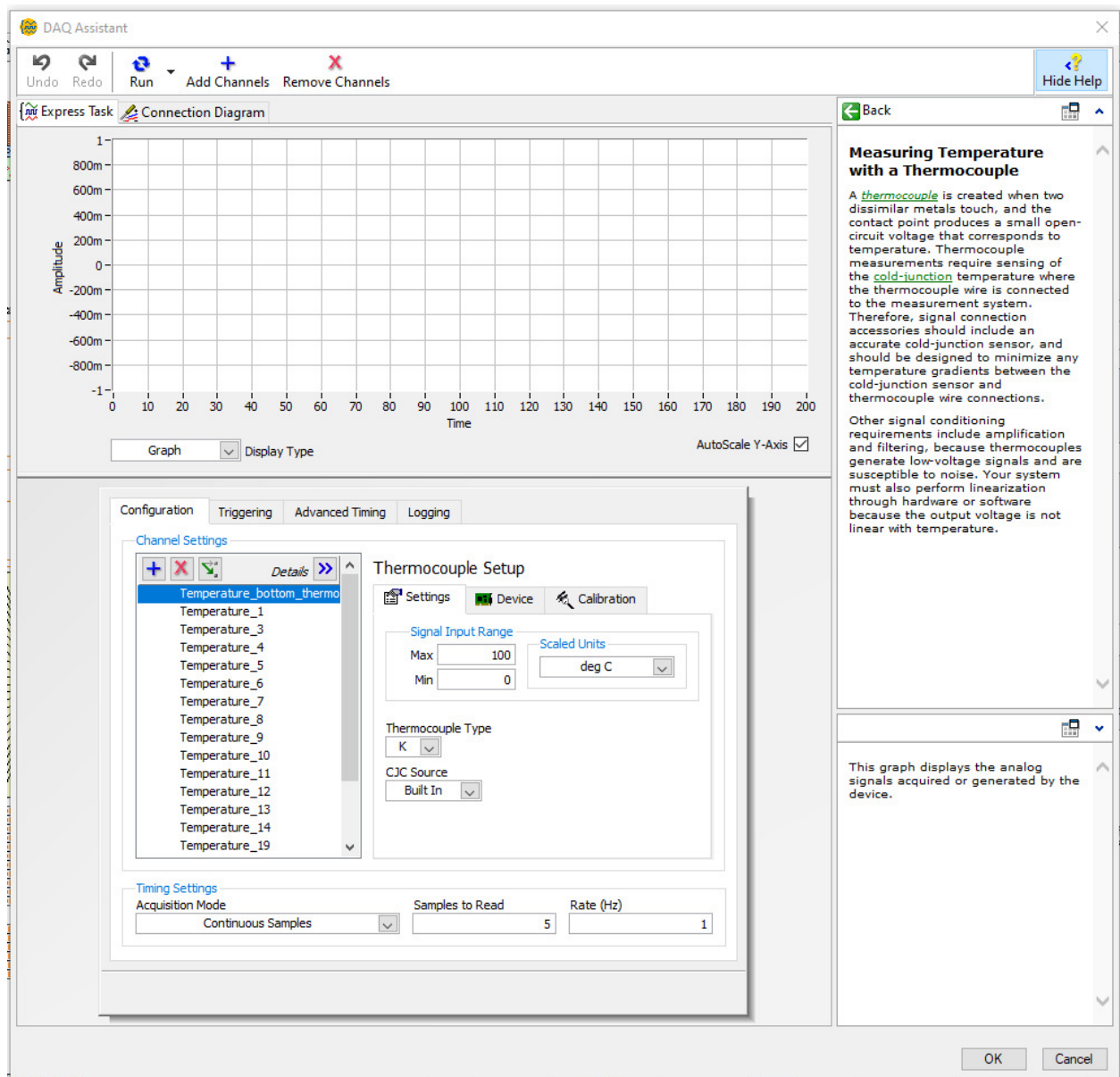


Figure 47: DAQ assistant who measures temperature with thermocouple.

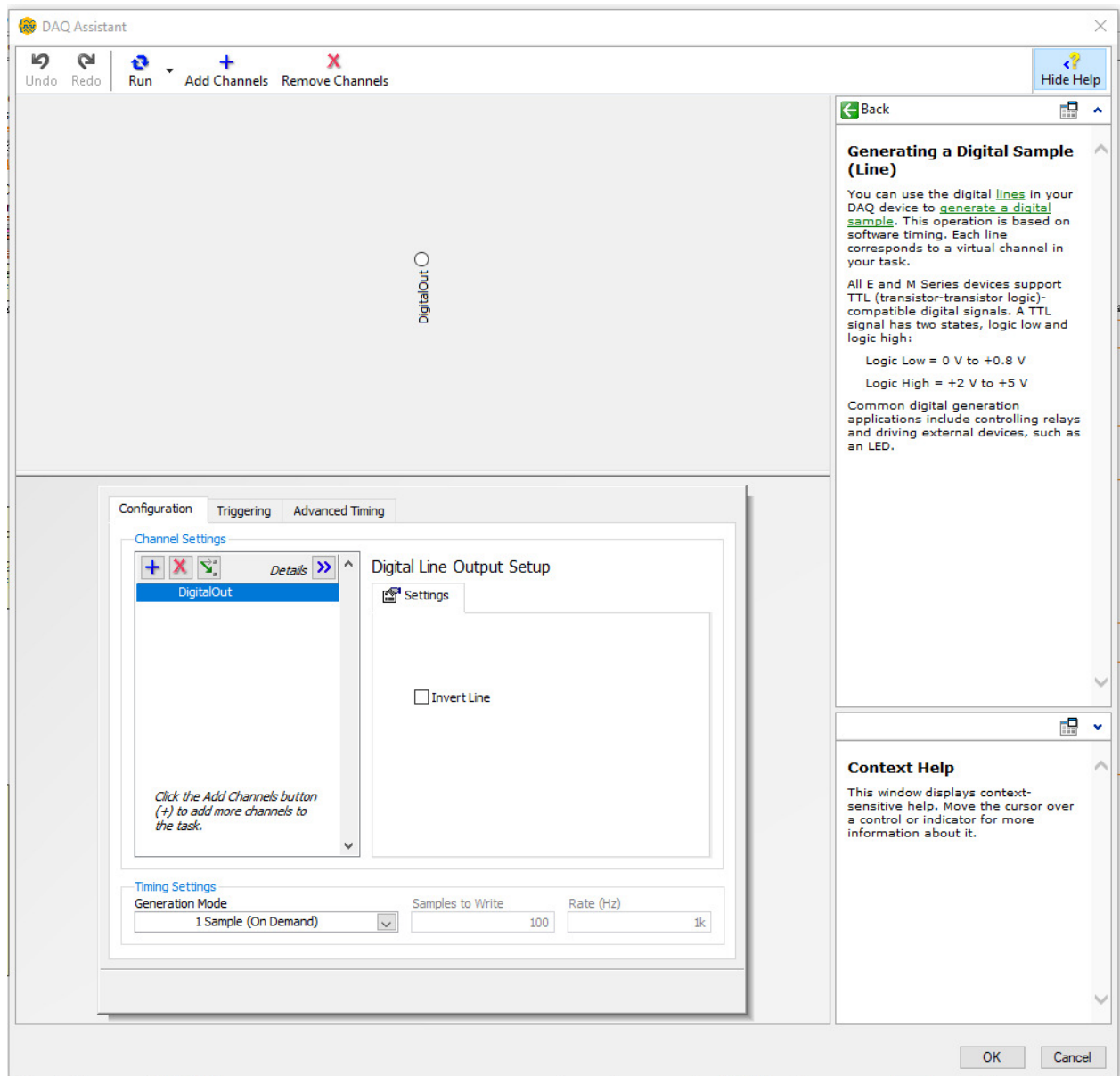


Figure 48: DAQ assistant who generates a digital sample.

Furthermore, in the LabVIEW code, three PID VI's are used to automatically control the two electrical valves, the pump in the cold circuit and resistance one and two of the heater. The PID controller transmits a voltage between zero and 10 Volts or a flow rate value in units kg/h to the components via the NI DAQ-system using a PID algorithm programmed in the PID VI. It also features an output range, a setpoint, a process variable, and a cluster control with the PID parameters. These PID parameters are found via a MATLAB program named Tunerfile, that was already in use by the research group.

To find the PID parameters using Tunerfile, firstly an input log file from LabVIEW is needed, where a step is created on the control variable. The control variables in this case are the two electrical valves, the pump in the cold circuit and resistance one and two of the heater. The process variables are different for each

control variable. The Tuner program finally finds PID and PI parameters for the PID controllers. These parameters are not always correct, so some of them had to be changed during the preparation of the tests.

In Figure 49, the true/false case structure containing the PID VI of the heater is shown. The PID of the heater ensures that the temperature at the inlet of the coils is constant by modifying the voltage over the heater.

The third resistance of the heater is manually controlled and this is because only one numeric control (containing the first and second resistance in parallel) can be connected to the PID VI of the heater. Also, as the load tests continue, the set voltage over the heater will drop to a very small value. If three resistances are used throughout the test, the set voltage on the heater must be smaller than if two resistances are used. Because the transmitted voltage in LabVIEW has a two decimal accuracy, it will be more difficult to control the heater at the end of each charging test. The third resistance of the heater was also only used during the preparations of the (dis)charging test and not during the actual tests.

The process variable of the heater PID is normally the inlet temperature of the coils, but this temperature cannot be selected, since the heater PID was also needed to heat up the tank as preparations for the discharging tests. When heating up the tank water, the water does not flow through the coils, but directly into the tank. That is why the outlet temperature of the heater is chosen as process variable. During load testing, there has been checked if the coils' inlet temperature remains the desired value, that is 30°C, 40°C, or 50°C, depending on which load test. The output range goes from zero to ten Volts.

The PI parameters selected by the Tunerfile are demonstrated in Table 11. Most PID parameters that the Tunerfile selected were too unstable and insufficient to hold the process variables constant.

	Heater	Valve hot circuit	Pump cold circuit	Valve cold circuit
K_c [min]	0.6627	0.0182	0.003	-0.0353
T_i [min]	0.7952	0.2351	0.0675	0.0913
T_d [min]	0	0	0	0.0168

Table 11: PI parameters for control variables, calculated by the Tunerfile.

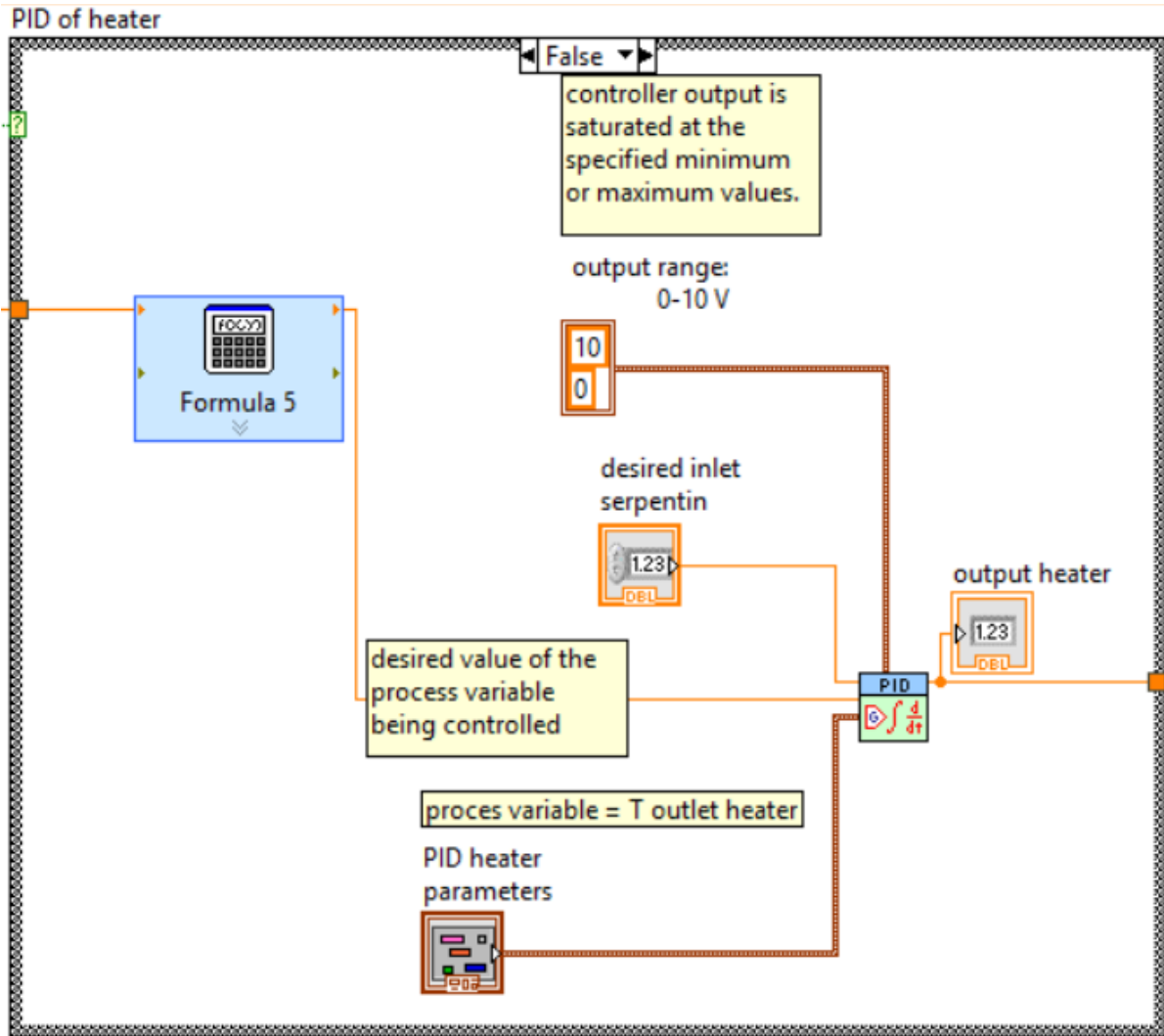


Figure 49: PID VI of heater in a true/false case structure.

The PID controllers for the valves and the pump are the same as for the heater but with other connected features. The process variable of the cold circuit pump PID and the process variable of the hot circuit valve PID are the desired mass flow rate in the cold circuit and desired mass flow rate in the hot circuit respectively. The process variable of the valve in the chiller circuit is the desired cold temperature at the outlet of the plate heat exchanger during discharging, which is approximately 19°C for the inlet coil temperature to remain 20°C. Selecting the coil inlet temperature as process variable for the chiller valve PID for finding the PID parameters would have been better, but there was no time left to reselect the PID parameters using the Tunerfile.

Finally, on the front panel, there can be chosen to enable the writing to a data file. Almost all data in the block diagram is connected to the Write To Measurement File function which transports this data to an Excel file. This Excel file contains the time of each sample (every five seconds), the mass flow rates in the hot and cold circuit, the values of all thermocouples and the voltages over the two electrical valves, over the pump of the cold circuit, and over the first and second heater resistance.

3.4 Measurement procedure

All process parameters during testing are known by measurement equipment and the communication between the NI DAQ-system and LabVIEW. All data is analysed using MATLAB.

3.4.1 Accuracies

The mass flow in the hot circuit is measured by the Coriolis flowmeter Proline Promass 80F and in the cold circuit by Electromagnetic flowmeter Krohne OPTIFLUX 4300. The temperatures in the whole set-up are measured with the same type of thermocouples type K which have an accuracy of 0.1°C. The accuracy of the measurement equipment can be found in Table 12.

Measurement equipment	Accuracy
Electromagnetic flowmeter Krohne OPTIFLUX 4300	±0.20-0.22% (for 5-10 m/s)
Coriolis flowmeter Proline Promass 80F	±0.15%
K-type thermocouple (°C)	0.1°C

Table 12: measurement equipment and their accuracies

Two types of tests are used: charging tests and discharging tests.

3.4.2 Charging tests

The procedure of a charging test is the following: the water in the tank must have an initial temperature of 20°C and the water at the inlet of the coils must have a temperature of 30, 40 or 50°C. The mass flow rates must be 150, 300 and 450 kg/h throughout the whole test, as can be seen in Table 13. The cycle ends when the tank water has the same temperature as the coils' inlet.

	30°C	40°C	50°C
150 kg/h	X	X	X
300 kg/h	X	X	
450 kg/h	X		

Table 13: Charging test matrix.

Before the actual start of the charging test, preparations are performed. The first step of the preparation of the charging test is cooling the tank water down to 15°C (for the 30°C charging tests) and 10°C (for the 40 and 50°C test) before heating up the HTF, as can be seen in Figure 50. The reason why will be explained in a following paragraph.

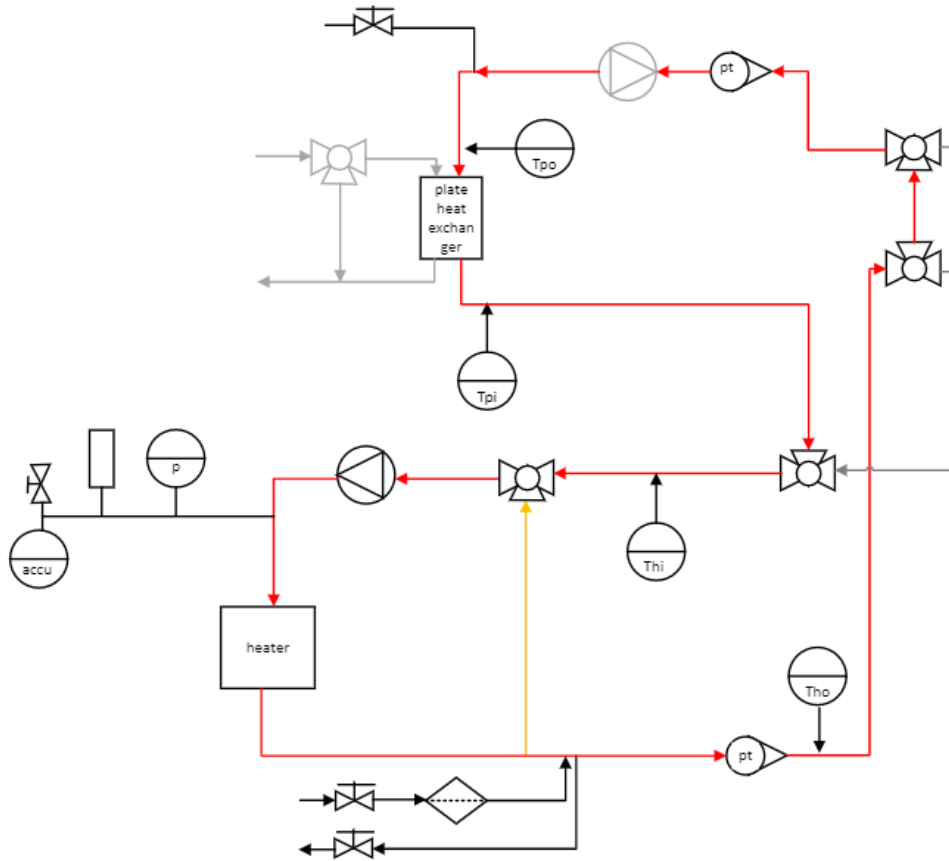


Figure 51: Preparations of the charging test: bringing the tank water to a constant temperature.

The heater is set on 80% of his power to not overheat the heater and the third heater is turned up. The mixing valve in the hot circuit is set on one Volt, which means 90% retour (yellow arrow). As the temperature of the heater's outlet approaches the desired temperature (30, 40 or 50°C), the mixing valve is set gradually from one to ten Volts.

At this moment of test preparation, the water volume of the coils is on the same low temperature of the tank water. When the HTF in the tubes has the desired temperature, the third step is to switch the hot circuit directly to the tank, as can be seen in Figure 52.

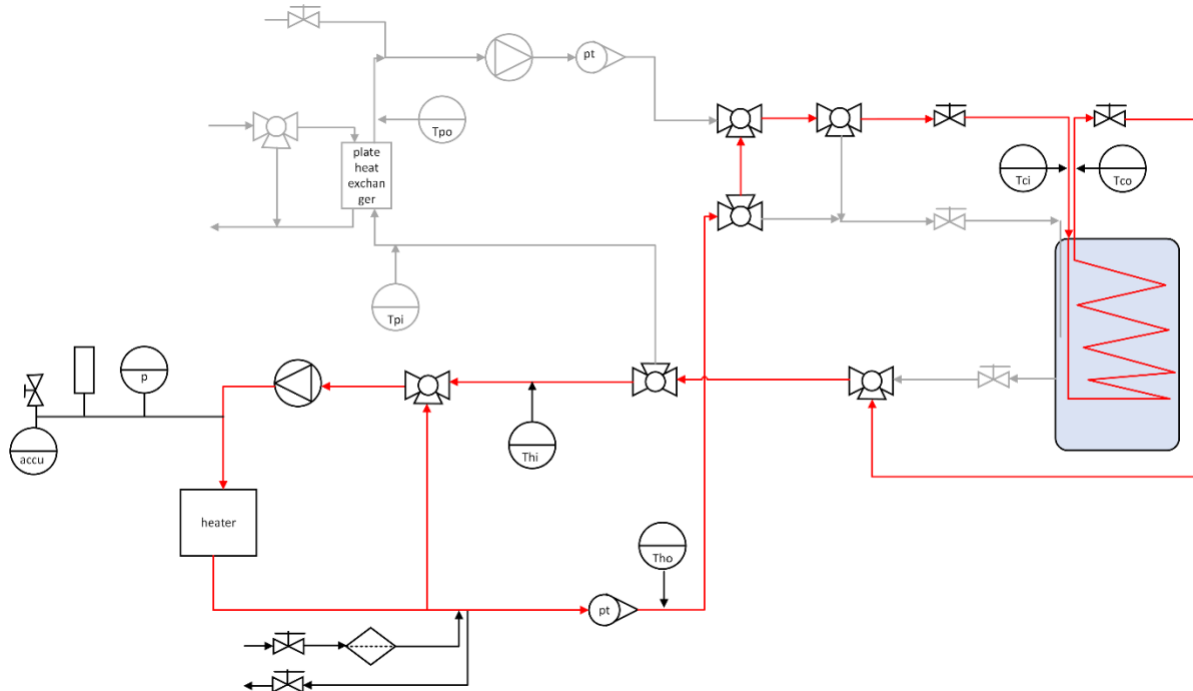


Figure 52: Scheme of solar boiler set-up during charging.

Now the HTF is flowing through the tubes of the hot circuit and through the coils in the tank. The volume of coil water which has a low temperature, is now mixed with the warmed up tube water. This causes the HTF to drop in temperature. The heater is now running at full capacity to heat up the HTF to the desired temperature, still using the third heater. This causes the tank water to increase in temperature, because hot water is flowing through the coils. The mixing valve in the hot circuit is set on 10% of his maximum opening to heat up the tank as little as possible, but to still have a read-out thermocouple value at the outlet of the mass flow rate meter in the hot circuit. So almost all hot water is bypassed by the valve back to the heater, except the 10% that flows through the mass flow meter to read out the temperature there. When the HTF temperature at the outlet of the heater is equal to the desired temperature, the PID of the hot circuit valve is turned on and the voltage over the third heater resistance is shut off. The PID of the heater is also turned on.

The preparations are now done and the actual charging test can start. This is done by enabling the writing to the measurement Excel file when the tank water has a temperature of 20°C, the coil inlet has a constant temperature of 30, 40 or 50°C and the mass flow rate of the HTF remains 150, 300 or 450 kg/h. Then, the official test is started. The test is stopped when the difference between the coil inlet and outlet temperature remains the same.

3.4.3 Discharging tests

The procedure of a discharging test is the following: the water at the inlet of the coils must have a temperature of 20°C and the water in the tank must have a temperature of 30 or 50°C.

To execute the tests, the pump's control mode 'constant curve' is chosen, because the external PID pump controller is installed in the LabVIEW program. Depending on the value of the external signal, the pump can

switch from one constant curve to another. The factory setting for the minimum curve is 28%, but this is manually changed to 21%, the lowest setting possible, as preparations for the tests. As a result, the minimum flow rate possible is 240 kg/h. That is the reason why flow rates 300, 450 and 600 kg/h are chosen, as presented in Table 14.

	30°C	50°C
300 kg/h	X	X
450 kg/h	X	X
600 kg/h	X	X

Table 14: Discharging test matrix.

Before the actual start of the discharging test, preparations must be performed. The first step of the preparation of a discharge test is heating up the tank water. This is done by connecting the hot circuit directly to the tank's in- and outlet and not via the coils, as Figure 53 displays. The third heater resistance is set to full capacity, the valve of the hot circuit is completely open so there is no return, and the PID of the heater is set to 10°C more than the desired temperature that the tank must have. The reason for this is the same as for the charging test and will be explained in the next paragraph.

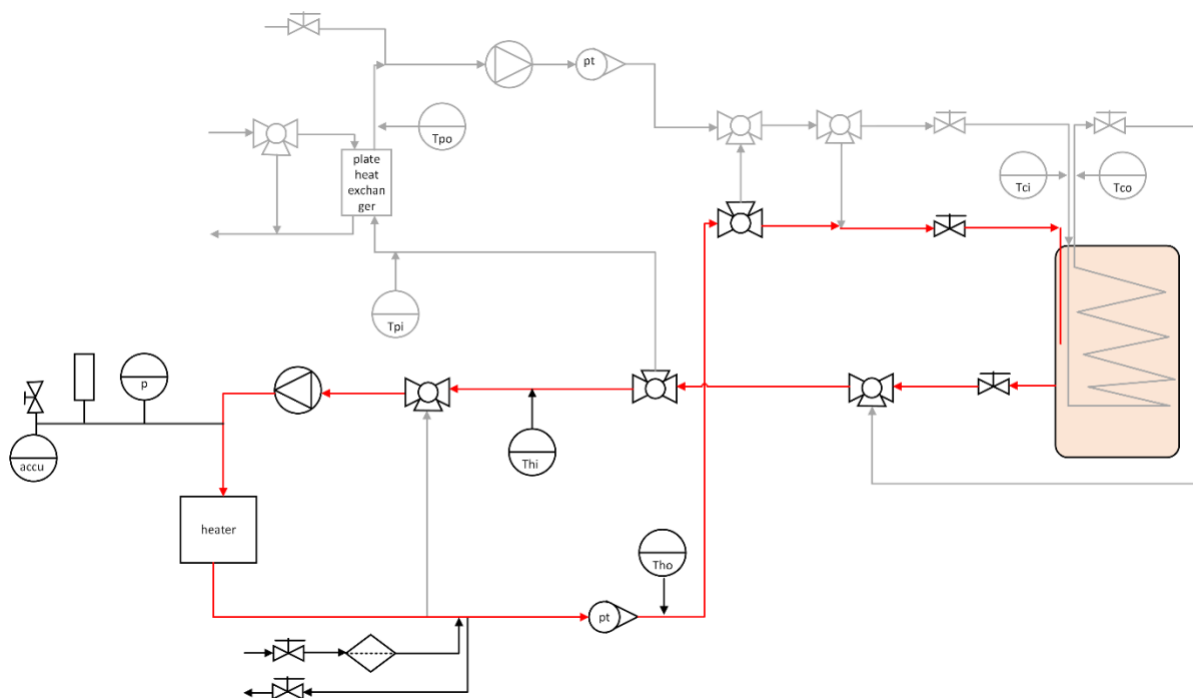


Figure 53: Heating up the tank.

The second step in the preparation before the discharge test is connecting the cold circuit to the coils, as can be seen in Figure 54. The PID controller of the plate heat exchanger is turned on in order to set the temperature at the outlet of the plate heat exchanger at approximately 19°C, so that the temperature at the coils' inlet would remain 20°C. The plate heat exchanger is able to directly transfer all necessary heat.

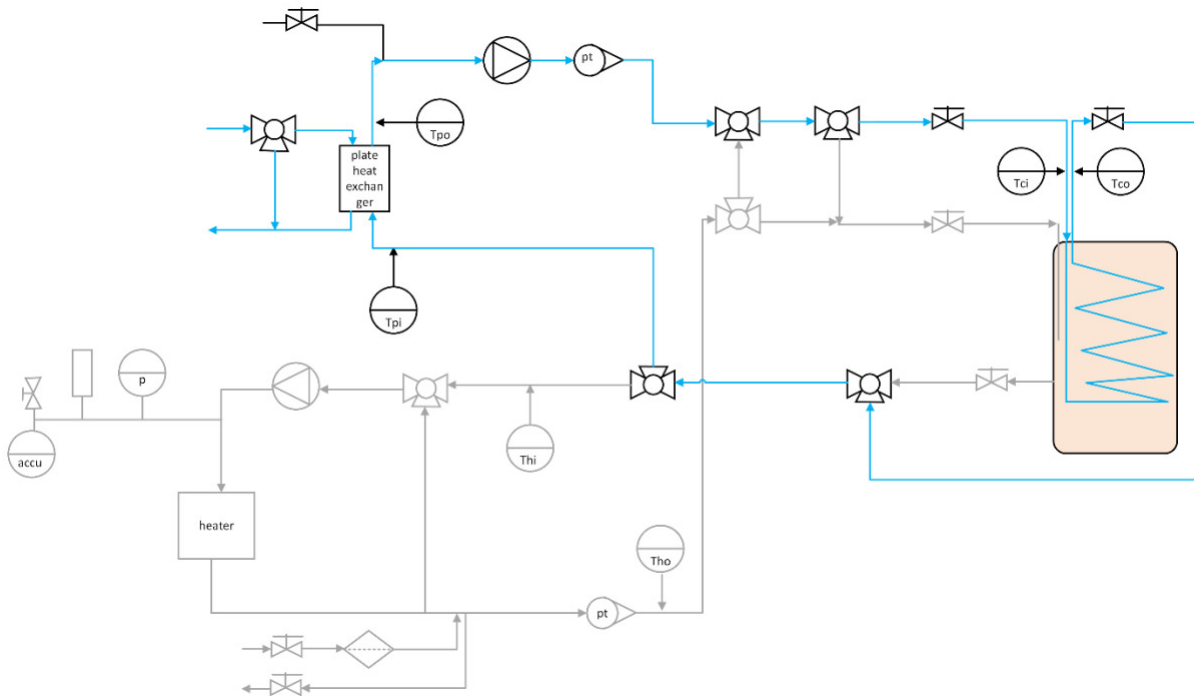


Figure 54: Scheme of solar boiler set-up during discharging.

When the pump delivers the desired constant mass flow rate and the chiller valve ensures that the inlet temperature of the coils is a constant 20°C, discharge preparation process is now fully performed and the actual test can start. That is enabling the writing to the Excel file at the moment that the tank temperature is 30 or 50°C, depending on which type of test.

3.5 Data reduction

To be able to perform the CTEFM, the mass flow rate and the inlet temperature of the HTF, the water in the coils, should be constant. When these two conditions are met, there must be looked at the energy balance firstly to observe if the tank energy throughout the test is the same as the heat transferred through the coil.

For the charging tests, as well as for the discharging tests, the energy balance should be correct if the heat loss to the environment is neglected. When assuming the total solar boiler as a control volume, it is an open system that does not work in steady state, as can be seen in Figure 55. To find the energy balance, the first law of an open system is first established, as presented in Eq. (41).

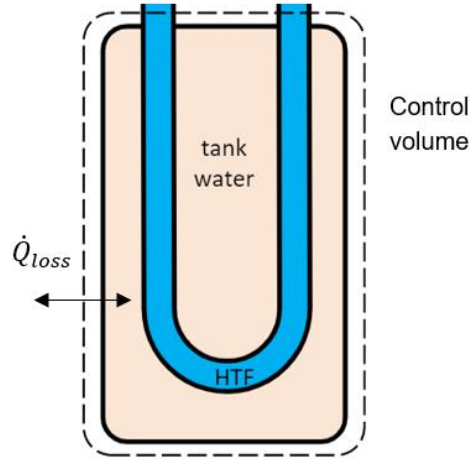


Figure 55: Simplified scheme of solar boiler as control volume.

$$\dot{Q} - \dot{W} + \sum_{inlet} \dot{m} \left(h + \frac{v^2}{2} + gz \right) - \sum_{outlet} \dot{m} \left(h + \frac{v^2}{2} + gz \right) = \frac{dE_{cv}}{dt} \quad (41)$$

$\frac{dE_{cv}}{dt}$ is the rate of change of the internal, kinetic and potential energy. The rate of change of the kinetic and potential energy is zero, so $\frac{dE_{cv}}{dt}$ is the rate of change of the internal energy, as can be seen in Eq. (42). The control volume also does not move, nor undergoes a displacement, nor performs work.

$$\dot{Q}_{loss} + \sum_{inlet} \dot{m}h - \sum_{outlet} \dot{m}h = \frac{dU}{dt} \quad (42)$$

\dot{Q}_{loss} is not measured and is neglected since the solar boiler is covered in insulation. This reduces the first law of this open system to Eq. (43). The mass flow rate at the inlet is the same as at the outlet of the coils. T_{ci} and T_{co} are the coils' in- and outlet temperatures. T_{tank1} and T_{tank2} are the start and end temperatures of the tank water, and \dot{m}_c is the mass flow in the coils. Eq. (43) shows that the heat capacity at constant volume is the same as the heat capacity at constant pressure for incompressible substances such as solids and liquids.

$$\dot{m}(h_{inlet} - h_{outlet}) = \dot{m}_c c_p (T_{ci} - T_{co}) = \frac{dU}{dt}$$

$$U(t) = m_t c_v (T_{tank}(t) - T_{tank,initieel})$$

$$\frac{dU}{dt} = m_t c_v \left(\frac{dT_{tank}}{dt} \right) \approx m_t c_v \left(\frac{T_{tank}(t + \Delta t) - T_{tank}(t)}{t + \Delta t - t} \right) = m_t c_v \left(\frac{T_{tank}(t + \Delta t) - T_{tank}(t)}{\Delta t} \right)$$

$$\dot{m}_c c_p (T_{ci} - T_{co}) = m_t c_v \left(\frac{T_{tank}(t + \Delta t) - T_{tank}(t)}{\Delta t} \right)$$

$$c_p = \left(\frac{\partial h}{\partial T} \right)_p = \frac{du}{dt} = c_v$$

$$\dot{m}_c c_p (T_{ci} - T_{co}) \cdot \Delta t = m_t c_v (T_{tank}(t + \Delta t) - T_{tank}(t)) \quad (43)$$

Eq. (43) is the energy balance, at any given moment during the charging or discharging cycle, t . Rewriting of the equations finally gives Eq. (44).

$$\dot{m}_c c_{p,c} (T_{ci}(t) - T_{co}(t)) * \Delta t = \rho_t V_t c_{p,t} (T_{tank}(t + \Delta t) - T_{tank}(t)) \quad (44)$$

ρ_t is the mass density of the tank water and V_t is the tank water's volume. $c_{p,c}$ is the heat capacity of the coil water and $c_{p,t}$ is het heat capacity of the tank water. $T_{tank}(t + \Delta t)$ and $T_{tank}(t)$ are the temperatures of the tank at any given moment, t . In order to discretise the derivative in time of the internal energy, the difference of the internal energies at a time, $t + \Delta t$ and t is divided by the elapsed time between these two measurements, Δt . As mentioned in section 3.2.4 Thermocouples, the tank volume is divided in 8 control volumes, as can be seen in Figure 56.

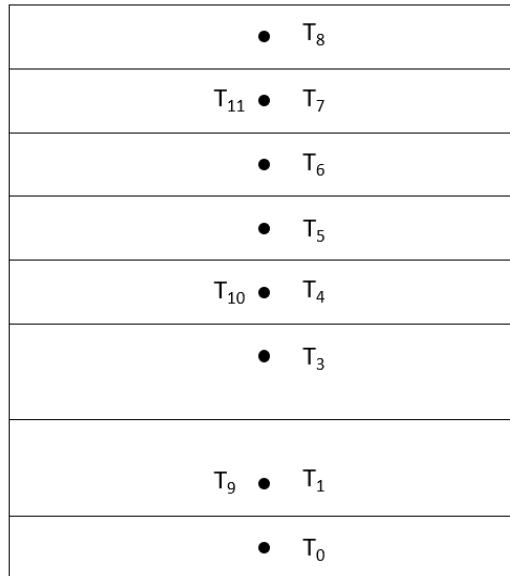


Figure 56: Control volumes of the tank.

Because the LabVIEW program exports data every five seconds, Eq. (44) can be expanded to Eq. (45). $c_{p,c,av}$ is the heat capacity of the average between the coils' in- and outlet temperature. $c_{p,t,av}$ is the heat capacity of the average control volume's temperatures between 5 seconds.

$$\begin{aligned}
 Q_c(t) &= \dot{m}_c c_{p,c,av} (T_{co}(t) - T_{ci}(t)) \cdot \Delta t_{5s} = \sum_{k=cv0}^{cv8} \rho_k V_k c_{p,t,av} (T_k(t + \Delta t_{5s}) - T_k(t)) = Q_t(t) \\
 Q_{total} &= Q_{previous} + Q_{new} = Q_{previous} + \dot{m}_c c_{p,c,av} (T_{co}(t) - T_{ci}(t)) \cdot \Delta t_{5s} \\
 Q_{total,c}(t) &= \sum_{i=0}^t \dot{m}_c c_{p,c,av} (T_{co}(i) - T_{ci}(i)) * \Delta t_{5s} \\
 Q_{total,t}(t) &= \sum_{i=0}^t \sum_{k=cv0}^{cv8} \rho_k V_k c_{p,t,av} (T_k(i + \Delta t_{5s}) - T_k(i))
 \end{aligned} \tag{ 45 }$$

Q_c is the amount of energy which is transferred from the coils to the tank water at any given moment t . Q_t is the amount of energy added to the tank water at any given moment t , added in an arbitrary time interval Δt . In order to get the total stored energy, these values therefore must be calculated for every period of time and be added to the previous value. These values are thus integrated values.

It is now possible to calculate the energy that is delivered to the tank by using the left-hand side of the equation, but also by using the right-hand side of the equation. If there are no or negligible heat losses present, both should be equal. This is called closing the energy balance. Both the left-hand side and the right-hand side of the equation quantify an energy, expressed in Joules.

According to the theory of Beyne et al. [71], the energy fraction is given by Eq. (46) and is defined as the stored energy divided by the maximum amount of energy that is stored in the tank at the end of the charging cycle, $Q_{c,max}$, and where $Q_{total,c}(t)$ the amount of heat is that is stored at any given time, t .

$$\alpha(t) = \frac{Q_{total,coils}(t)}{Q_{c,max}} \tag{ 46 }$$

The problem of fitting the energy fraction function $\alpha(t)$, is divided into solving for a correlation between $t_c(\alpha_i)$ values as can be seen in Eq. (47).

$$t_c(\alpha_i) \text{ for which } Q_c(t) = \alpha_i \max Q_c(t) \tag{ 47 }$$

After this, a function for the charging time is found and the parameters p of that function is determined for several energy fractions α_i , as Eq. (48) demonstrates.

$$t_c(\alpha_i) = f(\dot{m}; h_{in}; p(\alpha_i)) \tag{ 48 }$$

Mean efflux of energy between two energy fractions is shown in Eq. (49).

$$\bar{Q}_f^{\alpha_1, \alpha_2} = \frac{\alpha_1 - \alpha_2}{f(\dot{m}; h_{in}; p(\alpha_2)) - f(\dot{m}; h_{in}; p(\alpha_1))} \Delta U \quad (49)$$

Mean outlet state between energy fractions is shown in Eq. (50).

$$\bar{h}_{out}^{\alpha_1, \alpha_2} = h_{in}(t_m) - \frac{\bar{Q}_f^{\alpha_1, \alpha_2}}{\dot{m}(t_m^{\alpha_1, \alpha_2})} \text{ with } t_m^{\alpha_1, \alpha_2} = \frac{f(\dot{m}; h_{in}; p(\alpha_2)) + f(\dot{m}; h_{in}; p(\alpha_1))}{2} \quad (50)$$

Eq. (45), (48), (49), and (50) are necessary in the CTEF model to define the outlet state of the solar boiler as heat exchanger. A general correlation for the total charging time is found in Eq. (51) with correlation parameters $A(\alpha)$, $B(\alpha)$, $C(\alpha)$ and $D(\alpha)$ in Eq. (52) and (53) [3], [70], [69]. The charging time is now written in function of ΔT , which is the difference between the coils' inlet temperature and the tank's initial temperature. The inlet temperature and mass flow rate experience variations throughout the course of the experiment. Therefore, these inlet conditions are not completely constant, and consequently, it is necessary to average the mass flow rate and inlet temperature in time.

$$t_c = \frac{Slope}{\Delta T} + Intercept \quad (51)$$

$$Slope = A(\alpha) + \frac{B(\alpha)}{\dot{m}} \quad (52)$$

$$Intercept = C(\alpha) + \frac{D(\alpha)}{\dot{m}} \quad (53)$$

4 RESULTS AND DISCUSSION

The six charging and six discharging experiments were executed. During all tests, the initial conditions were met, which are a constant inlet mass flow rate of the HTF and a constant inlet HTF temperature.

4.1 Linear regression

The uncertainty analysis can be found in Appendix P. The reason for these high values can be because of the fact that only a linear regression is performed on the thermocouple values and the thermocouples are not calibrated.

Because the thermocouples in the tank are not calibrated, linear regression was performed on the values estimated by the thermocouples and this using MATLAB. To do this, three calibration tests were executed.

During these tests, the hot circuit was connected to the tank's in- and outlet. Water on 30°C, 40°C and on 50°C was flowing through the tank's inlet. The tests were only stopped when the tank had reached 30°C, 40°C or 50°C and the tank temperature had stabilized. The 30°C, 40°C and 50°C temperatures were measured by the thermocouple at the outlet of the heater, so these temperatures needed to be constant. It is assumed that the value of the thermocouple after the heater is correct, even though it was not calibrated. The displayed tank thermocouple values were always higher than the tank's inlet temperature, as can be seen in Figure 57. All thermocouples were then reset according to Eq. (54) with y representing the new thermocouple value.

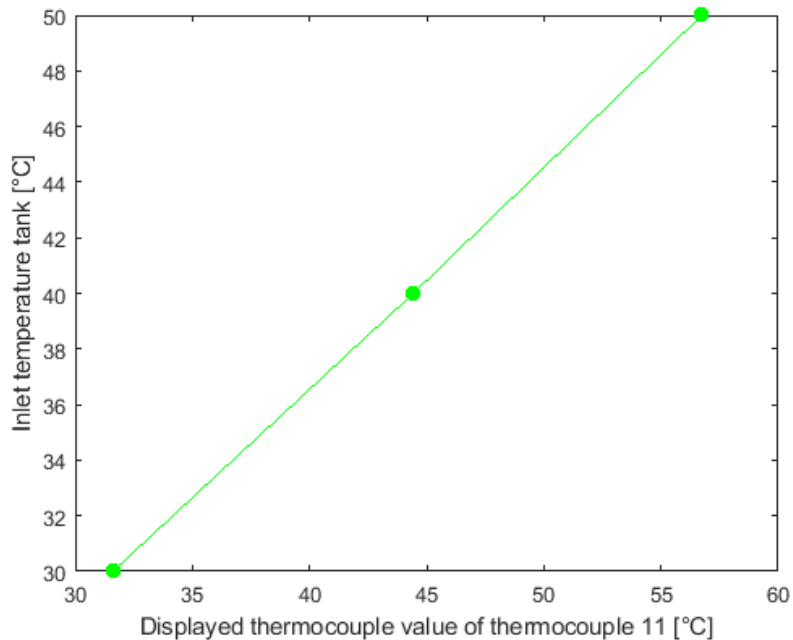


Figure 57: Linear regression on thermocouple 11.

$$y = \beta_0 + \beta_1 x$$

(54)

4.2 Charging tests

4.2.1 Initial conditions

The initial conditions for each experiment are a constant inlet mass flow rate of the HTF flowing through the coils as can be seen in Figure 58 and a constant inlet temperature. The tank's initial temperature is 20°C. To meet the initial conditions, PID controllers in LabVIEW are used. The used PI parameters for the heater and valve in the hot circuit can be found in Table 15.

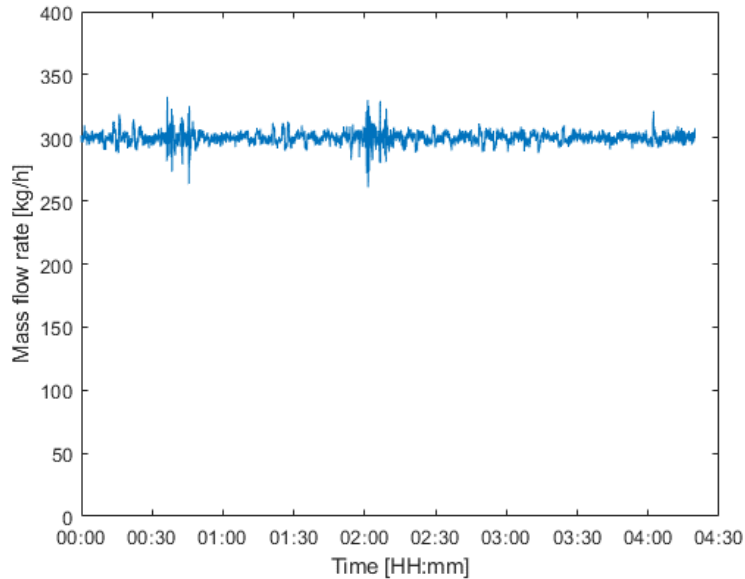


Figure 58: 300 kg/h mass flow rate of the 30° charging test.

		30°C		40°C		50°C	
		Heater	Valve	Heater	Valve	Heater	Valve
150 kg/h	K_c	0.6627	0.0182	0.6627	0.009	0.663	0.015
	T_i	0.7952	0.2351	0.7952	0.488	0.795	0.235
300 kg/h	K_c	0.6627	0.015	0.6627	0.015		
	T_i	0.95	0.2351	0.7952	0.2351		
450 kg/h	K_c	0.6627	0.007				
	T_i	0.2351	0.125				

Table 15: PI parameters of heater and valve for charging experiments.

4.2.2 Model calibration

4.2.2.1 Energy balance

To be able to perform the CTEFM, the mass flow rate and the inlet temperature of the HTF should be constant. When these two conditions are met, there must be looked at the energy balance firstly to observe if the tank energy throughout the test is the same as the heat released from the coils. For the charging tests,

as well as for the discharging tests, the energy balance should be correct if the heat loss to the environment is neglected.

Figure 59 shows that the mass flow rate at the inlet is constant. The inlet temperature of the heater is nearing the outlet temperature of the heater and the outlet temperature of the coils is nearing the inlet coil temperature. The temperature difference between the heater's outlet and the coils' inlet is due to heat loss to the environment, as well as for the temperature difference between the coils' outlet and heater's inlet. The heat loss between the coils' outlet and the heater's inlet is less than that between the heater's outlet and coils' inlet, because the HTF possesses a lower temperature after going out of the tank. The wide band of temperatures in Figure 59 is the values of the tank thermocouples. These are not all equal because of stratification. The band also ends higher than the heater's inlet temperature. That may be because the heat loss between the heater's outlet and coils' inlet is unknown and is thus not deducted from the new thermocouple values after linear regression.

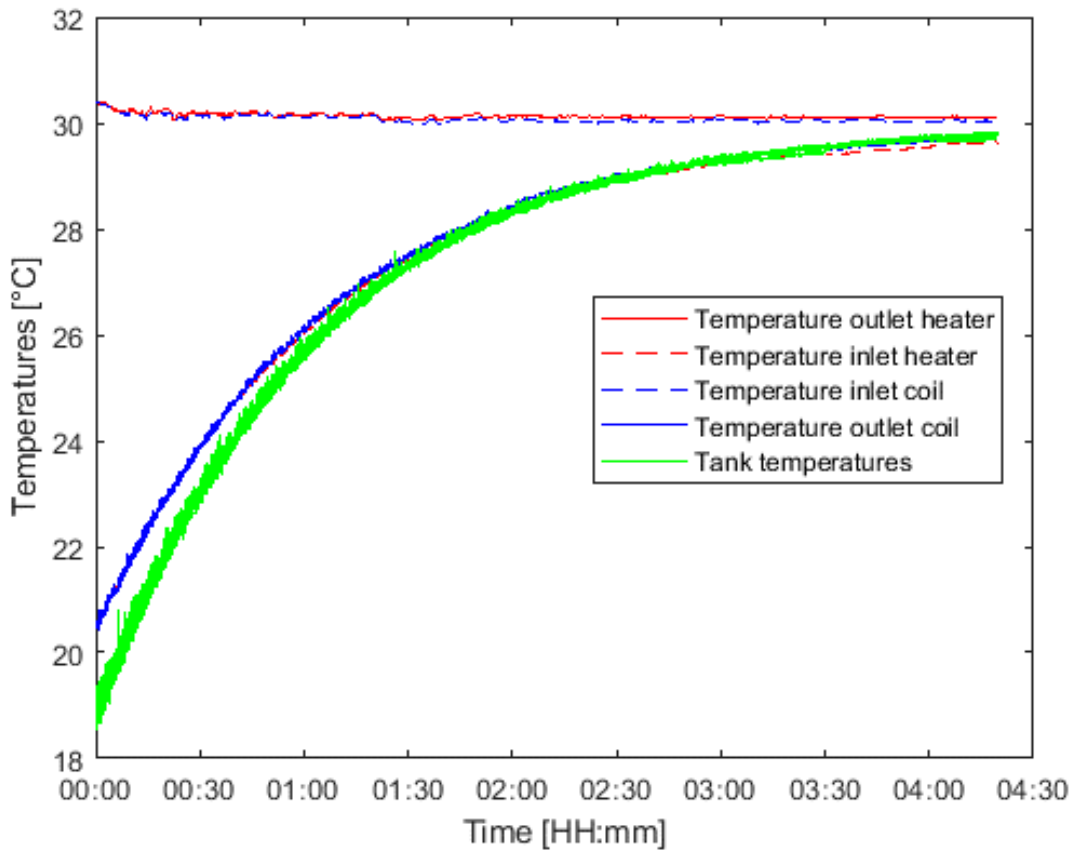


Figure 59: Temperatures of 30°C 300 kg/h charging test.

Eq. (55) is the energy balance, at any given moment during the charging or discharging cycle, t .

$$\dot{m}_c c_{p,c} (T_{ci}(t) - T_{co}(t)) * \Delta t = \rho_t V_t c_{p,t} (T_{tank}(t + \Delta t) - T_{tank}(t)) \quad (55)$$

Because the LabVIEW program exports data every five seconds, Eq. (55) can be expanded to Eq. (56).

$$Q_c(t) = \dot{m}_c c_{p,c,av}(T_{co}(t) - T_{ci}(t)) \cdot \Delta t_{5s} = \sum_{k=cv0}^{cv8} \rho_k V_k c_{p,t,av}(T_k(t + \Delta t_{5s}) - T_k(t)) = Q_t(t)$$

$$Q_{total,c} = Q_{previous} + Q_{new} = Q_{previous} + \dot{m}_c c_{p,c,av}(T_{co}(t) - T_{ci}(t)) \cdot \Delta t_{5s}$$

$$Q_{total,c}(t) = \sum_{i=0}^t \dot{m}_c c_{p,c,av}(T_{co}(i) - T_{ci}(i)) * \Delta t_{5s}$$

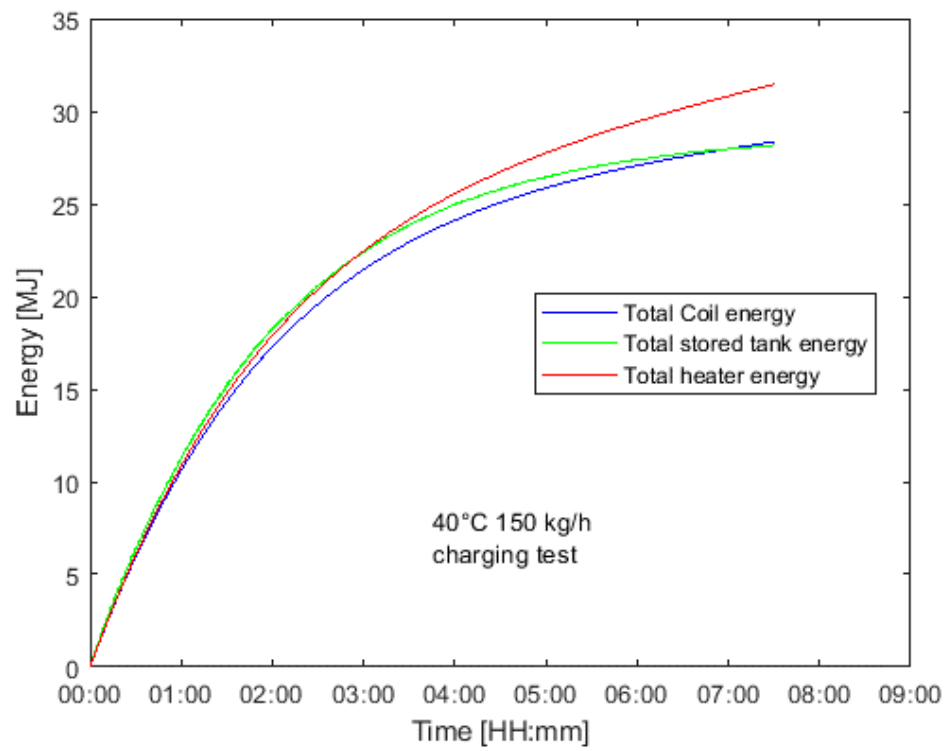
$$Q_{total,t}(t) = \sum_{i=0}^t \sum_{k=cv0}^{cv8} \rho_k V_k c_{p,t,av}(T_k(i + \Delta t_{5s}) - T_k(i))$$

$$Q_{total,c}(t) = \sum_{i=0}^t \dot{m}_c c_{p,c,av}(T_{co}(i) - T_{ci}(i)) * \Delta t_{5s} = \sum_{i=0}^t \sum_{k=cv0}^{cv8} \rho_k V_k c_{p,t,av}(T_k(i + \Delta t_{5s}) - T_k(i)) = Q_{total,t}(t) \quad (56)$$

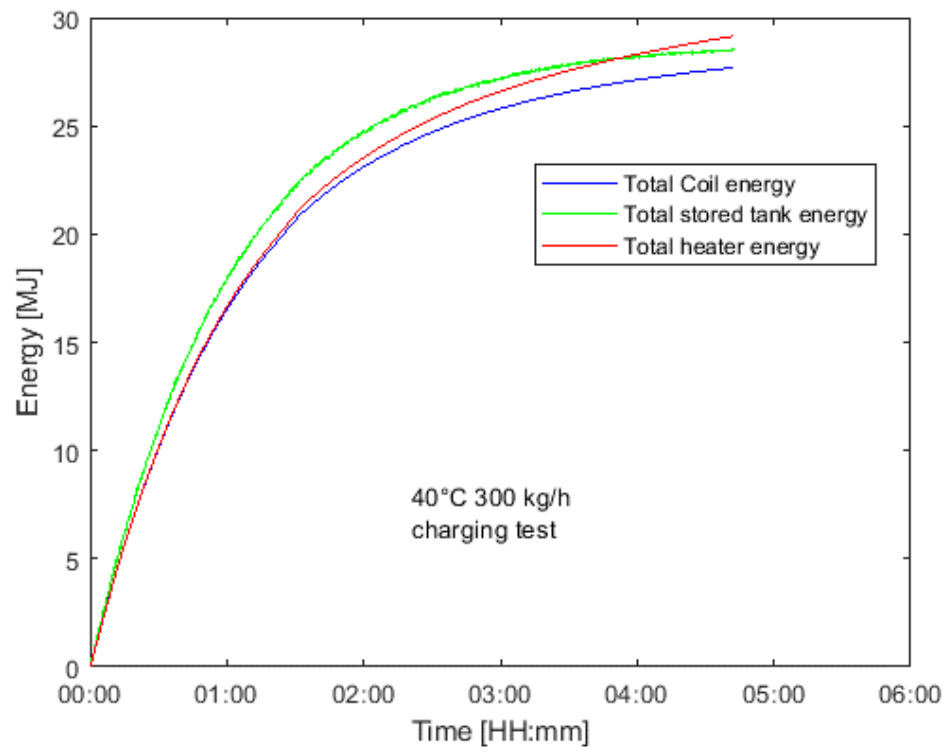
Q_c is the amount of energy which is transferred from the coils to the tank water at any given moment t . Q_t is the amount of energy added to the tank water at any given moment t , added in an arbitrary time interval Δt . In order to get the total stored energy, these values therefore must be calculated for every period of time and be added to the previous value. These values are thus integrated values.

It is now possible to calculate the energy that is transferred to the tank by using the left-hand side of the equation, but also by using the right-hand side of the equation. If there are no or negligible heat losses present, both should be equal. This is called closing the energy balance. Both the left-hand side and the right-hand side of the equation quantify an energy, expressed in Joules.

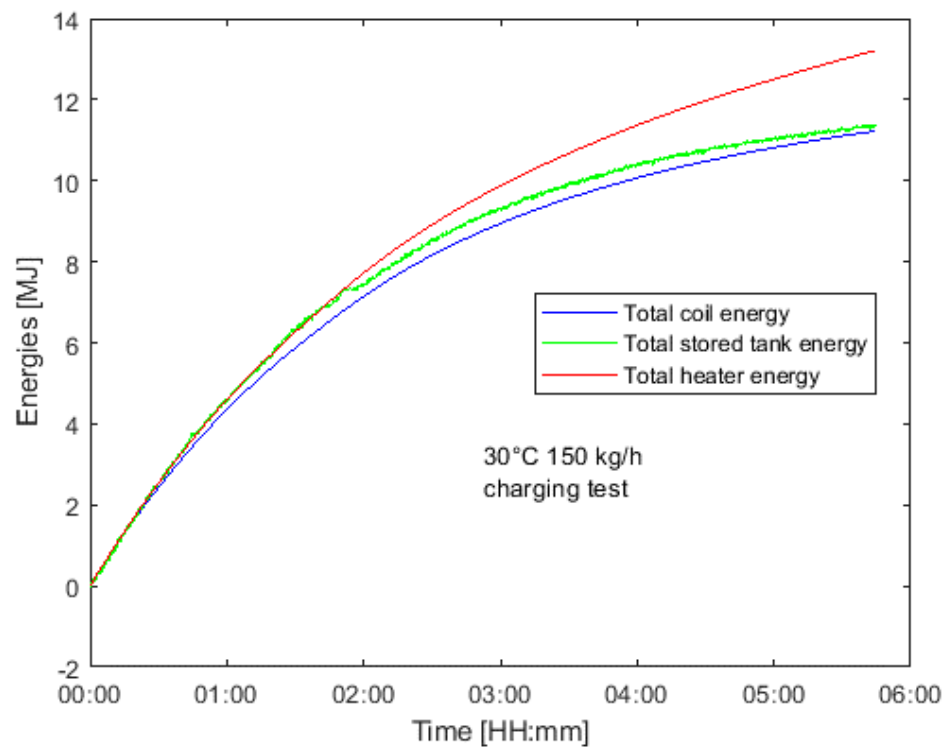
Figure 60 shows that the total energy released by the coils and heater are not completely equal. The difference is due to the heat loss to the environment. The heat absorbed by the tank water exceeds the delivered coils' heat in the beginning of the test but is caught up towards the end. This can be the result of the tank thermocouples that are calibrated based on the thermocouple at the inlet of the coil, which is not calibrated and because the heat loss between the heater's outlet and coils' inlet is unknown and is thus not deducted from the new thermocouple values after linear regression. The tests with a mass flow rate of 150 kg/h show the same pattern, same as the tests with a mass flow rate of 300 kg/h. During the 300 kg/h tests, the difference between the stored tank energy and the total coil energy is larger than the 150 kg/h tests, but also bigger than the 450 kg/h test, which should not be possible because the greater the mass flow rate, the greater the turbulence, the better the exchange of heat [80].



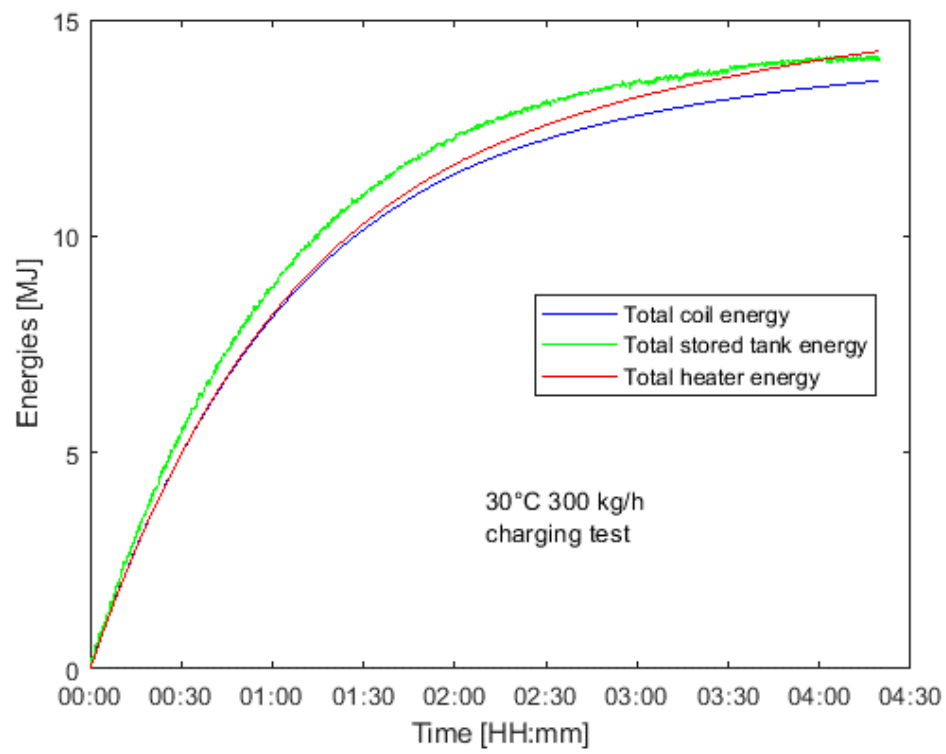
a)



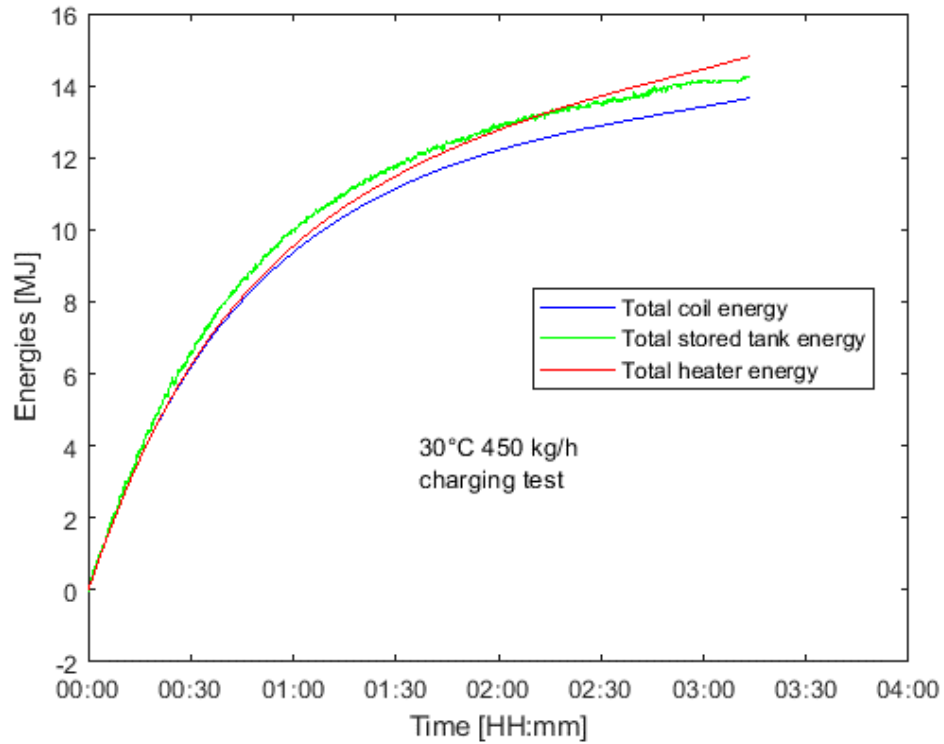
b)



c)



d)



e)

Figure 60: Total energies of coils, tank and heater of a) the charging test with an inlet temperature of 40°C and mass flow of 150 kg/h b) the 40°C 300 kg/h charging test c) the 30°C 150 kg/h charging test d) the 30°C 300 kg/h charging test and e) the 30°C 450 kg/h charging test.

4.2.2.2 Charging time measurements

The charging time in function of the energy fraction of the 30°C 450 kg/h test is shown in Figure 61. It increases faster in the beginning of the test but slows down near the end. The energy fraction equation is shown in Eq. (57).

$$\alpha(t) = \frac{Q_c(t)}{\max(Q_c(t))} \quad (57)$$

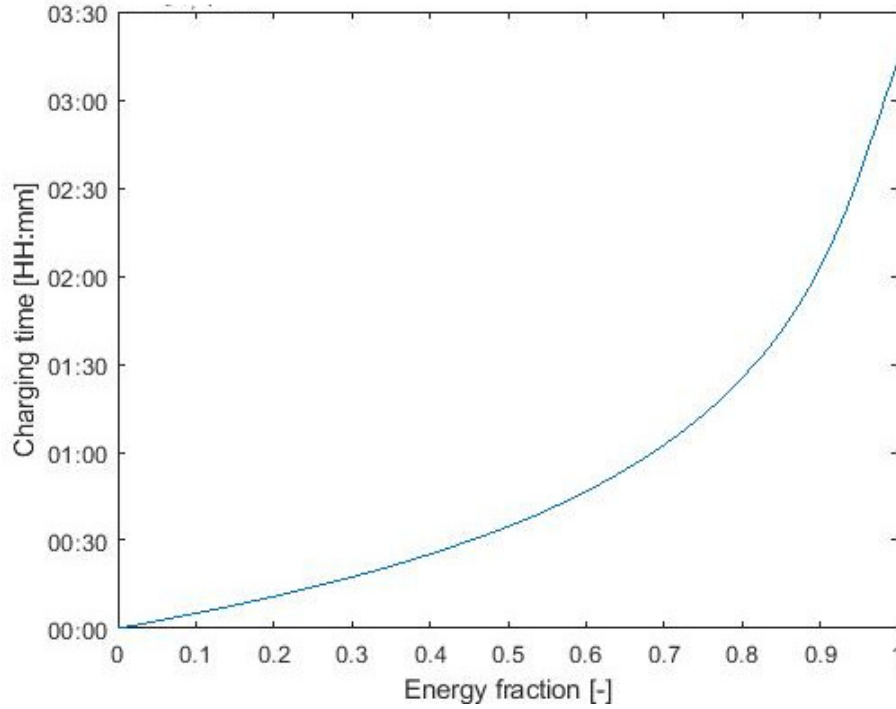


Figure 61: Energy fraction function of the 30°C 450 kg/h charging test.

4.2.2.3 Charging time correlation

In Eq. (58), the full charging time equation is shown with correlation parameters $A(\alpha)$, $B(\alpha)$, $C(\alpha)$ and $D(\alpha)$ in Eq. (59) and (60). The charging time is now written in function of ΔT , which is the difference between the coils' inlet temperature and the tank's initial temperature. The inlet temperature and mass flow rate experience variations throughout the course of the experiment. Therefore, these inlet conditions are not completely constant, and consequently, it is necessary to average the mass flow rate and inlet temperature in time.

$$t_c(\alpha) = \frac{Slope}{\Delta T} + Intercept \quad (58)$$

$$Slope = A(\alpha) + \frac{B(\alpha)}{\dot{m}} \quad (59)$$

$$Intercept = C(\alpha) + \frac{D(\alpha)}{\dot{m}} \quad (60)$$

To obtain the charging time correlation, first the energy fraction from zero till one is split up in 99 equal pieces $\alpha = 0, \alpha = 0.01, \alpha = 0.02$ until $\alpha = 0.99$. Eq. (61) shows the used formula for $\alpha(t)$.

$$\alpha(t) = \frac{Q_c(t)}{\max(Q_c)} \quad (61)$$

For each α , each experiment had its own duration till it reaches an energy fraction. For all 150 kg/h charging tests and all 300 kg/h charging tests, these durations were plotted with on the y-axis the duration (a.k.a. the charging time) and x-axis $\frac{1}{\Delta T}$, with ΔT being the temperature difference between the HTF inlet temperature and the initial tank temperature being 20°C, as can be seen in Figure 62 for an $\alpha = 0.20$.

The *slopes* of the charging times as function of $\frac{1}{\Delta T}$ can be plotted as a function of $\frac{1}{\dot{m}_{HTF}}$, as can be seen in Figure 63 for an $\alpha = 0.20$. The slope of this function is then $A(\alpha)$ and the intersect of this function is $B(\alpha)$.

The *intersects* of the charging times as function of $\frac{1}{\Delta T}$ can also be plotted as a function of $\frac{1}{\dot{m}_{HTF}}$, as can be seen in Figure 64 for an $\alpha = 0.20$.

Figure 65 shows the correlation parameters for all energy fractions. $B(\alpha)$ is negative, because the charging time of 300 kg/h is descending more than the charging time of 150 kg/h generally considered across all energy fractions. As a result, the *Slope* graphs are generally descending which results in the slope of *Slope*, which is equal to $B(\alpha)$, to be negative. All correlation parameters are plotted for $\alpha = 0.01$ till $\alpha = 0.90$ in Figure 65, because the charging time increases exponentially for $\alpha \geq 0.90$, as shown in Figure 66 for parameter C. The charging time t_c of the 40°C 150 kg/h test and 40°C 300 kg/h test is higher than the t_c of the 30°C 150 kg/h and 30°C 300 kg/h, respectively. This is due to the fact that the total stored heat is larger for the 40°C charging test than for the 30°C charging test, so it takes longer for the tank to reach the 40°C than to reach the 30°C. The charging time for the 150 kg/h tests is bigger than the charging time for 300 kg/h tests, because the heat transfer rate is proportional to the mass flow rate, so it takes less time for the 300 kg/h tests to store the total amount of heat than for the 150 kg/h tests.

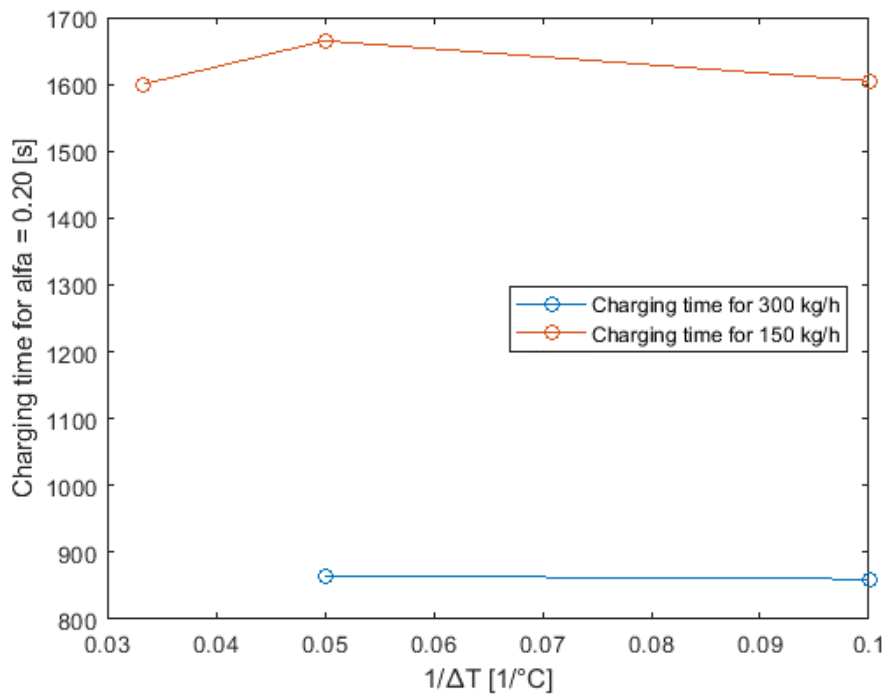


Figure 62: Charging times of 300 kg/h and 150 kg/h charging tests in function of $1/\Delta T$ for $\alpha = 0.2$.

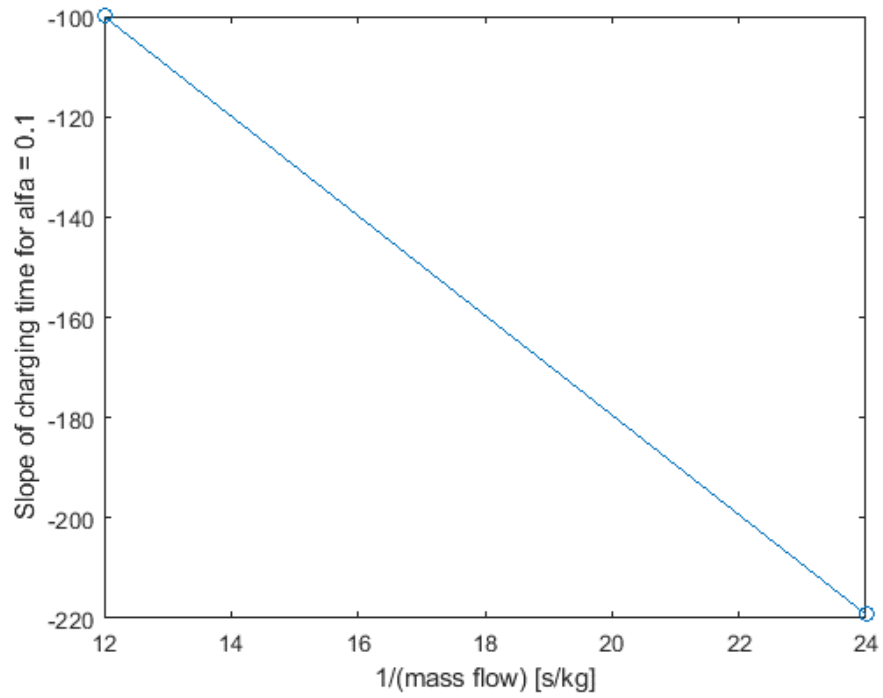


Figure 63: Slope of charging time for alfa = 0.2 in function of 1/(mass flow).

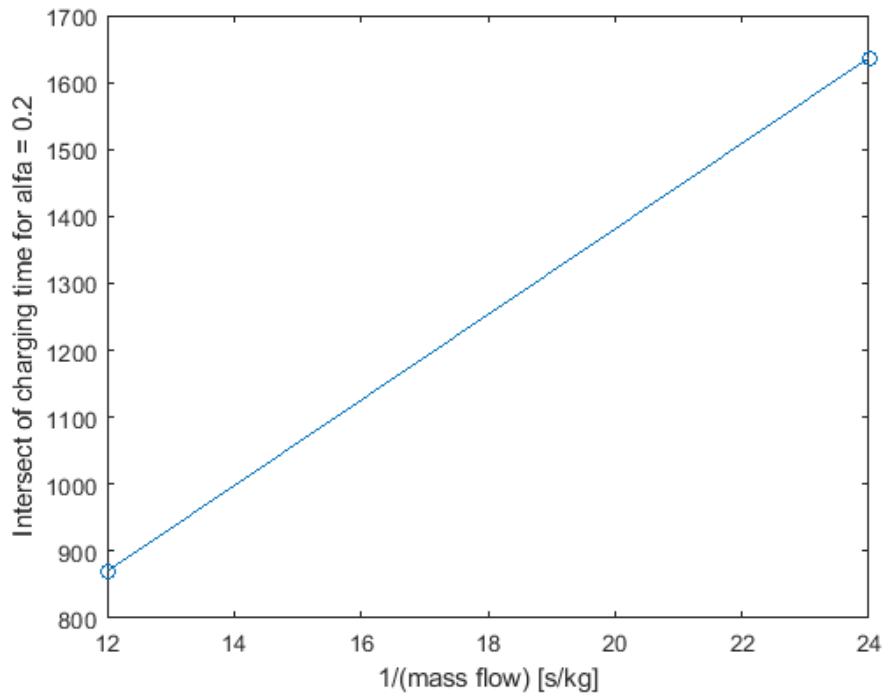


Figure 64: Intersect of charging time for alfa = 0.2 in function of 1/(mass flow).

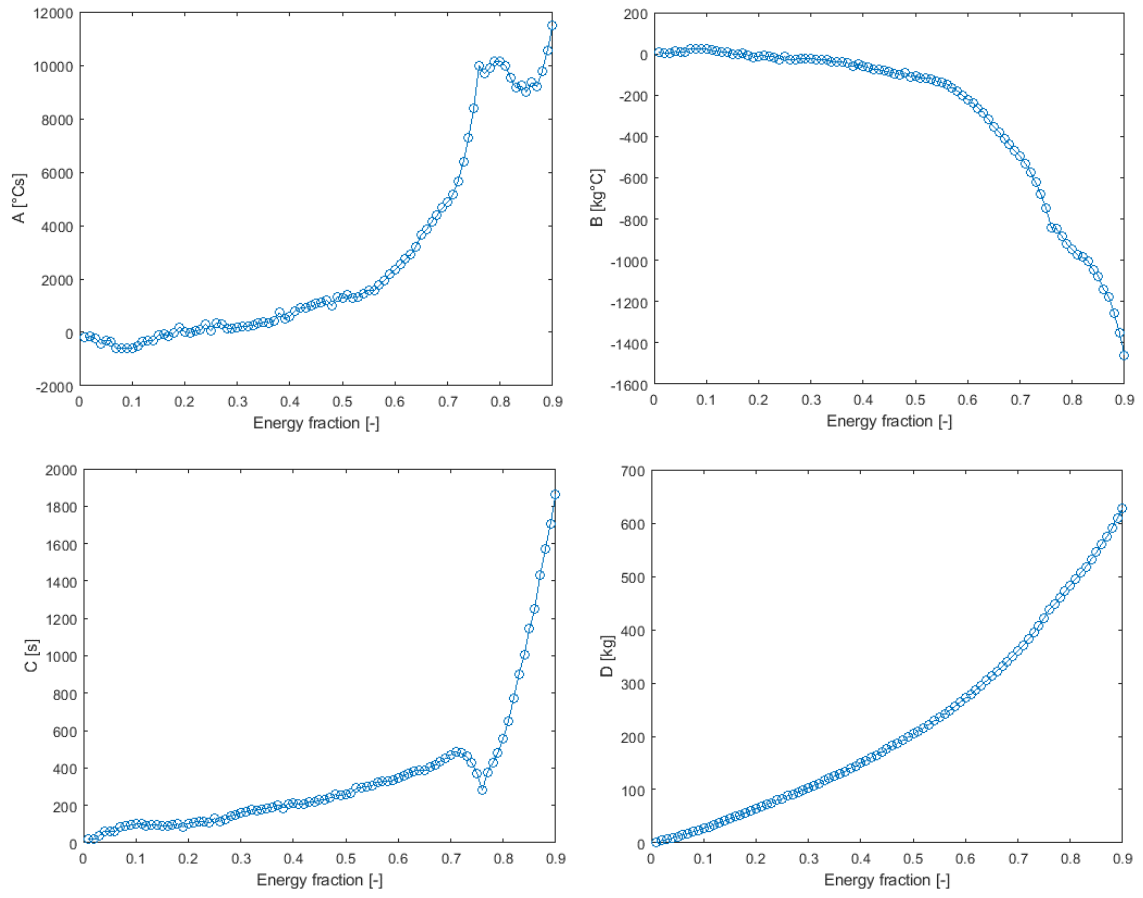


Figure 65: Correlation parameters for alle six charging tests.

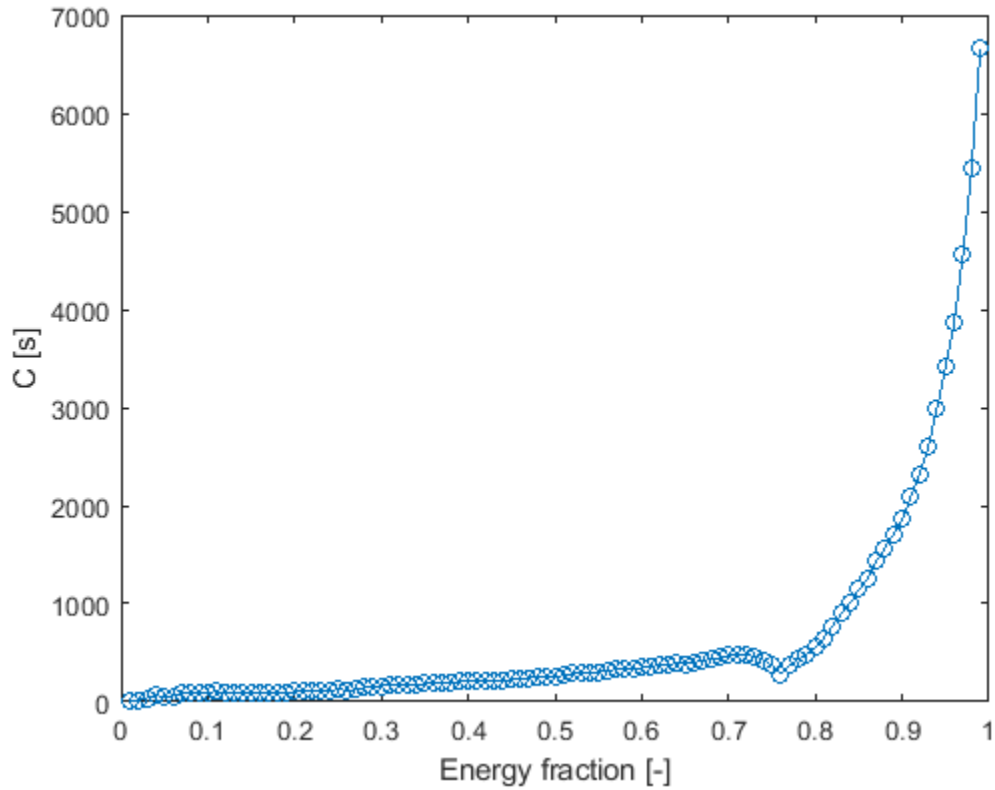


Figure 66: Correlation parameter C for all six charging tests from alfa = 0.01 till alfa = 0.99.

4.2.3 Model evaluation

The formula of ΔU is given by Eq. (62). The predicted energy $\alpha(t)\Delta U$ and the stored coil energy $Q_{total,c}$ of the 50°C 150 kg/h test are displayed in Figure 67. The curves are almost equal, but not completely, because $\alpha(t)\Delta U$ assumes that the average tank temperature will over time be exactly equal to the coils' inlet temperature, but this does not actually happen. So according to $\alpha(t)\Delta U$, the tank has absorbed more heat than it actually does.

$$\Delta U = U(state_{end} - state_{start}) = m_t c_{p,t} (T_{tank,end} - T_{tank,start}) \quad (62)$$

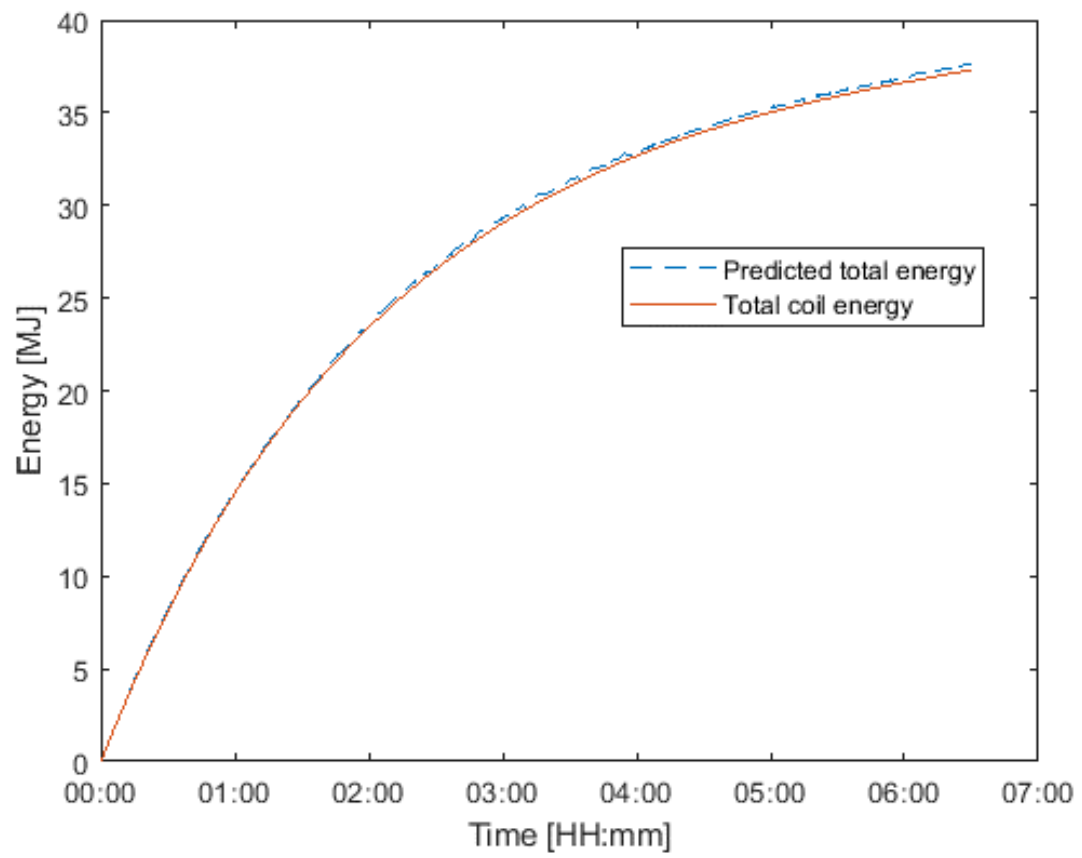


Figure 67: Predicted total energy and the stored coil energy of the 50°C 150 kg/h charging test.

4.3 Discharging tests

4.3.1 Initial conditions

The initial conditions for each discharging experiment are a constant inlet mass flow rate of the HTF flowing through the coils (300, 450 or 600 kg/h) as can be seen in Figure 68 and a constant inlet coil temperature of 20°C. The tank is initially 30 or 50°C warm. The used PID parameters for the pump in the cold circuit and valve in the chiller circuit can be found in Table 16.

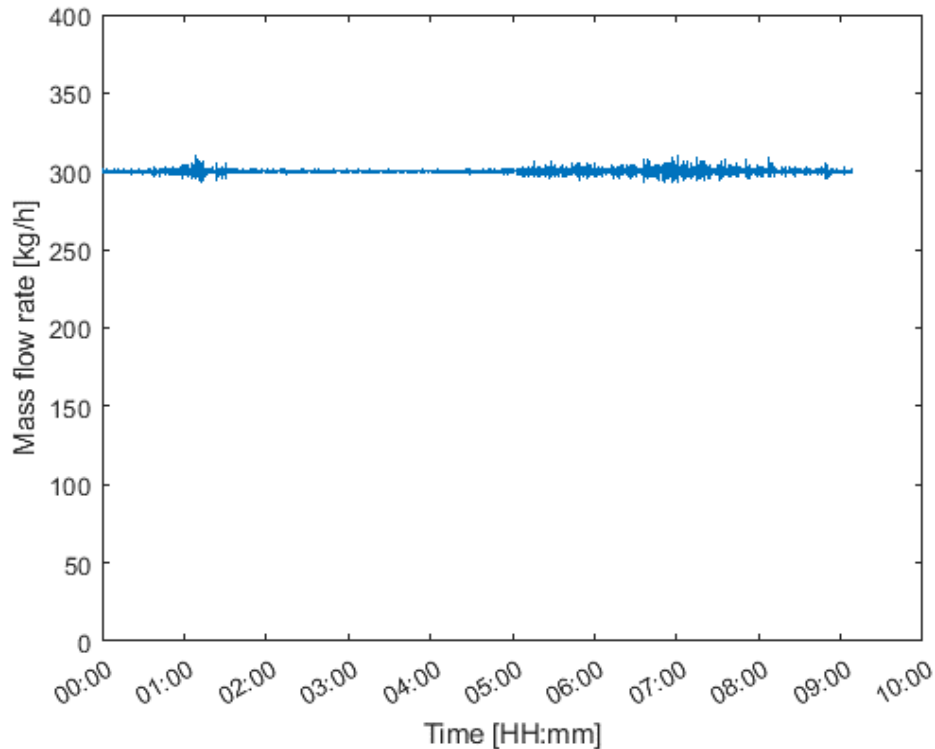


Figure 68: 300 kg/h mass flow rate of the 30°C discharging test.

		30°C		50°C	
		Pump	Valve	Pump	Valve
300 kg/h	K_c	0.003	-0.012	0.003	-0.035
	T_i	0.068	0.189	0.068	0.063
	T_d	0	0.029	0	0.017
450 kg/h	K_c	0.003	-0.035	0.003	-0.035
	T_i	0.068	0.063	0.068	0.076
	T_d	0	0.017	0	0.017
600 kg/h	K_c	0.003	-0.035	0.003	-0.004
	T_i	0.068	0.063	0.057	0.120
	T_d	0	0.017	0	0

Table 16: PID parameters of the pump and chiller valve for the discharging experiments.

Figure 69 shows all temperatures of the set-up. The temperature of the plate heat exchanger's outlet is almost equal to the temperature of the coils' inlet. The temperature of the coils' outlet is equal to the temperature of the plate heat exchanger's inlet. These temperatures are nearing the coils' inlet temperature, such as the tank temperatures do. This graph clearly shows the stratification in the tank. The temperature difference between the exchanger's outlet and coils' inlet and the temperature difference between the coils' outlet and exchanger's inlet are due to heat loss to the ambient air. Figure 70 shows all tank thermocouples after six hours of the 50°C 300 kg/h discharge test as a function of tank height. The stratification is clearly visible. The top control volume is still at a high temperature and it will take a long time for that control volume to cool down. The graph shows that thermocouples 10 and 11 probably give wrong values. Thermocouples 9 till 11 were not taken into account during the data analysis.

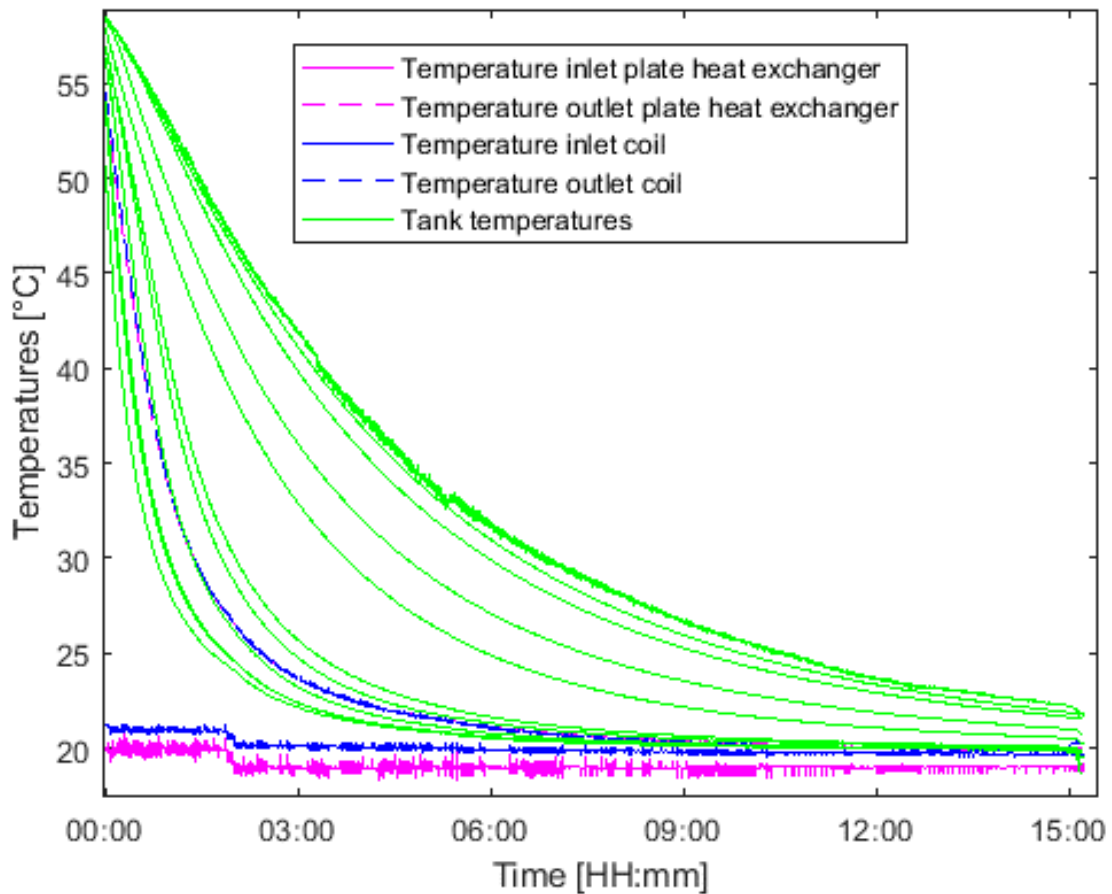


Figure 69: Temperatures of set-up during 50°C 300 kg/h discharging test.

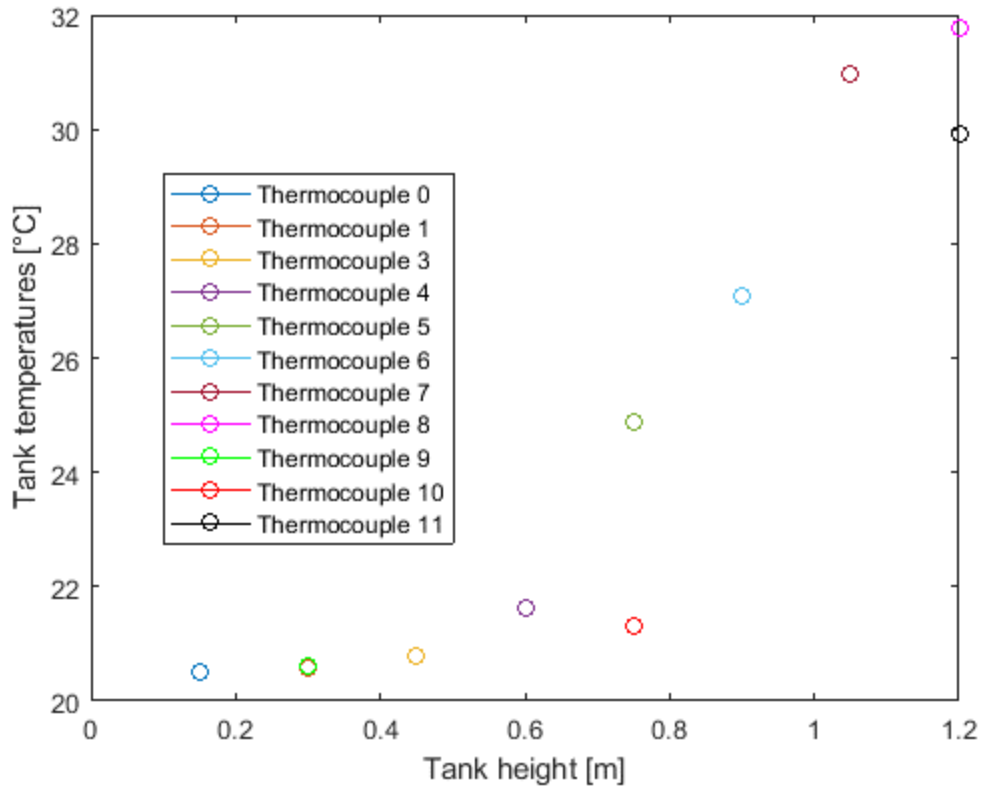


Figure 70: Tank temperatures of the 50°C 300 kg/h discharging test as a function of tank height after six hours.

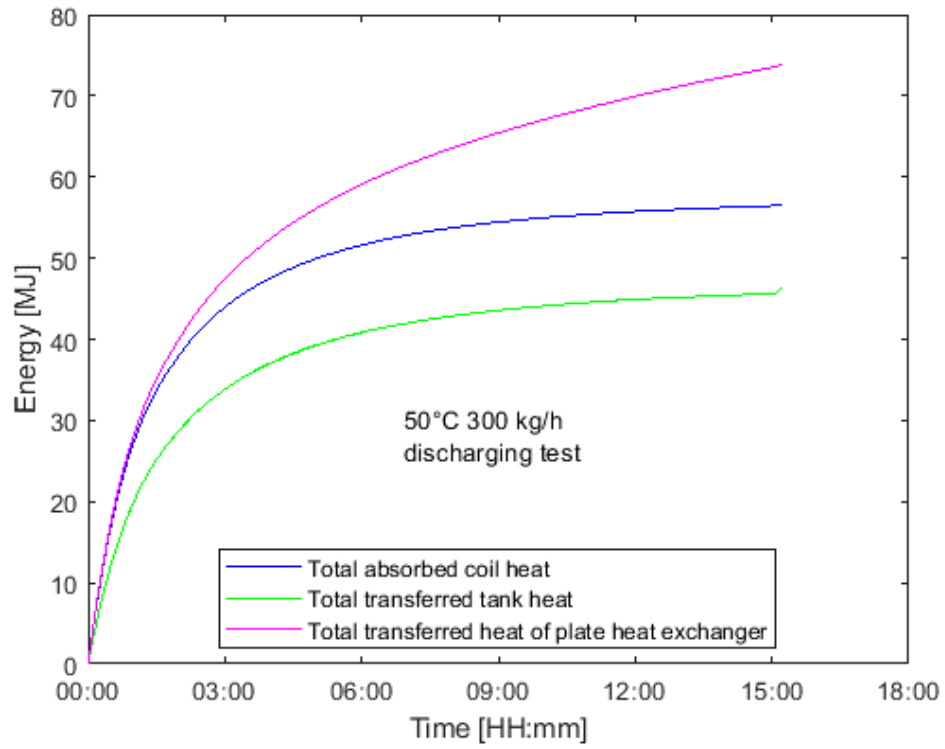
4.3.2 Model calibration

4.3.2.1 Energy balance

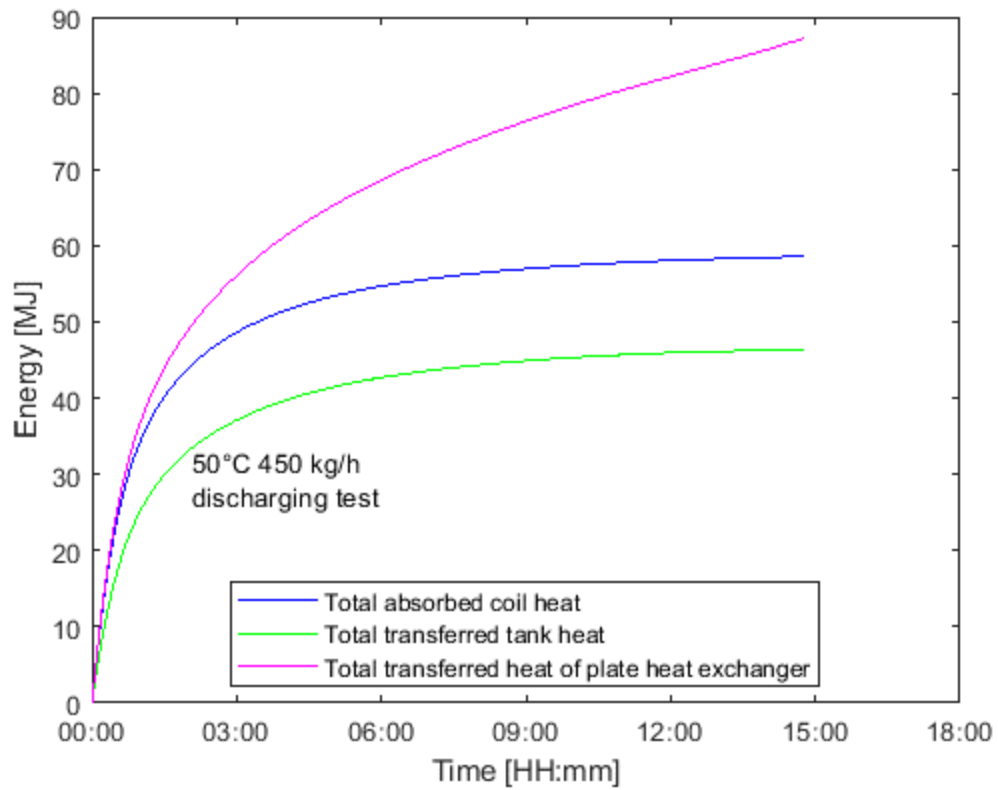
In Figure 71 the transferred coil heat, transferred heat of plate heat exchanger and released tank heat are displayed for a discharging test of 50°C and 300 kg/h. The difference in coil and tank energy can be the result of heat loss to the environment. However, the difference between the heat exchanger's energy and the energy of the coil and tank is great. The reason for this can be the fact that the thermocouples at the in- and outlet of the plate heat exchanger are newly bought thermocouples which are not calibrated. The read-out values of those thermocouples can have an offset in comparison with the older thermocouples in the tank and the older thermocouples at the in- and outlet of the heater. This can also be the result of the tank thermocouples that are calibrated based on the thermocouple at the inlet of the coil, which is not calibrated and because the heat loss between the coils' outlet and plate heat exchanger's inlet is unknown and is thus not deducted from the new thermocouple values after performing linear regression.

The total delivered heat from the plate heat exchanger keeps increasing towards the end while the coil and tank energy are flattening, as presented in Figure 71. This trend also occurs during the 30°C discharging tests. It does not occur during the 50°C 600 kg/h test, but that test may have been aborted too quickly. It may be that the control volumes in the lower part of the tank have already taken over the HTF inlet

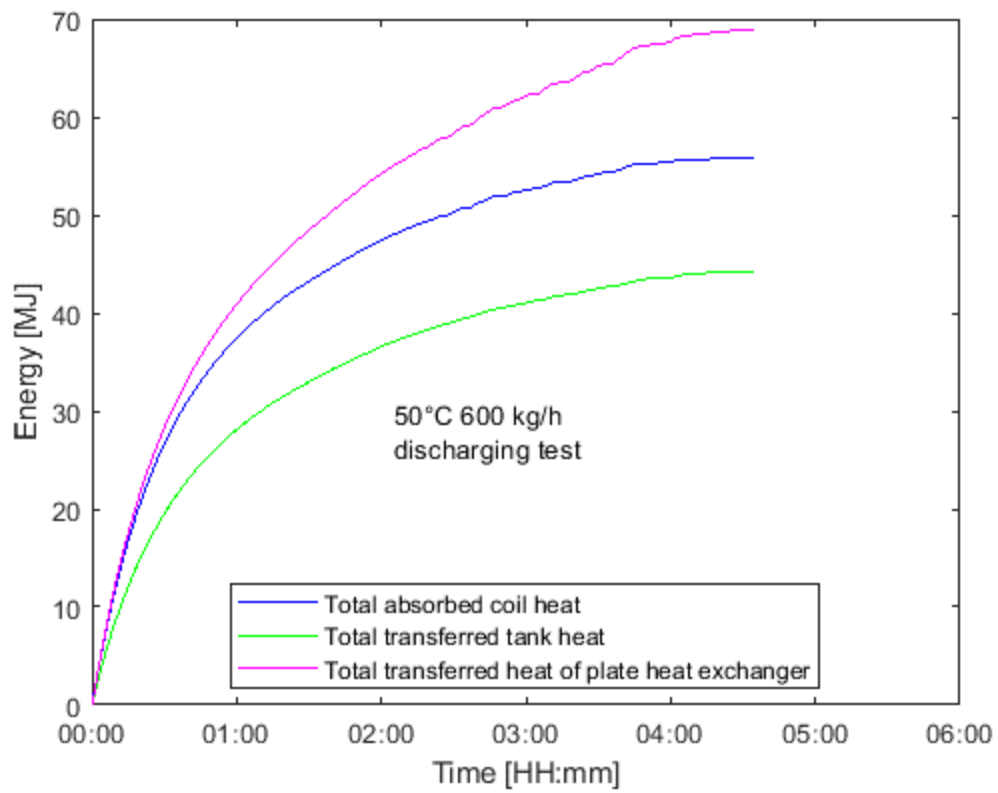
temperature, while the temperatures of the upper control volumes have not yet fully reached 20°C, so that the plate heat exchanger still must deliver power until the end.



a)



b)



c)

Figure 71: Total stored energies of the 50°C a) 300 kg/h discharging test b) 450 kg/h discharging test and c) 600 kg/h discharging test.

4.3.2.2 Discharging time measurement

The energy fraction of the 50°C 300 kg/h discharging test increases at a fast rate in the beginning of the test and increases slower at the end as can be seen in Figure 72. The formula used for $\alpha(t)$ is the same as the one used during charging testing.

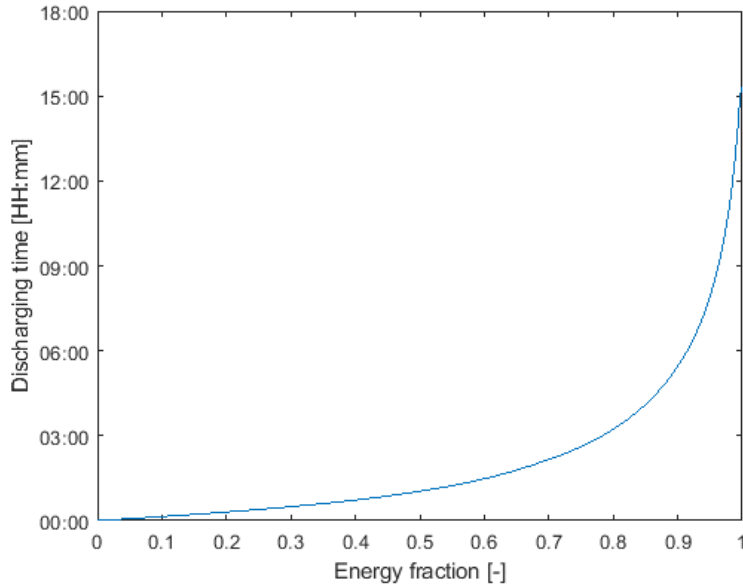


Figure 72: Discharging time of 50° 300 kg/h discharging test.

4.3.2.3 Discharging time correlation

For an $\alpha = 0.20$, the discharging times t_d for all mass flow rates of the discharging experiments in function of $\frac{1}{\Delta T}$ are plotted in Figure 73. ΔT is the initial temperature difference between the average tank water and the coils' inlet. The t_d curve for the 600 kg/h tests increases the most of the three curves, followed by the t_d curve for the 300 kg/h tests. The t_d curve for the 450 kg/h tests is rising the least. The discharging time is higher for a lower mass flow rate because the rate of heat transfer is proportional to the mass flow rate, so less heat per seconds is transferred to the coils and it takes longer for the tank to cool down. The discharging time increases with a higher $\frac{1}{\Delta T}$, because the lower the ΔT , the lower the heat transfer rate from the tank to the coils. So, for the same amount of stored heat, the discharge time is higher.

The function equation of the discharging time is the same as the function equation of the charging time, as can be seen in Eq. (63). The function equation of the *Slope* and *Intercept* with the correlation parameters are given in Eq. (64) and (65). The correlation parameters in function of the energy fraction are given in Figure 76 and are only plotted for $\alpha \leq 0.90$ for the same reason as the charging tests. The intercept function is shown in Figure 75 for an $\alpha = 0.20$.

$$t_d(\alpha) = \frac{Slope}{\Delta T} + Intercept \quad (63)$$

$$Slope = A(\alpha) + \frac{B(\alpha)}{\dot{m}} \quad (64)$$

$$Intercept = C(\alpha) + \frac{D(\alpha)}{\dot{m}} \quad (65)$$

Because the t_d as a function of $\frac{1}{\Delta T}$ of 450 kg/h is increasing the least (Figure 73), the *Slope* curve for $\alpha = 0.20$ looks the way it is shown in Figure 74.

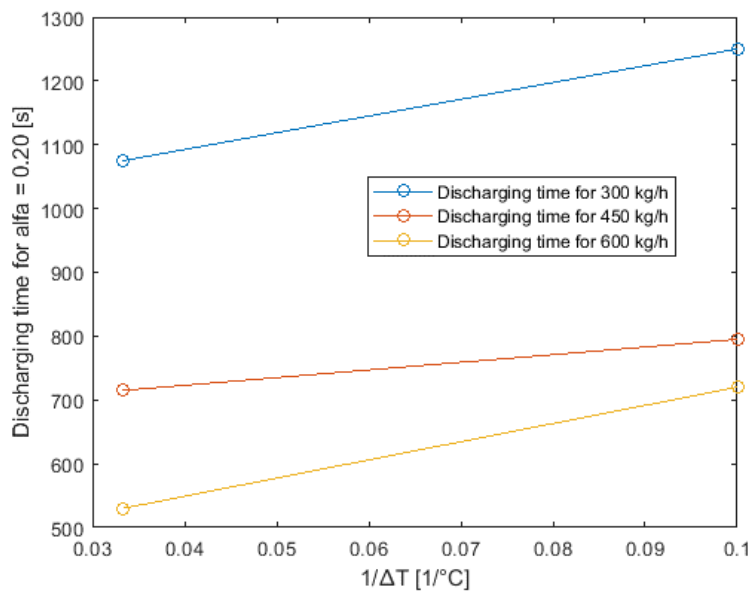


Figure 73: Discharging time functions for mass flow rates 300, 450 and 600 kg/h for an $\alpha = 0.20$.

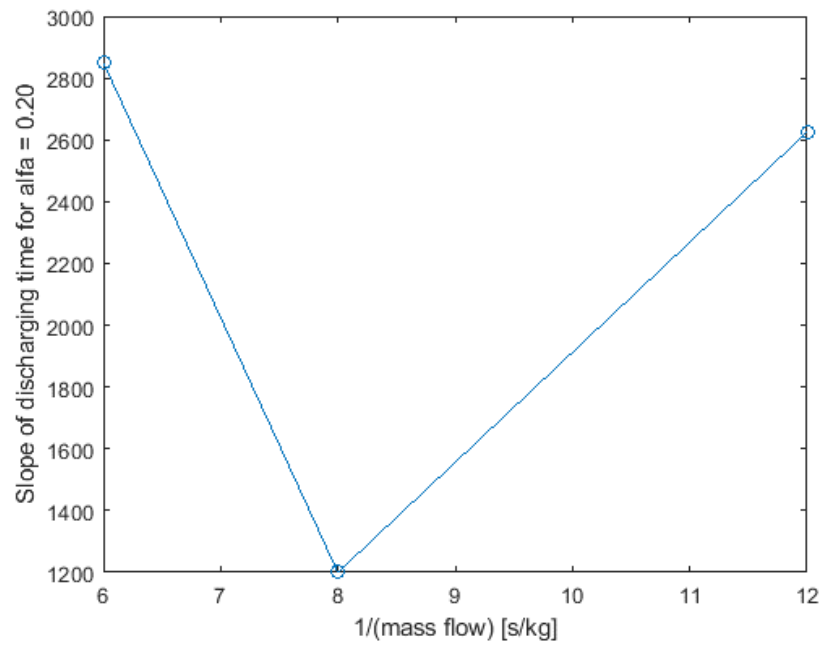


Figure 74: Slope curve of discharging time for an $\alpha = 0.20$.

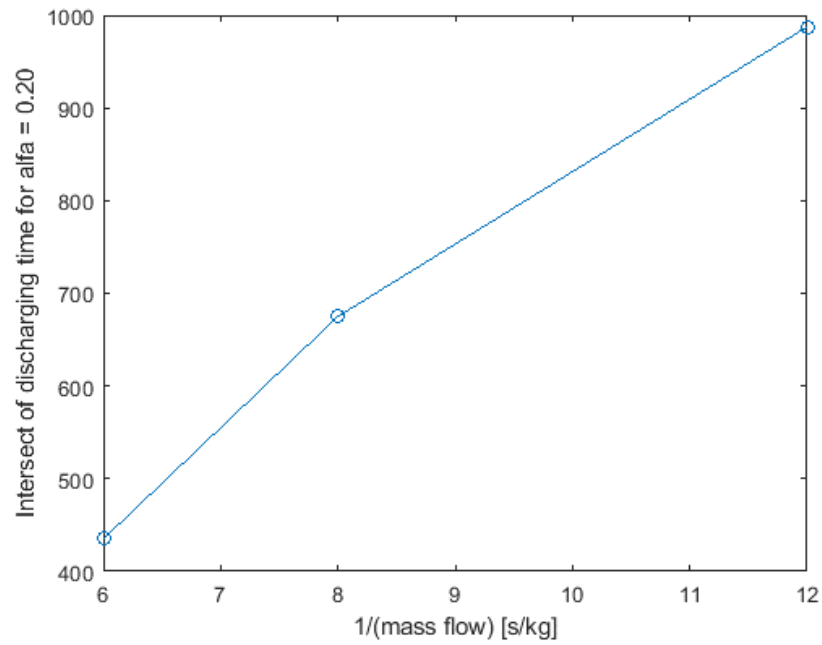


Figure 75: Intersect of discharging time for $\alpha = 0.20$.

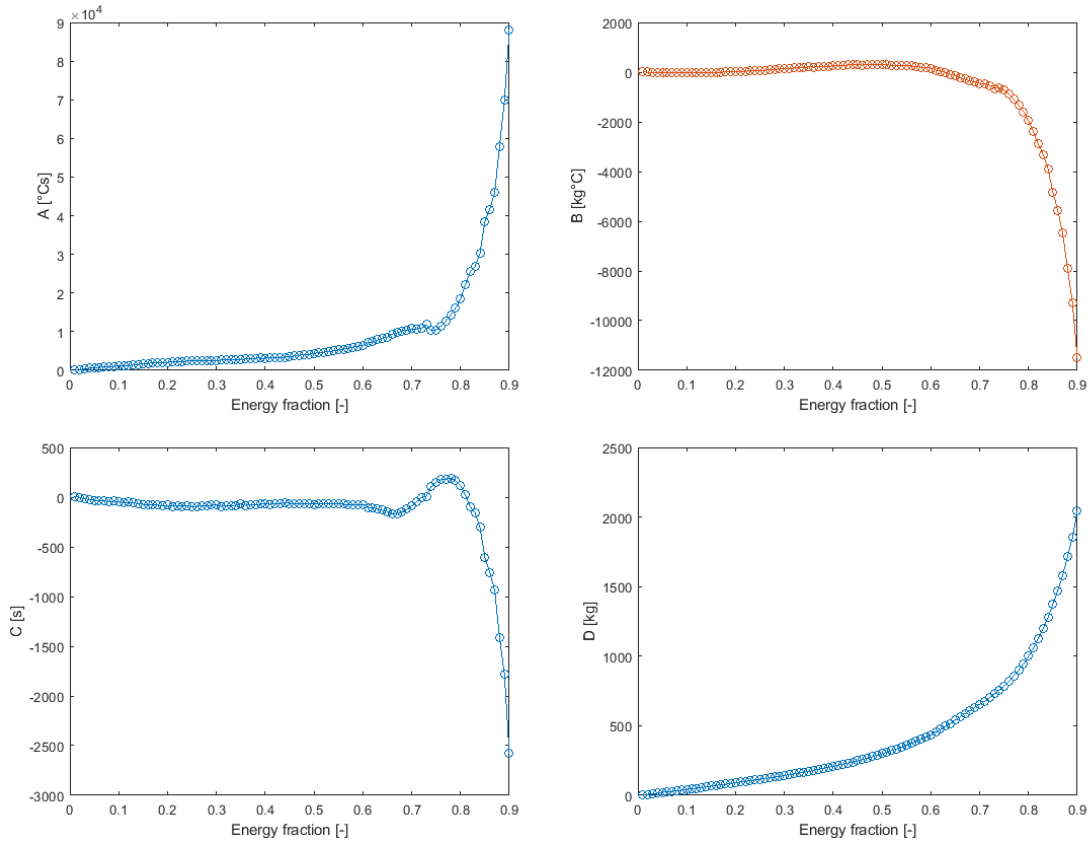


Figure 76: Correlation parameters for the discharging time.

4.3.3 Model evaluation

The predicted energy $\alpha(t)\Delta U$ and the stored coil energy Q_c of the 50°C 300 kg/h discharging test is displayed in Figure 77. The reason why the total predicted energy is lower than the stored coil energy can be due to the heat loss to the environment.

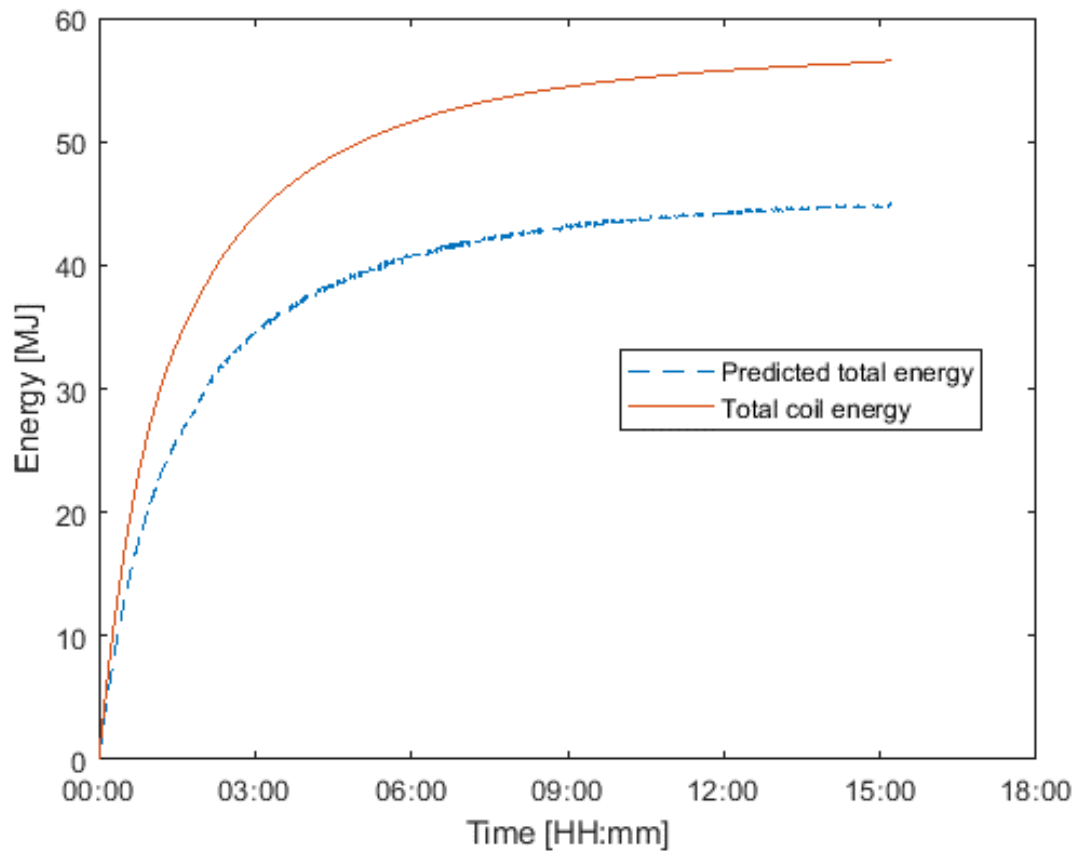


Figure 77: Predicted integrated efflux of energy and the stored coil energy of the 50°C 300 kg/h discharging test.

5 CONCLUSION

There are few ways to describe STES systems, however Beyne et al. [3] developed a method to investigate TES devices experimentally. Using this technology, it is now possible to define the dynamic behaviour of thermal energy storage devices, which was previously not possible using traditional heat exchanger methodologies.

The goal of this study is to determine whether a STES heat exchanger can use the CTEF model. If the model's coefficients can be determined based on the tank's shape, it is investigated if it may also be used as a design model for charging and discharging times. A cold circuit is added to an already constructed setup in order to conduct charging and discharging experiments. These tests were performed to determine whether a STES heat exchanger can use the CTEF model. Twelve experiments were run, each with a different flow rate and/or HTF input temperature. The energy fraction is fitted between zero and one as a function of time. The charging and discharging test correlation parameters are discovered. The integrated efflux of energy anticipated by this thesis and the energy stored in the coils differ, however the outlet temperature of the tests was not predicted by this thesis.

Although the CTEFM has not been fully applied to the solar boiler setup, a lot of new information has been provided about how the set-up works and how those components are connected to the NI DAQ system, which was not known before this thesis.

SUSTAINABILITY REFLECTION

Countries are forced to change their methods of energy production and usage as a result of the world's expanding population, rising energy consumption, and consequent worries about the effects on the environment. Therefore, the Sustainable Development Goals (SDGs), presented in Figure 78, were endorsed by the UN General Assembly in September 2015 with Agenda 2030 for Sustainable Development. 17 SDGs come together to establish an action plan over the course of the next 15 years in order to end global poverty and return the world to a sustainable course. These unified, undivided aims represent the economic, social, and environmental facets of sustainable development. TES can play a major role in this. The SDGs are divided into 5 goals: human, planet, wealth, peace and partnership [81].



Figure 78: Sustainable development goals [82].

Worldwide use of solar, biomass, wind, and hydroelectric energy sources is increasing. However, due to their high cyclical nature, these energy sources require efficient energy storage devices [1]. A thermal energy storage (TES) system is therefore a valuable asset to give society more effective, ecologically acceptable ways to use energy for utility applications, building heating and cooling, and aerospace energy. A TES system minimizes the overall energy consumption and, as a result, the usage of fossil fuels and pricey oil imports by using waste heat and natural resources [1], [2]. In this way it meets sustainability goal 13, which is climate action.

For thermal applications including space and water heating, cooling, and air conditioning, thermal energy storage (TES) is gaining popularity while being an advanced energy, so meeting goal nine. Because it is still a relatively new technology, the cost price is on the high side, but knowing that a solar water heater

lasts about 25 to 30 years, it is certainly an interesting investment by making use of an environmentally conscious, sustainable and clean energy, achieving goal seven [83].

During the construction of the installation, there has been looked to make it as sustainable as possible. The old set-up of the solar boiler consisted of an open cold circuit. To perform charging and discharging experiments on the solar boiler, the cold circuit has been redesigned and closed. With the new closed cold circuit, no hot water is discharged into the sewer and no water is wasted by using the same water each time for the tests, meeting goal 12. The water boiler has also only been filled twice and emptied once, so the water loss is only 300 litres. Had the cold circuit been open, much more water would have been wasted.

TES in combination with a solar water heater is an emerging technology and the solar water heater is an application of this. It is an environmentally friendly device which uses of the heat of the sun to heat/cool spaces and to heat sanitary water. TES systems are nowadays already used in a lot of applications, but there is still space for growth. These TES systems reduce the impact on the climate by reducing CO₂ emissions.

REFERENCES

- [1] I. Dinçer and M. (Marc A.) Rosen, "Thermal energy storage systems and applications", Accessed: Jan. 10, 2023. [Online]. Available: https://books.google.com/books/about/Thermal_Energy_Storage.html?hl=nl&id=4SY9EAAAQBAJ
- [2] P. Arce, M. Medrano, A. Gil, E. Oró, and L. F. Cabeza, "Overview of thermal energy storage (TES) potential energy savings and climate change mitigation in Spain and Europe," *Appl Energy*, vol. 88, no. 8, pp. 2764–2774, Aug. 2011, doi: 10.1016/J.APENERGY.2011.01.067.
- [3] W. Beyne, K. Couvreur, I. T' Jollyn, R. Tassenoy, S. Lecompte, and M. De Paepe, "A charging time energy fraction method for evaluating the performance of a latent thermal energy storage heat exchanger," *Appl Therm Eng*, vol. 195, Aug. 2021, doi: 10.1016/j.applthermaleng.2021.117068.
- [4] S. Danehkar and H. Yousefi, "A comprehensive overview on water-based energy storage systems for solar applications," *Energy Reports*, vol. 8. Elsevier Ltd, pp. 8777–8797, Nov. 01, 2022. doi: 10.1016/j.egyr.2022.06.057.
- [5] S. Martinez Fernandez De Cordova, "Thermal analysis and comparison of a metal helical coil heat exchanger and its plastic alternative for a domestic water storage tank."
- [6] "1. Is the climate warming? | Royal Society." <https://royalsociety.org/topics-policy/projects/climate-change-evidence-causes/question-1/> (accessed Jan. 11, 2023).
- [7] P. Arce, M. Medrano, A. Gil, E. Oró, and L. F. Cabeza, "Overview of thermal energy storage (TES) potential energy savings and climate change mitigation in Spain and Europe," *Appl Energy*, vol. 88, no. 8, pp. 2764–2774, 2011, doi: 10.1016/J.APENERGY.2011.01.067.
- [8] C. Sabine, "The IPCC fifth assessment report," *Carbon Manag*, vol. 5, no. 1, pp. 17–25, Feb. 2014, doi: 10.4155/CMT.13.80.
- [9] "Wind power storage plant." https://www.activesustainability.com/renewable-energy/wind-power-storage-plant/?_adin=02021864894 (accessed May 08, 2023).
- [10] D. Gilfillan and J. Pittock, "Pumped Storage Hydropower for Sustainable and Low-Carbon Electricity Grids in Pacific Rim Economies," *Energies (Basel)*, vol. 15, no. 9, p. 3139, May 2022, doi: 10.3390/EN15093139/S1.
- [11] K. Mensah-Darkwa, S. Akromah, and R. K. Gupta, "Advanced applications of biomass for energy storage," *Bio-Based Nanomaterials: Synthesis Protocols, Mechanisms and Applications*, pp. 171–209, Jan. 2022, doi: 10.1016/B978-0-323-85148-0.00005-1.
- [12] "Waste heat utilization in European energy intensive industries - Interreg." <https://www.interreg-central.eu/Content.Node/CE-HEAT/Waste-heat-utilization-in-European-energy-intensive-indus.html> (accessed Jan. 10, 2023).
- [13] "Economische ontwikkeling energie-intensieve sectoren - CE Delft." <https://ce.nl/publicaties/economische-ontwikkeling-energie-intensieve-sectoren/> (accessed Jan. 10, 2023).
- [14] "Underground thermal energy storage helps prevent peaks in power grid." <https://www.ecovat.eu/underground-thermal-energy-storage-helps-prevent-peaks-in-power-grid/?lang=en> (accessed May 07, 2023).
- [15] "Ecovat Small - Energy Storage NL." <https://www.energystoragenl.nl/projects/listing/ecovat-demo> (accessed May 25, 2023).
- [16] Y. H. Yau and B. Rismanchi, "A review on cool thermal storage technologies and operating strategies," *Renewable and Sustainable Energy Reviews*, vol. 16, no. 1, pp. 787–797, Jan. 2012, doi: 10.1016/J.RSER.2011.09.004.

- [17] A. Arteconi, N. J. Hewitt, and F. Polonara, "State of the art of thermal storage for demand-side management," *Appl Energy*, vol. 93, pp. 371–389, 2012, doi: 10.1016/j.apenergy.2011.12.045.
- [18] N. Mihaylov, B. Evstatiev, S. Kadirova, T. Gueorguiev, T. Georgieva, and A. Evtimov, "Load Profile of Typical Residential Buildings in Bulgaria," in *IOP Conference Series: Earth and Environmental Science*, Institute of Physics Publishing, Jul. 2018. doi: 10.1088/1755-1315/172/1/012035.
- [19] "(PDF) Electrical flexibility in the chemical process industry." https://www.researchgate.net/publication/351021032_Electrical_flexibility_in_the_chemical_process_industry/figures?lo=1&utm_source=google&utm_medium=organic (accessed May 21, 2023).
- [20] "Solar Duck Curve Explained: What it Means in Western Australia." <https://www.synergy.net.au/Blog/2021/10/Everything-you-need-to-know-about-the-Duck-Curve> (accessed May 21, 2023).
- [21] "IEEE Xplore Full-Text PDF:" <https://ieeexplore.ieee.org/stamp/stamp.jsp?tp=&arnumber=29331> (accessed Jan. 12, 2023).
- [22] "(PDF) Energy Management of Industrial Loads In a Smart Micro grid Using Particle Swarm Optimization Algorithm." https://www.researchgate.net/publication/286556977_Energy_Management_of_Industrial_Loads_In_a_Smart_Micro_grid_Using_Particle_Swarm_Optimization_Algorithm (accessed May 07, 2023).
- [23] "Electric Storage Heaters For Off Peak Tariffs Explained | EDF." <https://www.edfenergy.com/heating/advice/storage-heaters-explained> (accessed May 07, 2023).
- [24] "Energy Machines." <https://www.energymachines.com/cases/bispebjerg-hospital> (accessed May 07, 2023).
- [25] "Thermal Power Generation." <https://www.tepco.co.jp/en/hd/about/facilities/thermal-e.html> (accessed May 07, 2023).
- [26] J. Arijis, J. Meul, M. Naessens, K. Uyttenhove, and S. Verammen, "Technologieën voor het optimaliseren van de efficiëntie van BEO-systemen."
- [27] F. Marias, P. Neveu, G. Tanguy, and P. Papillon, "Thermodynamic analysis and experimental study of solid/gas reactor operating in open mode," *Energy*, vol. 66, pp. 757–765, Mar. 2014, doi: 10.1016/J.ENERGY.2014.01.101.
- [28] X. Guo, A. P. Goumba, C. Wang, and W. Cheng, "Comparison of Direct and Indirect Active Thermal Energy Storage Strategies for Large-Scale Solar Heating Systems," vol. 12, no. 10, p. 1948, 2019, doi: 10.3390/en12101948.
- [29] P. Garcia, V. Vuillerme, M. Olcese, and N. El Mourchid, "Design and modelling of an innovative three-stage thermal storage system for direct steam generation CSP plants," *AIP Conf Proc*, vol. 1734, May 2016, doi: 10.1063/1.4949113.
- [30] G. Alva, Y. Lin, and G. Fang, "An overview of thermal energy storage systems," *Energy*, vol. 144. Elsevier Ltd, pp. 341–378, Feb. 01, 2018. doi: 10.1016/j.energy.2017.12.037.
- [31] F. Hussain, M. Z. Rahman, A. N. Sivasengaran, and M. Hasanuzzaman, "Energy storage technologies," *Energy for Sustainable Development: Demand, Supply, Conversion and Management*, pp. 125–165, Jan. 2020, doi: 10.1016/B978-0-12-814645-3.00006-7.
- [32] A. Dahash, F. Ochs, M. B. Janetti, and W. Streicher, "Advances in seasonal thermal energy storage for solar district heating applications: A critical review on large-scale hot-water tank and pit thermal energy storage systems," *Appl Energy*, vol. 239, pp. 296–315, Apr. 2019, doi: 10.1016/J.APENERGY.2019.01.189.
- [33] J. E. B. Nelson, A. R. Balakrishnan, and S. Srinivasa Murthy, "Experiments on stratified chilled-water tanks," *International Journal of Refrigeration*, vol. 22, no. 3, pp. 216–234, 1999, doi: 10.1016/S0140-7007(98)00055-3.

- [34] C. Solé, M. Medrano, A. Castell, M. Nogués, H. Mehling, and L. F. Cabeza, "Energetic and exergetic analysis of a domestic water tank with phase change material," *Int J Energy Res*, vol. 32, no. 3, pp. 204–214, 2008, doi: 10.1002/ER.1341.
- [35] L. F. Cabeza, M. Ibáñez, C. Solé, J. Roca, and M. Nogués, "Experimentation with a water tank including a PCM module," *Solar Energy Materials and Solar Cells*, vol. 90, no. 9, pp. 1273–1282, May 2006, doi: 10.1016/J.SOLMAT.2005.08.002.
- [36] A. Castell, C. Solé, M. Medrano, M. Nogués, and L. F. Cabeza, "Comparison of stratification in a water tank and a PCM-water tank," *Journal of Solar Energy Engineering, Transactions of the ASME*, vol. 131, no. 2, pp. 0245011–0245015, May 2009, doi: 10.1115/1.3097277.
- [37] T. Bouhal, S. Fertahi, Y. Agrouaz, T. el Rhafiki, T. Kousksou, and A. Jamil, "Numerical modeling and optimization of thermal stratification in solar hot water storage tanks for domestic applications: CFD study," *Solar Energy*, vol. 157, pp. 441–455, Nov. 2017, doi: 10.1016/J.SOLENER.2017.08.061.
- [38] D. Erdemir, H. Atesoglu, and N. Altuntop, "Experimental investigation on enhancement of thermal performance with obstacle placing in the horizontal hot water tank used in solar domestic hot water system," *Renew Energy*, vol. 138, pp. 187–197, Aug. 2019, doi: 10.1016/J.RENENE.2019.01.075.
- [39] J. Dragsted, S. Furbo, M. Dannemand, and F. Bava, "Thermal stratification built up in hot water tank with different inlet stratifiers," *Solar Energy*, vol. 147, pp. 414–425, May 2017, doi: 10.1016/J.SOLENER.2017.03.008.
- [40] Y. P. Chandra and T. Matuska, "Numerical prediction of the stratification performance in domestic hot water storage tanks," *Renew Energy*, vol. 154, pp. 1165–1179, Jul. 2020, doi: 10.1016/J.RENENE.2020.03.090.
- [41] B. Kurşun and K. Ökten, "Effect of rectangular hot water tank position and aspect ratio on thermal stratification enhancement," *Renew Energy*, vol. 116, pp. 639–646, Feb. 2018, doi: 10.1016/J.RENENE.2017.10.013.
- [42] M. A. Karim, "Experimental investigation of a stratified chilled-water thermal storage system," *Appl Therm Eng*, vol. 31, no. 11–12, pp. 1853–1860, Aug. 2011, doi: 10.1016/J.APPLTHERMALENG.2010.12.019.
- [43] J. Fourdrinoy, J. Dambrine, M. Petcu, M. Pierre, and G. Rousseaux, "The dual nature of the dead-water phenomenology: Nansen versus Ekman wave-making drags," *Proceedings of the National Academy of Sciences*, vol. 117, no. 29, pp. 16770–16775, Jul. 2020, doi: 10.1073/pnas.1922584117.
- [44] Y. P. Chandra and T. Matuska, "Stratification analysis of domestic hot water storage tanks: A comprehensive review," *Energy Build*, vol. 187, pp. 110–131, Mar. 2019, doi: 10.1016/J.ENBUILD.2019.01.052.
- [45] C. Bott, I. Dressel, and P. Bayer, "State-of-technology review of water-based closed seasonal thermal energy storage systems," *Renewable and Sustainable Energy Reviews*, vol. 113, p. 109241, Oct. 2019, doi: 10.1016/J.RSER.2019.06.048.
- [46] S. Fantucci, A. Lorenzati, G. Kazas, D. Levchenko, and G. Serale, "Thermal Energy Storage with Super Insulating Materials: A Parametrical Analysis," *Energy Procedia*, vol. 78, pp. 441–446, Nov. 2015, doi: 10.1016/J.EGYPRO.2015.11.691.
- [47] R. Abbas Ahmmed, K. AlwanHussien, S. Mohammed Hadi, and A. Ibrahim Owaid, "Article ID: IJMET_08_10_003 Aero Gel as Insulator," *International Journal of Mechanical Engineering and Technology (IJMET)*, vol. 8, no. 10, pp. 19–24, 2017, [Online]. Available: <http://www.iaeme.com/IJMET/issues.asp?JType=IJMET&VType=8&IType=10>

- [48] K. Kaminski, P. Znaczkó, M. Lyczko, T. Krolikowski, and R. Knitter, "Operational Properties Investigation of The Flat-Plate Solar Collector with Poliuretane Foam Insulation," *Procedia Comput Sci*, vol. 159, pp. 1730–1739, Jan. 2019, doi: 10.1016/J.PROCS.2019.09.344.
- [49] J. Kalder, A. Annuk, A. Allik, and E. Kokin, "Increasing Solar Energy Usage for Dwelling Heating, Using Solar Collectors and Medium Sized Vacuum Insulated Storage Tank," *Energies 2018, Vol. 11, Page 1832*, vol. 11, no. 7, p. 1832, Jul. 2018, doi: 10.3390/EN11071832.
- [50] A. Al-Masri, "Effect of Tank Size on the Temperature Distributions for Hybrid Photovoltaic/Thermal Water Heaters," 2016.
- [51] "Solar Energy | EESI." <https://www.eesi.org/topics/solar/description> (accessed Jan. 11, 2023).
- [52] N. A. Aziz, N. Amri, M. Amin, M. Shukry, A. Majid, and I. Zaman, "Thermal energy storage (TES) technology for active and passive cooling in buildings: A Review", doi: 10.1051/mateconf/201822503022.
- [53] P. K. Vijayan, A. K. Nayak, and N. Kumar, "Review of applications of natural circulation systems," *Single-Phase, Two-Phase and Supercritical Natural Circulation Systems*, pp. 31–68, Jan. 2019, doi: 10.1016/B978-0-08-102486-7.00002-0.
- [54] "Direct-Gain Passive Solar | BuildingGreen." <https://www.buildinggreen.com/blog/direct-gain-passive-solar> (accessed May 07, 2023).
- [55] "Passive heating | YourHome." <https://www.yourhome.gov.au/passive-design/passive-heating> (accessed May 07, 2023).
- [56] "GreenSpec: Passive Solar Design: Sunspaces." <https://www.greenspec.co.uk/building-design/passive-solar-sunspaces/> (accessed May 07, 2023).
- [57] S. Chen, B. J. Dewancker, S. Yang, J. Mao, and J. Chen, "Study on the Roof Solar Heating Storage System of Traditional Residences in Southern Shaanxi, China," *Int J Environ Res Public Health*, vol. 18, no. 23, Dec. 2021, doi: 10.3390/IJERPH182312600.
- [58] "How Does a Thermosiphon Work | Arrow.com." <https://www.arrow.com/en/research-and-events/articles/how-does-a-thermosiphon-work> (accessed May 07, 2023).
- [59] R. G. Razo, B. Cárdenas Castañeda, and N. L. Rovira, "Design for a Solar Thermal Energy Storage System; Design for a Solar Thermal Energy Storage System," pp. 8–12, 2015.
- [60] N. Kannan and D. Vakeesan, "Solar energy for future world: - A review," *Renewable and Sustainable Energy Reviews*, vol. 62, pp. 1092–1105, Sep. 2016, doi: 10.1016/J.RSER.2016.05.022.
- [61] E. Kabir, P. Kumar, S. Kumar, A. A. Adelodun, and K. H. Kim, "Solar energy: Potential and future prospects," *Renewable and Sustainable Energy Reviews*, vol. 82, pp. 894–900, Feb. 2018, doi: 10.1016/J.RSER.2017.09.094.
- [62] I. Sarbu and C. Sebarchievici, "Thermal Energy Storage," *Solar Heating and Cooling Systems*, pp. 99–138, Jan. 2017, doi: 10.1016/B978-0-12-811662-3.00004-9.
- [63] M. Moradi, M. Farrokhi, A. Rahimi, and M. S. Hatamipour, "Modeling strategies for sensible heat thermal energy recovery through packed beds," *J Energy Storage*, vol. 54, p. 105297, Oct. 2022, doi: 10.1016/J.EST.2022.105297.
- [64] H. Khurana, R. Majumdar, and S. K. Saha, "Experimental investigation of heat dispatch controllability through simultaneous charging-discharging and stand-alone discharging operations in vertical cylindrical sensible heat storage tank," *J Energy Storage*, vol. 54, Oct. 2022, doi: 10.1016/j.est.2022.105268.
- [65] S. Li, Y. Zhang, K. Zhang, X. Li, Y. Li, and X. Zhang, "Study on Performance of Storage Tanks in Solar Water Heater System in Charge and Discharge Progress," *Energy Procedia*, vol. 48, pp. 384–393, Jan. 2014, doi: 10.1016/J.EGYPRO.2014.02.045.

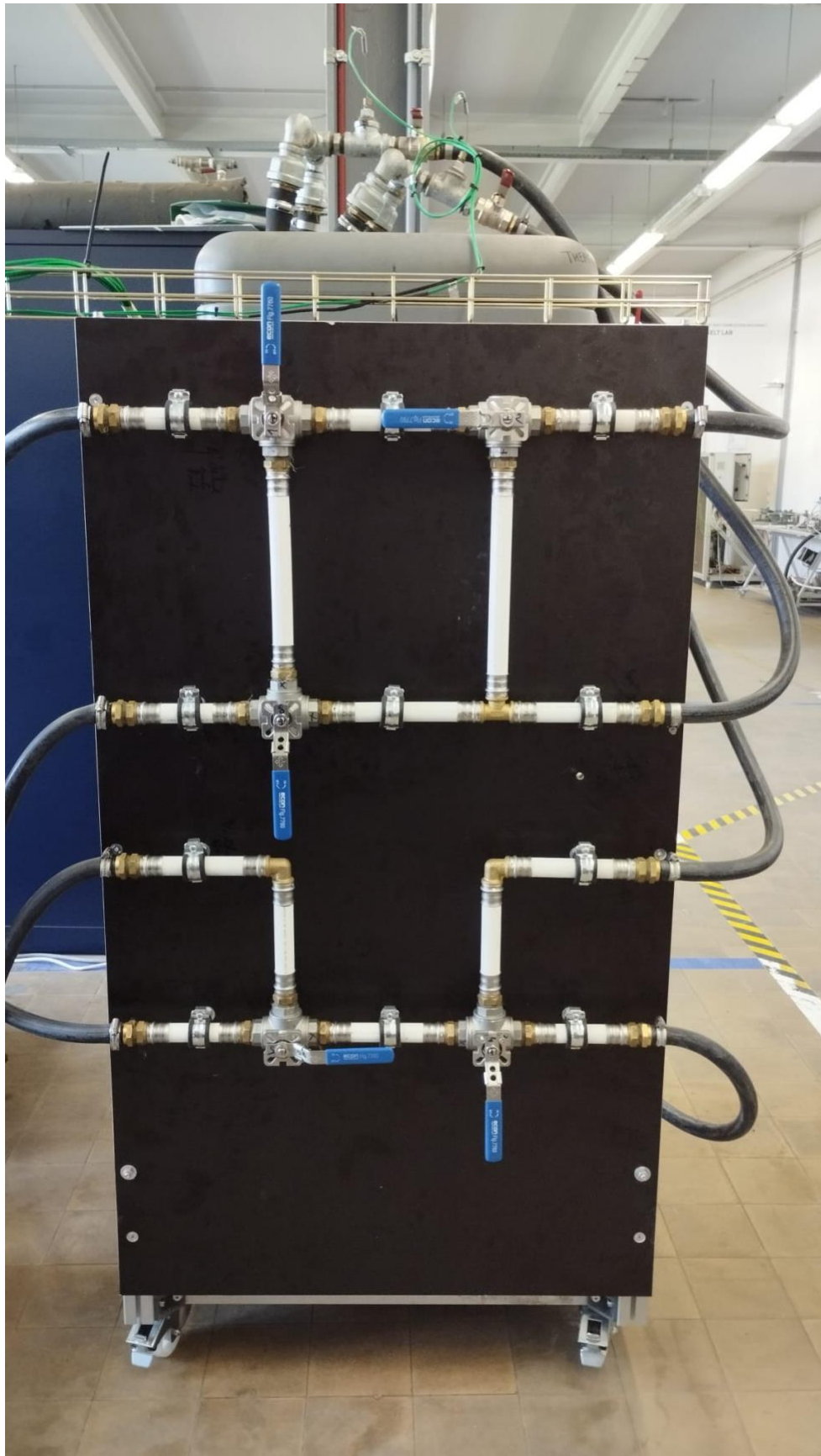
- [66] M. Smyth, P. Quinlan, J. D. Mondol, A. Zacharopoulos, D. McLarnon, and A. Pugsley, "The experimental evaluation and improvements of a novel thermal diode pre-heat solar water heater under simulated solar conditions," *Renew Energy*, vol. 121, pp. 116–122, Jun. 2018, doi: 10.1016/j.renene.2017.12.083.
- [67] S. Kuboth, A. König-Haagen, and D. Brüggemann, "Numerical Analysis of Shell-and-Tube Type Latent Thermal Energy Storage Performance with Different Arrangements of Circular Fins," *Energies* 2017, Vol. 10, Page 274, vol. 10, no. 3, p. 274, Feb. 2017, doi: 10.3390/EN10030274.
- [68] M. Martinelli, F. Bentivoglio, A. Caron-Soupart, R. Couturier, J. F. Fourmigue, and P. Marty, "Experimental study of a phase change thermal energy storage with copper foam," *Appl Therm Eng*, vol. 101, pp. 247–261, May 2016, doi: 10.1016/J.APPLTHERMALENG.2016.02.095.
- [69] W. Beyne, K. Couvreur, S. Lecompte, and M. de Paepe, "A technical, financial and CO2 emission analysis of the implementation of metal foam in a thermal battery for cold chain transport," *J Energy Storage*, vol. 35, p. 102324, Mar. 2021, doi: 10.1016/J.EST.2021.102324.
- [70] T. Bauer, "Approximate analytical solutions for the solidification of PCMs in fin geometries using effective thermophysical properties," *Int J Heat Mass Transf*, vol. 54, no. 23–24, pp. 4923–4930, Nov. 2011, doi: 10.1016/J.IJHEATMASSTRANSFER.2011.07.004.
- [71] K. Couvreur, W. Beyne, R. Tassenoy, S. Lecompte, and M. De Paepe, "Characterization of a latent thermal energy storage heat exchanger using a charging time energy fraction method with a heat loss model," *Appl Therm Eng*, vol. 219, p. 119526, Jan. 2023, doi: 10.1016/J.APPLTHERMALENG.2022.119526.
- [72] "Actuators for modulating control AME 25, AME 35 Data sheet Ordering Actuators".
- [73] "Promass 80F | Endress+Hauser." <https://www.nl.endress.com/nl/flowmeting-niveaumeting-drukmeting-temperatuurmeting-analysemeting/Flowmeting-vloeistoffen-gassen-stoom/coriolis-flowmeter-promass-80f?t.tabId=product-specification> (accessed Apr. 11, 2023).
- [74] S. Dthermx, "HEAT EXCHANGER: BX8THx10/1P SINGLE PHASE-DESIGN." [Online]. Available: www.swep.net
- [75] "PRODUCT SHEET BX8T." [Online]. Available: www.swep.net
- [76] "OPTIFLUX 4000 OPTIFLUX 4000 OPTIFLUX 4000 OPTIFLUX 4000 Technical Datasheet Electromagnetic flow sensor", Accessed: Mar. 13, 2023. [Online]. Available: www.krohne.com
- [77] L. Bokisova, Ö. Bağcı, A. Sharif, D. Daenens, W. Beyne, and M. De Paepe, "Thermal analysis of a plastic helical coil heat exchanger for a domestic water storage tank," *Proceedings of the 9th World Conference on Experimental Heat Transfer, Fluid Mechanics and Thermodynamics (ExHFT-9)*, p. PT72, 2017, Accessed: Mar. 17, 2023. [Online]. Available: <http://hdl.handle.net/1854/LU-8652912>
- [78] "Grundfos België | Pompen en innovatieve pompoplossingen | The full range supplier of pumps and pump solutions. As a renowned pump manufacturer, Grundfos delivers efficient, reliable, and sustainable solutions all over the globe. Step into our world." <https://www.grundfos.com/be> (accessed Apr. 03, 2023).
- [79] "Grundfosliterature-5564196".
- [80] "RUG01-001311673_2010_0001_AC".
- [81] "SDGs | sdgs." <https://www.sdgs.be/nl/sdgs> (accessed May 21, 2023).
- [82] "Sustainable Development Goals launch in 2016." <https://www.un.org/sustainabledevelopment/blog/2015/12/sustainable-development-goals-kick-off-with-start-of-new-year/#> (accessed May 21, 2023).
- [83] "Terugverdiëntijd zonneboiler 2023: info & berekening." <https://www.zonneboiler.be/terugverdiëntijd-zonneboiler> (accessed May 21, 2023).

- [84] "MAGNA 32-100 - 96281016 | Grundfos." <https://product-selection.grundfos.com/be/products/magna/magnaue-series-2000/magna-32-100-96281016?tab=variant-curves&pumpsystemid=2100847007> (accessed May 13, 2023).
- [85] "VRB 3, 10.00 m³/h, Rp 1 | Valves for Heating and Cooling | Globe Valves | Motorised Control Valves | Climate Solutions for heating | Danfoss Great Britain Product Store." https://store.danfoss.com/gb/en_GB/Climate-Solutions-for-heating/Motorised-Control-Valves/Globe-Valves/Valves-for-Heating-and-Cooling/VRB-3%2C-10-00-m%C2%B3-h%2C-Rp-1/p/065Z0217 (accessed May 13, 2023).
- [86] "Electrical actuators, AME 25, Supply voltage [V] AC: 24 | Actuators Without Safety Function | Actuators for Globe Valves | Motorised Control Valves | Climate Solutions for heating | Danfoss Great Britain Product Store." https://store.danfoss.com/gb/en_GB/Climate-Solutions-for-heating/Motorised-Control-Valves/Actuators-for-Globe-Valves/Actuators-Without-Safety-Function/Electrical-actuators%2C-AME-25%2C-Supply-voltage-%5BV%5D-AC%3A-24/p/082G3025 (accessed May 13, 2023).
- [87] "BX8T - SWEP." <https://www.swep.net/products/bx8t/> (accessed May 13, 2023).
- [88] "MAGNA3 32-100 - 97924257 | Grundfos." <https://product-selection.grundfos.com/be/products/magna/magna3/magna3-32-100-97924257?tab=variant-specifications&pumpsystemid=2038376967> (accessed Mar. 13, 2023).
- [89] "Electrical actuators, AME 35, Supply voltage [V] AC: 24 | Actuators Without Safety Function | Actuators for Globe Valves | Motorised Control Valves | Climate Solutions for heating | Danfoss Global Product Store." <https://store.danfoss.com/en/Climate-Solutions-for-heating/Motorised-Control-Valves/Actuators-for-Globe-Valves/Actuators-Without-Safety-Function/Electrical-actuators%2C-AME-35%2C-Supply-voltage-%5BV%5D-AC%3A-24/p/082G3022?language=sl> (accessed May 13, 2023).

APPENDICES



Appendix A: Photo of hot circuit.





Appendix B: Photos of solar boiler.



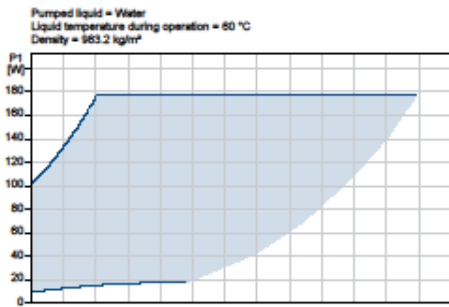
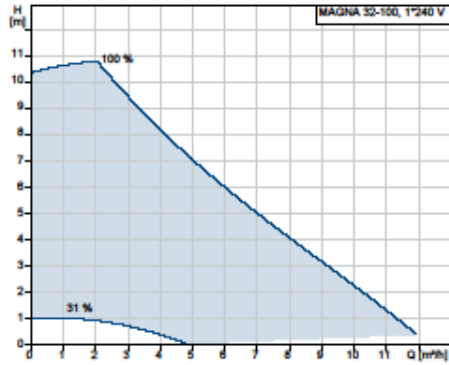
Appendix C: Photo of cold circuit and chiller circuit.



Company name:
Created by:
Phone:

Date: 13/05/2023

Description	Value
General information:	
Product name:	MAGNA 32-100
Product No:	96281016
EAN number:	5700830267790
Price:	
Technical:	
Head max:	100 dm
TF class:	110
Approvals:	CE, TSE, GOST2
Materials:	
Pump housing:	Cast Iron
Pump housing:	EN-JL1040
Pump housing:	ASTM 35 B - 40 B
Impeller:	Composite, PES
Installation:	
Range of ambient temperature:	0 .. 40 °C
Maximum operating pressure:	10 bar
Pipe connection:	G 2
Port-to-port length:	180 mm
Liquid:	
Pumped liquid:	Water
Liquid temperature range:	2 .. 95 °C
Selected liquid temperature:	60 °C
Density:	983.2 kg/m ³
Electrical data:	
Power input - P1:	10 .. 180 W
Mains frequency:	50 / 60 Hz
Rated voltage:	1 x 230-240 V
Maximum current consumption:	0.1 .. 1.23 A
Enclosure class (IEC 34-5):	X4D
Insulation class (IEC 85):	F
Controls:	
Pos term box:	3H
Others:	
Energy (EEI):	0.22
Net weight:	4.4 kg
Gross weight:	5.58 kg
Danish VVS No.:	380682600
Nonwegian NRF no.:	9043064



Appendix D: Datasheet of Grundfos MAGNA 32-100 pump [84].

Data sheet

Seated valves (PN 16)

VRB 2 – 2-way valve, internal and external thread

VRB 3 – 3-way valve, internal and external thread

Description



Features:

- Bubble tight design
- Snap mechanical connection together with AMV(E) 335, AMV(E) 435
- Dedicated 2 and 3-port valv
- Suitable for diverting applications (3-port)

Main data:

- DN 15-50
- k_{vs} 0,63-40 m³/h
- PN 16
- Temperature:
 - Circulation water / glycolic water up to 50 %: 2 (-10^o) ... 130 °C
 - * At temperatures from -10 °C up to +2 °C use stem heater
- Connections:
 - External thread
 - Internal thread

VRB valves provide a quality, cost effective solution for most water and chilled applications.

The valves are designed to be combined with following actuators:

- With AMV(E) 335, AMV(E) 435 or AMV(E) 438 SU actuators.
- With AMV(E) 25, 25 SU/SD, 35 actuators (with adapter 065Z0311).

Combinations of actuators is evident under section "Dimension".

Ordering

Example:
3-way valve; DN 15; k_{vs} 1,6; PN 16;
 T_{max} 130 °C; ext. thread

- 1x VRB 3 DN 15 valve
Code No.: 065Z0153

Option:
- 3x Tailpieces
Code No.: 065Z0291

2&3-way valves VRB (external thread)

DN	k_{vs} (m ³ /h)	Code No.	
		VRB 2	VRB 3
15	0,63	065Z0171	065Z0151
	1,0	065Z0172	065Z0152
	1,6	065Z0173	065Z0153
	2,5	065Z0174	065Z0154
	4,0	065Z0175	065Z0155
20	6,3	065Z0176	065Z0156
25	10	065Z0177	065Z0157
32	16	065Z0178	065Z0158
40	25	065Z0179	065Z0159
50	40	065Z0180	065Z0160

2 & 3-way valves VRB (internal thread)

DN	k_{vs} (m ³ /h)	Code No.	
		VRB 2	VRB 3
15	0,63	065Z0231	065Z0211
	1,0	065Z0232	065Z0212
	1,6	065Z0233	065Z0213
	2,5	065Z0234	065Z0214
	4,0	065Z0235	065Z0215
20	6,3	065Z0236	065Z0216
25	10	065Z0237	065Z0217
32	16	065Z0238	065Z0218
40	25	065Z0239	065Z0219
50	40	065Z0240	065Z0220

**082G3025**

Electrical actuators, AME 25, Supply voltage [V] AC: 24
AME 25 24V 11s/mm 15mm 1000N

PRODUCT DETAILS

Gross weight	1.65 Kg
Net weight	1.503 Kg
Volume	3.62 Liter
EAN	5702421513132
Actuator speed [s/mm]	11 s/mm
Actuator type	Electrical
Ambient temperature [°C] [Max]	55 °C
Ambient temperature [°C] [Min]	0 °C
Application	HVAC
Closing force [N]	1000 N
Control input signal Y [mA]	0(4) - 20 mA
Control input signal Y [mA], Impedance [Ohm]	500
Control input signal Y [V]	0(2) - 10 V
Control input signal Y [V], Impedance [kOhm]	24 kOhm
Control signal type	Modulating/3-point
Description	AME 25 24V 11s/mm 15mm 1000N
Grade of enclosure	IP54
Manual operation	Yes
Position feedback	Yes
Power consumption [W]	4 W
Product Group	Electrical actuators
Protection Class	II
REACH Candidate List substances	Lead (CAS no. 7439-92-1)
0,1	
Safety function	NO
SCIP dossier no.	c5b6fd67-cf6c-493f-8f13-2d65fca1997f
SCIP dossier product name	AMV(E) 20 - 35
Speed type	Standard
Spring down (return)	No
Spring up	No
Storage temperature [°C] [Max]	70 °C
Storage temperature [°C] [Min]	-40 °C
Stroke [mm]	15 mm
Supply voltage [V] AC	24 V
Turn time per 90° [s]	0 *

Danfoss can accept no responsibility for possible errors in catalogs, brochures and other printed material. Danfoss reserves the right to alter its products without notice. This also applies to products already in order provided that such alterations can be made without subsequent changes being necessary in specifications already agreed. All trademarks in this material are property of the respective companies. Danfoss and the Danfoss logotype are trademarks of Danfoss A/S. All rights reserved.

Promass 80F



More information and current pricing:

www.endress.com/80F

Benefits:

- Highest process safety – immune to fluctuating and harsh environments
- Fewer process measuring points – multivariable measurement (flow, density, temperature)
- Space-saving installation – no in/outlet run needs
- Cost-effective – dedicated design for standard applications
- Safe operation – display provides easy readable process information
- Fully industry compliant – IEC/EN/NAMUR

Specs at a glance

- **Max. measurement error** Mass flow (liquid): $\pm 0.15\%$ (standard), 0.1% (option) Volume flow (liquid): $\pm 0.15\%$ Mass flow (gas): $\pm 0.35\%$ Density (liquid): $\pm 0.0005\text{ g/cm}^3$
- **Measuring range** 0 to 2 200 000 kg/h (0 to 80 840 lb/min)
- **Medium temperature range** Standard: -50 to $+200\text{ }^\circ\text{C}$ (-58 to $+392\text{ }^\circ\text{F}$) High temperature: -50 to $+350\text{ }^\circ\text{C}$ (-58 to $+662\text{ }^\circ\text{F}$)
- **Max. process pressure** PN 100, Class 600, 63K
- **Wetted materials** Measuring tube: 1.4539 (904L); 1.4404 (316/316L); Alloy C22, 2.4602 (UNS N06022) Connection: 1.4404 (316/316L); Alloy C22, 2.4602 (UNS N06022)

Field of application: Promass F has a long standing reputation as a highly accurate and robust device. It is suited for a broadest range of applications. Combined with the proven Promass 80 transmitter with push buttons, Promass 80F offers highest measurement performance for liquids and gases under varying, demanding process conditions.

Features and specifications

Liquids

Measuring principle
Coriolis

Endress+Hauser 

Appendix G: Datasheet of Coriolis mass flow measuring system Endress+Hauser PROMASS 80F [73].



OPTIFLUX 4300

Electromagnetic flowmeter for advanced process and custody transfer (CT) applications

- High accuracy ($\pm 0.2\%$), certified for custody transfer
- For low conductivity media ($> 1 \mu\text{S}/\text{cm}$) and high solid contents ($\leq 70\%$)
- Flange: DN2.5...3000 / γ_0 ...120°, max. PN40 / ASME CI 600
- 3 x 4...20 mA, HART®, Modbus, FF, Profibus-PA/DP, PROFINET

General information

Product type	Flowmeter
Product family name	OPTIFLUX
Product positioning	For advanced process and custody transfer (CT) applications
Measurement principle	Electromagnetic
Measured media	Liquids

Operating conditions

Process pressure	max. 40 barg/ 580 psig
Process temperature	-40...+180°C/ -40...+356°F

Materials

Liner	Ethylene tetrafluoroethylene (ETFE), Hard rubber, Perfluoroalkoxy alkane (PFA), Polytetrafluoroethylene (PTFE), Polyurethane (PUR)
-------	--

Process connections

Flange connections	EN (1092-1): DN2.5...3000 ASME (B 16.5): 1/2...120" JIS (B 2220): 2.5...1000A
Pressure rating (EN 1092-1)	PN40
Pressure rating (JIS B 2220)	20k
Pressure rating (ASME B 16.5)	Cl 300#, Cl 600#

Approvals/Standards

Certificates/Approvals Ex	ATEX, cQPSus, CSA, EAC Ex, FM, IA, IECEx, INMETRO, KCs, NEPSI, PESO
Certificates/Approvals Hygienic	FDA
Certificates/Approvals Marine	ABS, BV, CCS, CRS, DNV, IRS, KR, LR, NK, PRS, RINA, RS

Communication

Analogue outputs	4...20 mA
------------------	-----------

Discrete outputs	Frequency, Limit switches, Pulse, Status
Digital outputs	FOUNDATION™ fieldbus, HART®, Modbus RTU, Profibus-DP, Profibus-PA, PROFINET

Appendix H: Datasheet of KROHNE OPTIFLUX 4300 Electromagnetic flowmeter [76].

SINGLE PHASE - DESIGN

SWEP DThermX

HEAT EXCHANGER: BX8THx10/1P

Date: 12/04/2023

SSP Alias: BX8T

DUTY REQUIREMENTS		Side 1	Side 2
Fluid		Water	Water
Flow type		Counter-Current	
Circuit		Inner	Outer
Heat load	kW	12.00	
Inlet temperature	°C	60.00	10.00
Outlet temperature	°C	19.00	23.27
Flow rate	kg/s	0.07004	0.2161
Pressure drop (Design PD)	kPa	3.61 (20.00)	21.0 (20.00)
Thermal length		2.079	0.673
PLATE HEAT EXCHANGER		Side 1	Side 2
Total heat transfer area	m ²		0.184
Heat flux	kW/m ²		85.2
Mean temperature difference	K		19.72
O.H.T.C. (available/required)	W/m ² , °C		4100/3310
Pressure drop - total*	kPa	3.61	21.0
- in ports	kPa	0.0579	0.547
Port diameter (up/down)	mm	16.0/16.0	16.0/16.0
Number of channels per pass		4	5
Number of plates			10
Oversurfacing	%		24
Fouling factor	m ² , °C/kW		0.053
Reynolds number		727.2	1085
Port velocity (up/down)	m/s	0.351/0.351	1.08/1.08
Channel velocity	m/s	0.121	0.296
Shear stress	kPa	0.0113	0.0650
Average wall temperature	°C	26.35	24.73
Largest wall temperature difference	K		6.00
Min./Max. wall temperature	°C	14.34/40.98	12.87/34.98
*Excluding pressure drop in connections.			
PHYSICAL PROPERTIES		Side 1	Side 2
Reference temperature	°C	39.50	16.64
Dynamic viscosity	cP	0.660	1.09
Dynamic viscosity - wall	cP	0.864	0.896
Density	kg/m ³	992.5	998.8
Heat capacity	kJ/kg, °C	4.179	4.185
Thermal conductivity	W/m, °C	0.6299	0.5923
Film coefficient	W/m ² , °C	7920	12900
TOTALS		Side 1	Side 2
Total weight empty (no connections)*	kg		1.13
Total weight filled (no connections)*	kg		1.48
Hold-up volume (Inner Circuit)	dm ³		0.16
Hold-up volume (Outer Circuit)	dm ³		0.2
Port size F1/P1	mm		16
Port size F2/P2	mm		16
Port size F3/P3	mm		16
Port size F4/P4	mm		16
Carbon footprint	kg		7.92



6c8e3869-76a9-4059-b507-6c6decf95712

www.swep.net

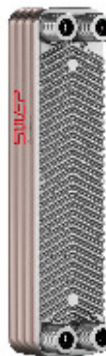
Date: 12/04/2023

Page: 1/2

PRODUCT SHEET

BX8T

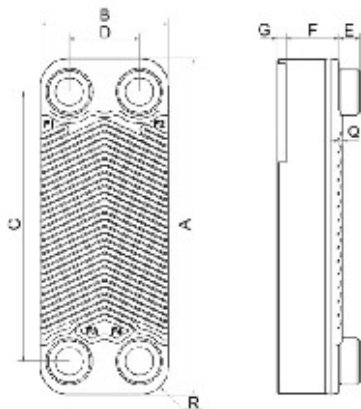
The X-marked BX8T is a good choice for a variety of one-phase and two-phase applications in many industries. Its efficient heat transfer can be utilized in applications such as container refrigeration and heat pumps. The X-plates on front and back give structural stability while being active heat transfer plates. This All-Active plate pack maximizes the material utilization and makes the product an efficient and competitive product for demanding applications.



Basic specifications

Maximum number of plates (NoP)	60
Max flow	4 m³/h (17.61 gpm)
Channel volume	0.039/0.039 dm³ (0.0014/0.0014 ft³)
Material	304 Stainless Steel Plates, Copper Brazing
Weight excl. connections	0.53+(0.075*NoP) kg 1.16+(0.165*NoP) lb
Max Particle Size (mm)	1

Standard dimensions



#	MM	IN
A	315	12.4
B	73	2.87
C	278	10.94
D	40	1.57
F	2,00+(2,24*(NoP-2,00))	0.08+(0.09*(NoP-7.87))
G	7	0.28
Q	2	0.08
R	16	0.63
E_1	20	0.79



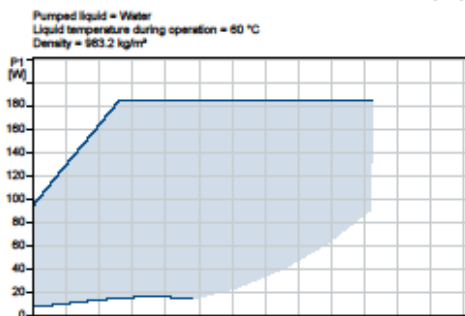
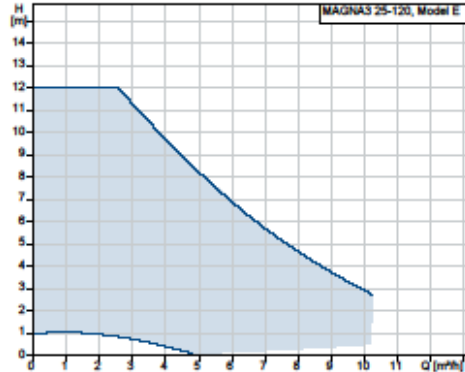
Company name:

Created by:

Phone:

Date: 13/05/2023

Description	Value
General information:	
Product name:	MAGNA3 25-120
Product No:	97924248
EAN number:	5710626493234
Price:	€ 1650
Technical:	
Rated flow:	5.56 m ³ /h
Rated head:	7.469 m
Head max:	120 dm
TF class:	110
Approvals:	CE, VDE, EAC, MOROCCO, UKCA, TSERCM, UkrSEPRO
Model:	E
Materials:	
Pump housing:	Cast iron
Pump housing:	EN-GJL-200
Pump housing:	ASTM A48-200B
Impeller:	PES 30%GF
Installation:	
Range of ambient temperature:	0 .. 40 °C
Maximum operating pressure:	10 bar
Pipe connection:	G 1 1/2"
Pressure rating:	PN 10
Port-to-port length:	180 mm
Liquid:	
Pumped liquid:	Water
Liquid temperature range:	-10 .. 110 °C
Selected liquid temperature:	60 °C
Density:	983.2 kg/m ³
Electrical data:	
Power input - P1:	9 .. 185 W
Mains frequency:	50 / 60 Hz
Rated voltage:	1 x 230 V
Maximum current consumption:	0.09 .. 1.56 A
Enclosure class (IEC 34-5):	X4D
Insulation class (IEC 85):	F
Others:	
Energy (EEI):	0.18
Net weight:	5.11 kg
Gross weight:	5.75 kg
Shipping volume:	0.015 m ³
Danish VVS No.:	380790120
Swedish RSK No.:	5732576
Finnish LVI No.:	4615101
Norwegian NRF no.:	9042329
Country of origin:	DE
Custom tariff no.:	84137030
Environmental approvals:	CN ROHS, WEEE



**082G3022**

Electrical actuators, AME 35, Supply voltage [V] AC: 24
AME 35 24V 3s/mm 15mm 600N

PRODUCT DETAILS

Gross weight	1.754 Kg
Net weight	1.742 Kg
Volume	3.508 Liter
EAN	5702421513071
Actuator speed [s/mm]	3 s/mm
Actuator type	Electrical
Ambient temperature [°C] [Max]	55 °C
Ambient temperature [°C] [Min]	0 °C
Application	HVAC
Closing force [N]	600 N
Control input signal Y [mA]	0(4) - 20 mA
Control input signal Y [mA], Impedance [Ohm]	500
Control input signal Y [V]	0(2) - 10 V
Control input signal Y [V], Impedance [kOhm]	24 kOhm
Control signal type	Modulating/3-point
Description	AME 35 24V 3s/mm 15mm 600N
Grade of enclosure	IP54
Manual operation	Yes
Position feedback	yes
Power consumption [W]	9 W
Product group	Electrical actuators
Protection Class	II
REACH Candidate List substances	Lead (CAS no. 7439-92-1)
Safety function	No
SCIP dossier no.	c5b6fd67- cf6c-493f-8f13-2d65fca1997f
SCIP dossier product name	AM(V)E 20 - 35
Speed type	Fast
Spring down (return)	No
Spring up	No
Storage temperature [°C] [Max]	70 °C
Storage temperature [°C] [Min]	-40 °C
Stroke [mm]	15 mm
Supply voltage [V] AC	24 V
Turn time per 90° [s]	0 *

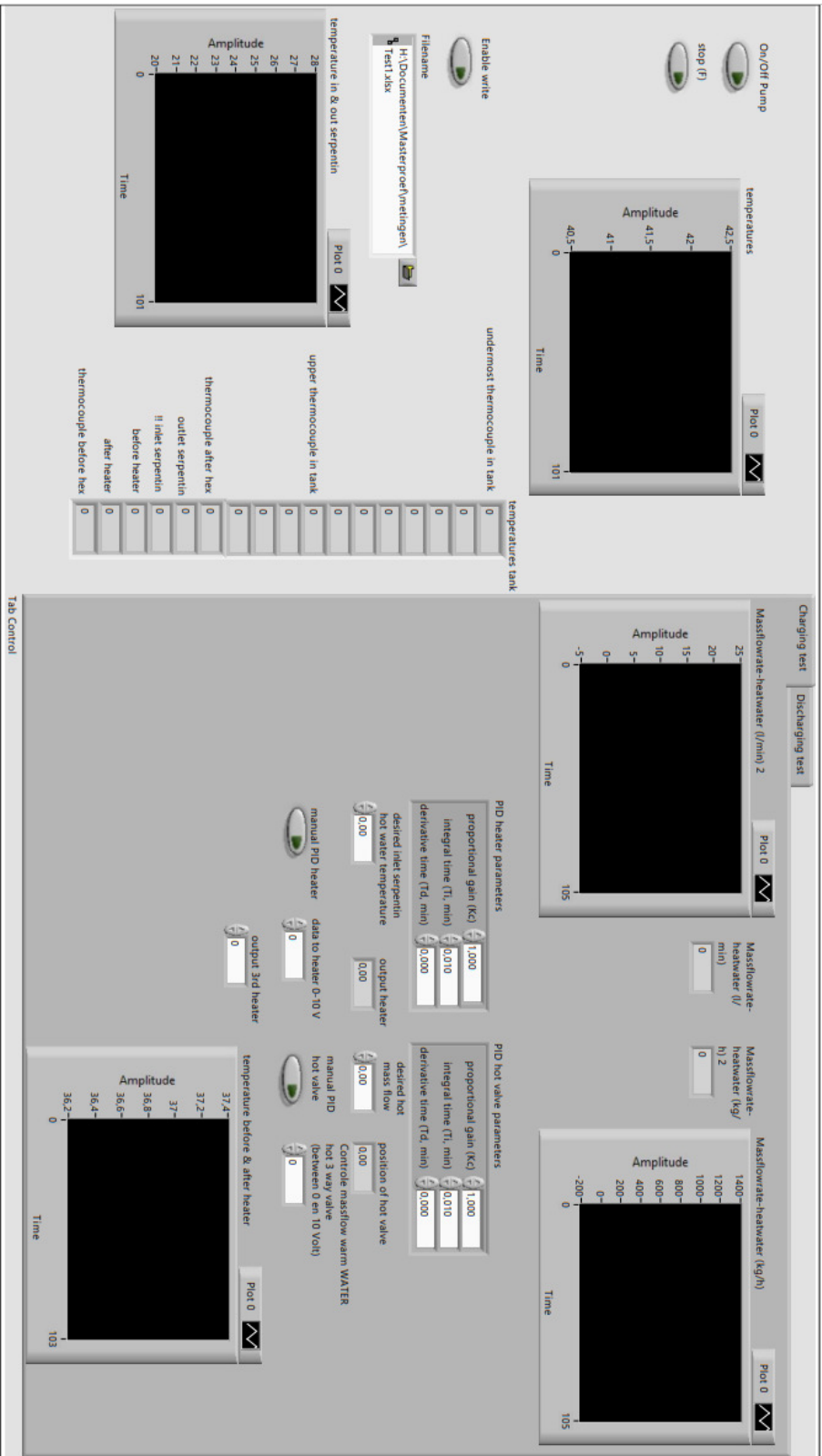
Danfoss can accept no responsibility for possible errors in catalogs, brochures and other printed material. Danfoss reserves the right to alter its products without notice. This also applies to products already on order provided that such alterations can be made without subsequent changes being necessary in specifications already agreed. All trademarks in this material are property of the respective companies. Danfoss and the Danfoss logo are trademarks of Danfoss A/S. All rights reserved.

Labview_test_sophie.vi

H:\Documenten\Masterproef\Labview_test_sophie.vi

Last modified on 18/04/2023 at 13:41

Printed on 12/05/2023 at 11:22



The screenshot displays the LabVIEW front panel for a water heating experiment. It is divided into two main test sections: 'Charging test' and 'Discharging test'. Each section contains a plot showing 'Amplitude' versus 'Time'. The 'Charging test' plots show temperature (40.5 to 42.5) and mass flow rate (0 to 25 l/min). The 'Discharging test' plots show temperature (36.2 to 37.4) and mass flow rate (0 to 1400 kg/h). The central control area includes two PID controllers: one for the heater and one for the hot valve. The heater PID parameters are: proportional gain (1.000), integral time (0.010), derivative time (0.000), desired inlet temperature (0.00), and output heater (0.00). The hot valve PID parameters are: proportional gain (1.000), integral time (0.010), derivative time (0.000), desired hot mass flow (0.00), and position of hot valve (0.00). A note indicates the hot valve is a 'hot 3 way valve (between 0 en 10 Volt)'. On the left, there are 'On/Off Pump' and 'stop (F)' indicators, and a 'Test 1.txt' file path. A 'Tab Control' is located at the bottom left.

Appendix M: Charge tab in front panel of LabVIEW program.

Labview_test_sophie.vi
 H:\Documenten\Masterproef\Labview_test_sophie.vi
 Last modified on 18/04/2023 at 13:41
 Printed on 12/05/2023 at 11:22

The screenshot displays the LabVIEW front panel for the 'Discharging test' tab. It features several data plots and control sections:

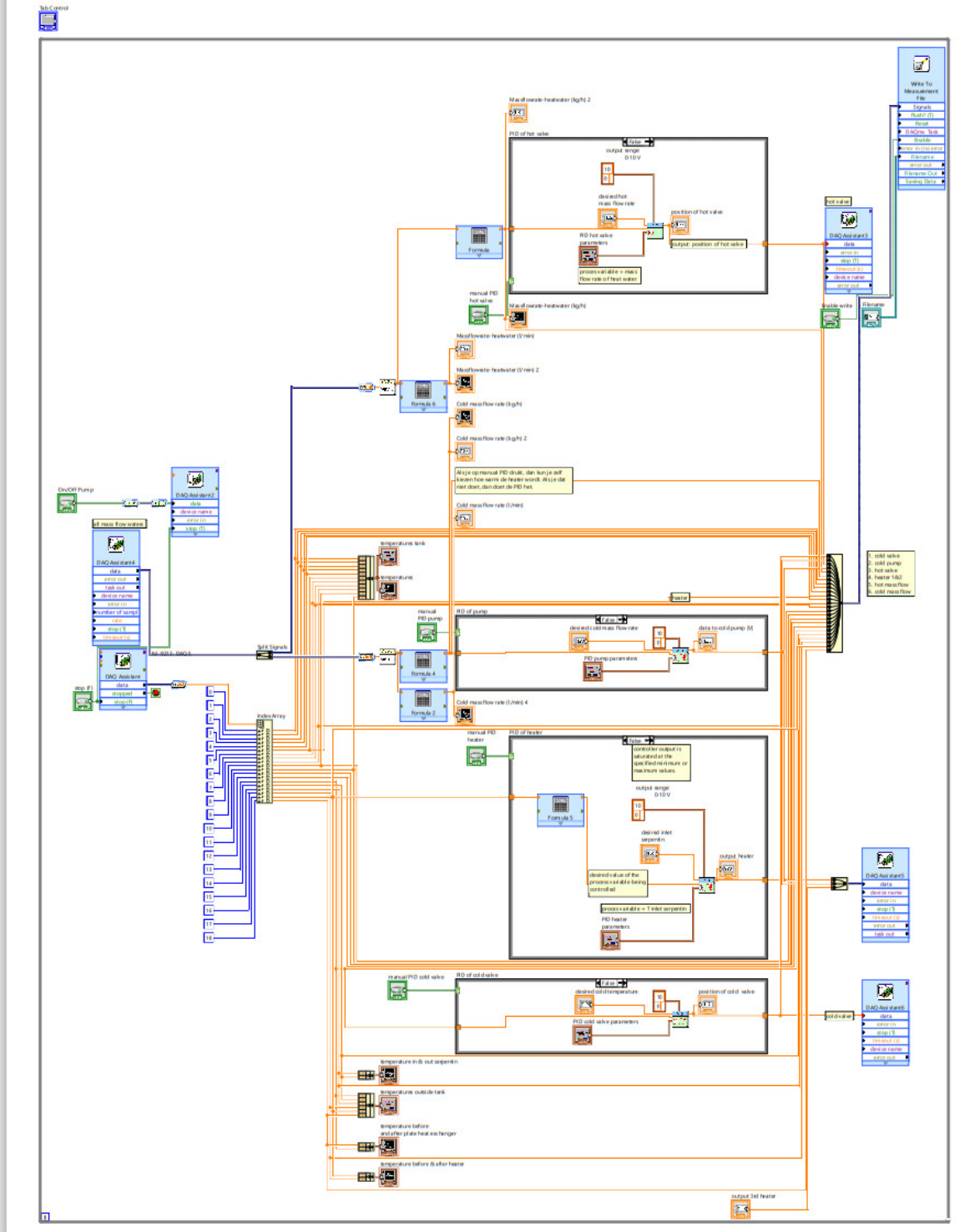
- On/Off Pump:** Includes 'stop (F)' and 'Test1.xlsx' buttons.
- temperatures:** A plot showing Amplitude vs Time with values ranging from 40.5 to 42.5.
- temperatures tank:** A table listing various temperature points:

undermost thermocouple in tank	0
upper thermocouple in tank	0
thermocouple after hex	0
outlet serpentin	0
inlet serpentin	0
before heater	0
after heater	0
thermocouple before hex	0
- Charging test / Discharging test:** Two tabs with associated plots. The 'Discharging test' plot shows Amplitude vs Time with values from -5 to 25.
- Massflowrate-heatwater (l/min) 2:** A control knob set to 0.
- Massflowrate-heatwater (kg/h) 2:** A control knob set to 0.
- Massflowrate-heatwater (kg/h) 2:** A plot showing Amplitude vs Time with values from -200 to 1400.
- PID heater parameters:**
 - proportional gain (Kc): 1.000
 - integral time (Ti, min): 0.010
 - derivative time (Td, min): 0.000
 - desired inlet serpentin hot water temperature: 0.00
 - output heater: 0.00
 - manual PID heater: 0
 - data to heater 0-10 V: 0
 - output 3rd heater: 0
- PID hot valve parameters:**
 - proportional gain (Kc): 1.000
 - integral time (Ti, min): 0.010
 - derivative time (Td, min): 0.000
 - desired hot mass flow: 0.00
 - position of hot valve: 0.00
 - manual PID hot valve: 0
 - Controlle massflow warm WATER hot 3 way valve (between 0 en 10 Volt): 0
- temperature before & after heater:** A plot showing Amplitude vs Time with values ranging from 36.2 to 37.4.
- Tab Control:** Located at the bottom left.

Appendix N: Discharge tab in front panel of LabVIEW program.



Labview_test_sophie.vi
H:\Documenten\Masterproef\Labview_test_sophie.vi
Last modified on 18/04/2023 at 13:41
Printed on 12/05/2023 at 9:07



Appendix O: Block diagram of LabVIEW program

Appendix P: Uncertainty analysis

An uncertainty analysis is done for the results of the coils' power and the tank power as can be seen in Table 17. Both mass flows, the heat capacity (0.1%), the water density (0.001%) and the temperatures have an uncertainty range. The uncertainty analysis is done based on the root-sum-square method [9]. For the uncertainty range of the coil energy the heat formula is used. That is the mass flow in the pipes and coils multiplied by the heat capacity of the heat transfer fluid multiplied with the temperature difference between the inlet and outlet of the coil.

For charging tests:

$$\dot{Q}_{coil} = \dot{m}c_p\Delta T$$

$$\delta\dot{Q}_{coil} = \sqrt{\left(\frac{\delta E}{\delta\dot{m}} * \delta\dot{m}\right)^2 + \left(\frac{\delta E}{\delta c_p} * \delta c_p\right)^2 + \left(\frac{\delta E}{\delta\Delta T} * \delta\Delta T\right)^2}$$

$$\begin{aligned} \frac{\delta\dot{Q}_{coil}}{\dot{Q}_{coil,min}} &= \sqrt{\left(\frac{c_p\Delta T}{\dot{m}c_p\Delta T} * \delta\dot{m}\right)^2 + \left(\frac{\dot{m}\Delta T}{\dot{m}c_p\Delta T} * \delta c_p\right)^2 + \left(\frac{\dot{m}c_p}{\dot{m}c_p\Delta T} * \delta\Delta T\right)^2} = \sqrt{\left(\frac{\delta\dot{m}}{\dot{m}}\right)^2 + \left(\frac{\delta c_p}{c_p}\right)^2 + \left(\frac{\delta\Delta T}{\Delta T}\right)^2} \\ &= \sqrt{0.0015^2 + 0.001^2 + \frac{0.1^2}{29.20}} = 0.39\% \end{aligned}$$

$$\frac{\delta\dot{Q}_{coil}}{\dot{Q}_{coil,max}} = \sqrt{0.0015^2 + 0.001^2 + \frac{0.1^2}{2.05}} = 4.88\%$$

For discharging tests:

$$\frac{\delta\dot{Q}_{coil}}{\dot{Q}_{coil,min}} = \sqrt{0.0022^2 + 0.001^2 + \frac{0.1^2}{35.30}} = 0.37\%$$

$$\frac{\delta\dot{Q}_{coil}}{\dot{Q}_{coil,max}} = \sqrt{0.0022^2 + 0.001^2 + \frac{0.1^2}{0.01}} = 10\%$$

As can be seen in Figure 79, the tank energy in the beginning of the test is higher than the other energies. At the end the tank energy is lower than the energy given by the heater, but higher than the energy delivered from the coil. The thermocouples are not calibrated and are measuring higher temperatures than they in reality are. Even though linear regression is applied on the values given by the thermocouples, the tank energy is still higher than the coil energy. This cannot be true since the tank water heats up due to the energy delivered by the heat transfer fluid flowing through the coil.

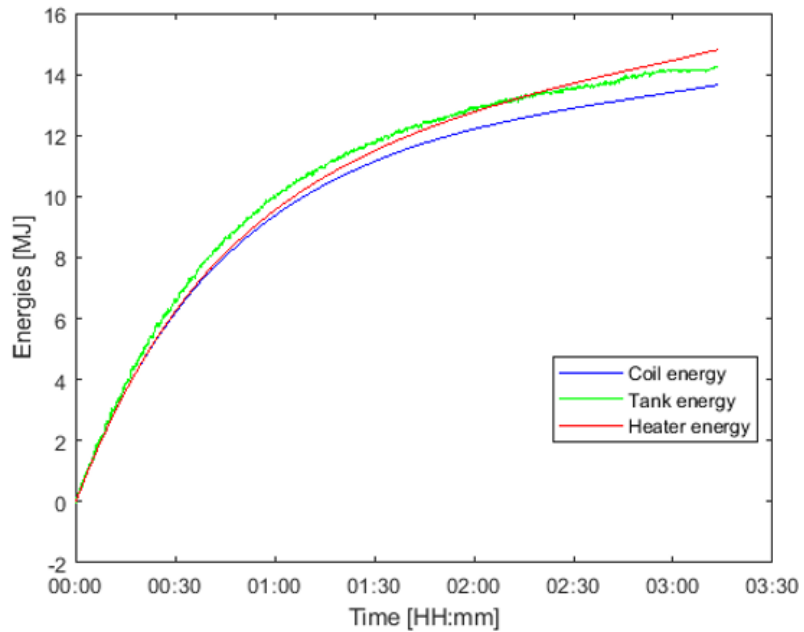


Figure 79: Coil, tank and heater energy of the 30°C 450 kg/h charging test.

The relative difference between the coil energy and tank energy of the 30°C 450 kg/h charging test is given in Figure 80. This is the error on the energy balance for that given working point.

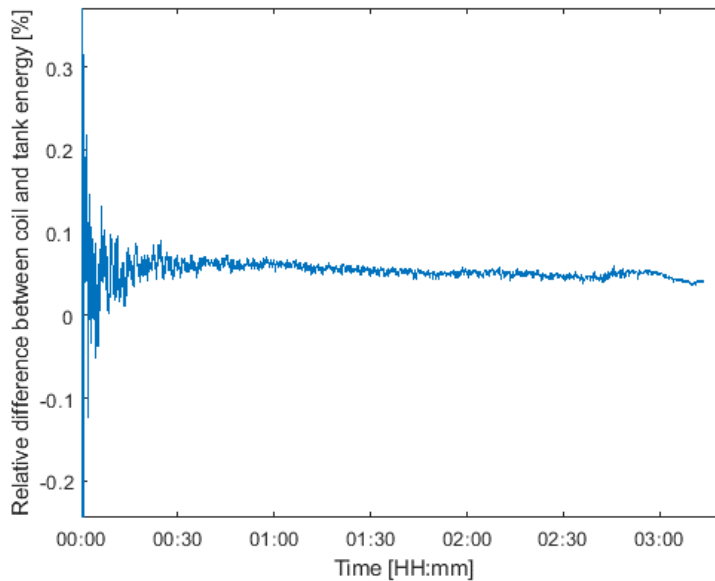


Figure 80: Relative difference between coil and tank energy of 30°C 450 kg/h charging test.

To determine the \dot{Q}_{heat} and \dot{Q}_{phex} , the same formula as for the \dot{Q}_{coil} is used, except the ΔT . Here, the fault of the temperature difference over the heater is measured by the thermocouples at the inlet and outlet of the heater. The fault of the temperature difference over the plate heat exchanger is measured by the thermocouple at the inlet and at the outlet of the plate heat exchanger.

Charging tests:

$$\frac{\delta \dot{Q}_{heat}}{\dot{Q}_{heat,min}} = \sqrt{0.0015^2 + 0.001^2 + \frac{0.1^2}{30,23}} = 0.38\%$$

$$\frac{\delta \dot{Q}_{heat}}{\dot{Q}_{heat,max}} = \sqrt{0.0015^2 + 0.001^2 + \frac{0.1^2}{3,41}} = 2.94\%$$

Discharging tests:

$$\frac{\delta \dot{Q}_{phex}}{\dot{Q}_{phex,min}} = \sqrt{0.0022^2 + 0.001^2 + \frac{0.1^2}{36.93}} = 0.36\%$$

$$\frac{\delta \dot{Q}_{phex}}{\dot{Q}_{phex,max}} = \sqrt{0.0022^2 + 0.001^2 + \frac{0.1^2}{0.37}} = 27.03\%$$

Quantity	Uncertainty range charging test	Uncertainty range discharging test
\dot{Q}_{serp}	0.39% - 4.88%	0.37% - 10%
\dot{Q}_{tank}	-4.99% - 2.78%	-3.08% - 16.13%
\dot{Q}_{heat}	0.38% - 2.94%	
\dot{Q}_{phex}		0.36% - 27.03%

Table 17: Uncertainty range for the results.

The reason for these high values can be because of the fact that only a linear regression is performed on the thermocouple values and the thermocouples are not calibrated.